Tyrosine kinases as therapeutic targets and their effect on the tumour microenvironment in oncogene-driven non-small-cell lung cancer

Inaugural-Dissertation

zur

Erlangung des Doktorgrades

der Mathematisch-Naturwissenschaftlichen Fakultät

der Universität zu Köln

vorgelegt von

Carolin Selenz

aus Bonn

Köln

2022

Berichterstatter: Prof. Dr. Dr. Roland T. Ullrich

(Gutachter) Prof. Dr. Björn Schumacher

Table of Contents

Summary 6

Chapter 1 – Introduction **8**

1.1 Non-small-cell lung cancer 8

1.2 Receptor tyrosine kinases in oncogene-driven NSCLC 6

1.2.1 EGFR *9*

1.2.2 EML4-ALK *10*

1.3 Components of the tumour microenvironment 11

1.4 Immune cell compartment of the tumour microenvironment 12

1.5 Treatment strategies for NSCLC 15

1.5.1 Targeted therapy in NSCLC *15*

1.5.2 Immunotherapy in NSCLC *17*

1.6 Aims of this work 18

Chapter 2 – Inhibition of tumour VEGFR2 induces serine 897 EphA2-dependent tumour cell invasion and metastasis in NSCLC **20**

Summary 22

2.1 Introduction 22

2.2 Results 24

2.2.1 Knockdown of Tumour VEGFR2 or Drug-Induced Inhibition of VEGFR2 Signalling in NSCLC Cells Induces an Invasive Phenotype In Vitro and In Vivo *24*

2.2.2 VEGFR2 Forms a Heterocomplex with EphA2 which Is Released upon VEGFR2 Inhibition *26*

2.2.3 EphA2 KD Prevents VEGFR2 Inhibition-Induced Tumour Cell Invasion In Vitro and In Vivo *27*

2.2.4 EphA2 S897 Is Required for Tumour Cell Invasion upon VEGFR2 Inhibition *27*

2.2.5 RSK Mediates Phosphorylation of S897 EphA2 ..... *28*

2.3 Discussion 30

2.4 References 32

2.5 STAR Methods 34

Chapter 3 – EGFR inhibition strongly modulates the tumour immune microenvironment in EGFR-driven non-small-cell lung cancer **40**

Simple Summary 41

Abstract 41

3.1 Introduction 42

3.2 Materials and Methods 43
3.3 Results 45
3.3.1 Inhibition of EGFR Mediates Higher Immune Cells Infiltration in TME of EGFR-Driven Tumours 45
3.3.2 EGFR Inhibition Enhances Proliferation and Activation of T-cells in TME .46
3.3.3 Inhibition of EGFR Increases Active Phenotype of Immune Cell Infiltrate in EGFR-Driven Tumours 47
3.3.4 Simultaneous EGFR Inhibition and ICB Indicates Slower Tumour Growth and Improved Anti-Tumour Response over EGFR Inhibition Alone in EGFR-Driven NSCLC Model 50
3.4 Discussion 51
3.5 Conclusion....53
3.6 References 53
Chapter 4 – Establishment of multiple EML4-ALK-driven NSCLC mouse models
4.1 Introduction....56
4.2 Materials and Methods 57
4.3 Results 62
4.3.1 Establishment of autochthonous EML4-ALK lung cancer model....62
4.3.2 In vitro validation of sensitivity to ALK inhibition in murine EML4-ALK/p53 NSCLC cell lines 64
4.3.3 Establishment of EML4-ALK/p53 subcutaneous mouse model....67
4.3.4 Investigation of different therapy approaches in autochthonous EML4-ALK model 69
4.4 Discussion 72
4.5 Conclusion....72
Chapter 5 – Discussion 73
5.1 Inhibition of tumour VEGFR2 induces serine 897 EphA2-dependent tumour cell invasion and metastasis in NSCLC 73
5.2 EGFR inhibition strongly modulates the tumour immune microenvironment in EGFR-driven non-small-cell lung cancer 75
5.3 Establishment of multiple EML4-ALK-driven NSCLC mouse models 77
5.4 Concluding remarks 80
General References 81
Erklärung zur Dissertation 94
Appendix 96
Chapter 2 Supplementary Materials 96

Chapter 3 Supplementary Materials 117
Chapter 4 Supplementary Materials 120
Danksagung 122

Summary

Lung cancer represents the most prevalent type of cancer and is responsible for the highest number of cancer-related deaths worldwide. Approximately 80 % of patients are non-small-cell lung cancer (NSCLC) cases. These can be further subcategorised depending on the histological and molecular composition of tumours. Oncogene-dependent NSCLC comprise a major subtype of NSCLC that harbours oncogenic driver mutations, for example in the receptor tyrosine kinase EGFR. These mutations induce aberrant activation of cell signalling, thus facilitating uncontrolled cell growth and tumorigenesis. Targeted therapy represents one essential treatment strategy that is well-established in the clinic for oncogene-driven NSCLC, for example in the form of tyrosine kinase inhibitors (TKIs). Other therapy approaches, such as anti-angiogenic compounds, aim to modulate the tumour microenvironment (TME) to become less advantageous to tumour cells, thus inhibiting cancer progression. Unfortunately, highly adaptive tumour cells and the dynamic nature of the TME limit the benefits of targeted therapy due to the emergence of resistance mechanisms or suppression of immune response. Therefore, it is essential to elucidate the effects of targeted therapy on the TME to increase our understanding of the underlying mechanisms responsible for the escape of immunosurveillance and tumour progression.

For this purpose, we investigated targeted therapy in the context of blood vessels in the TME. Anti-angiogenic treatment by targeting VEGFR2 signalling has demonstrated only limited benefits in lung cancer patients. We showed that inhibition of VEGFR2 induced a more aggressive phenotype of NSCLC with increase invasiveness and metastatic potential. Furthermore, we identified EphA2 signalling as a critical mediator for this aggressive phenotype, which is activated upon VEGFR2 inhibition. In particular, we shed light on the molecular mechanism that is dependent on phosphorylation of EphA2, which mediates the increased invasive phenotype in NSCLC.

To elucidate the impact oncogenic signalling inhibition in NSCLC on tumours and the TME, we examined EGFR-driven NSCLC and the immune cell infiltrate after EGFR inhibition by TKI. Interestingly, we found that inhibition of oncogenic signalling increased infiltration of immune cells into the TME and stimulated immune response against tumour cells. Additionally, we investigated potential benefits of combining EGFR inhibition with immune checkpoint blockade (ICB), which enhanced tumour response, providing grounds for further exploration of this matter.

Lastly, to contribute and expand our studies on the TME in oncogene-driven NSCLC, different *in vivo* NSCLC models were established harbouring the *EML4-ALK* fusion gene. These provide appropriate systems to study the direct and indirect impact of oncogenic signalling on the TME in more detail. Moreover, they offer unique opportunities to elucidate mechanisms of resistance and compare between oncogene-driven NSCLC tumours harbouring either the wildtype or mutated variant of the tumour suppressor gene *p53*.

Together, this thesis investigated the impact of targeted therapy on cancer cells and the TME in oncogene-driven NSCLC and evaluated the remaining difficulties associated with this therapy approach, which illustrate the need for optimisation of existing therapy options or development of alternative treatment strategies.

Chapter 1 – Introduction

1.1 Non-small-cell lung cancer

Lung cancer one of the most common cancer types and accounts for the highest cancer-related deaths worldwide. In 2020, an estimated 2.2 million people have been newly diagnosed with lung cancer, with 1.8 million deaths assigned to lung cancer [1,2]. The two main types of lung cancer are non-small-cell lung carcinoma (NSCLC) and small-cell lung carcinoma (SCLC), with NSCLC accounting for approximately 85% of lung cancer cases [3]. NSCLC can be further classified depending on histology of the tumour. Adenocarcinoma, squamous cell carcinoma and large cell carcinoma represent the three major subtypes of NSCLC, adenocarcinoma being by far the most frequently occurring in app. 40% of lung cancers [4]. NSCLC cases are not only stratified depending on their histological subtype, but further differentiated into classes based on the genetic composition of the tumours. Almost two-thirds of NSCLC patients have tumours harbouring genetic alterations that are classified as oncogenic driver mutations [5]. These mutations often occur in receptor tyrosine kinases (RTKs) that mediate multiple signalling pathways, such as cellular proliferation or differentiation, resulting in uncontrolled signal transmission by oncogenic receptor proteins. Tumour-suppressor gene mutations are another type of genetic alterations that frequently arise in tumours and affect genes that encode anti-proliferative signals and proteins. Loss of function of the affected genes and proteins contribute to an environment favourable for tumours [6]. Together, tumour-suppressing mutations and oncogenic driver mutations are factors in oncogene-driven NSCLC that are not only critical during initial stages in the development of cancer, but also over the course of tumour progression and metastasis [6–8].

1.2 Receptor tyrosine kinases in oncogene-driven NSCLC

Receptor tyrosine kinases (RTKs) constitute a family of proteins that are cell surface receptors and fulfil key regulatory functions in cellular signal transmission that are not only essential for normal cell survival, but also critical in development and progression of tumours. More specifically, RTKs can harbour different oncogenic mutations that promote initial tumorigenesis and also facilitates expansion of the tumour. One well-known/ well-established example for canonical RTK signalling, and one of the first RTKs to be discovered, is the epidermal growth factor receptor (EGFR) [9,10].

1.2.1 EGFR

EGFR, also called ErbB1, is a transmembrane tyrosine kinase that is part of the ErbB receptor protein. EGFR-mediated signalling is activated upon binding of its ligands, epidermal growth factor (EGF) or transforming growth factor-α (TGF-α), resulting in the formation of dimers of two receptor proteins. Subsequently, EGFR dimerization induces autophosphorylation of the intracellular tails via ATP-dependent activation of their tyrosine kinase domain [11] (Fig. 1.1A, C). This phosphorylation of intracellular tyrosine residues on EGFR activates several downstream pathways mediated by different signalling cascades, including the mitogen-activated protein kinase (MAPK), protein kinase B (AKT), and signal transducer and activator of transcription 3 (STAT3) pathways [12,13] (Fig. 1.1C). These pathways are key regulators for different vital cellular processes, such as cell growth, proliferation, and adhesion [14,15]. Therefore, EGFR signalling plays a significant role in facilitating multiple mechanisms that are essential to cell survival. Apart from its role in healthy cells, oncogenic driver mutations in *EGFR* can promote tumour development and growth by uncontrolled EGFR signalling. In NSCLC, oncogenic EGFR signalling is associated with formation and progression of tumours, as well as poor outcome for patients [11,15]. The most prevalent driver mutations in EGFR are either a leucine-to-arginine point mutation (L858R), or a deletion in exon 19 (del19) in the kinase domain. Driver mutations cause the EGFR tyrosine kinase to become constitutively active independent of ligands binding to the receptor [14]. Consequently, continuous EGFR signalling also leads to uncontrolled downstream signalling that eventually results in aberrant regulation of cellular processes, such as proliferation and adhesion, and promotes initial tumorigenesis and progression of established tumours [15,16].

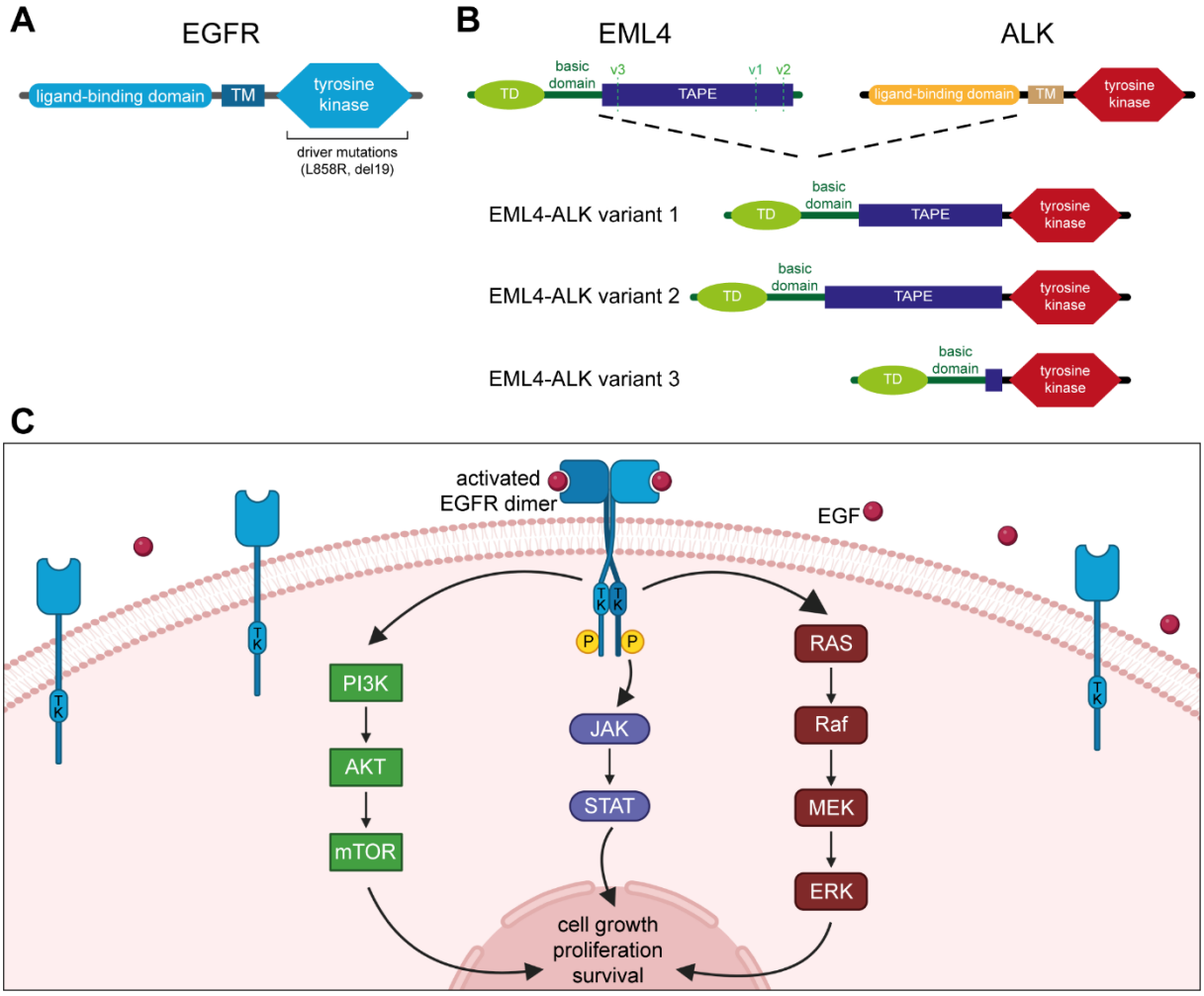

Figure 1.1 Oncogenic driver mutations in receptor tyrosine kinases in NSCLC (**A**) EGFR protein schematic of major protein domains: extracellular ligand-binding domain, transmembrane domain (TM) and tyrosine kinase domain, site of EGFR driver mutations such as point mutation L858R or deletion of exon 19 (del19). (**B**) Schematic of EML4-ALK chromosomal translocation, resulting in different variants of EML4-ALK fusion protein, depending on site of break point in EML4. TD: trimerisation domain, TAPE: tandem atypical beta-propeller domain, TM: transmembrane domain. (**C**) Canonical EGFR signalling pathway. EGFR dimerization is prompted by ligand-binding of EGF to receptor. Activated EGFR dimers initiate autophosphorylation via tyrosine kinase domain (TK). Phosphorylation (P) of intracellular tail induces downstream signalling cascades, including PI3K-AKT-mTOR, JAK-STAT and RAS-Raf-MEK-ERK pathways. Signal transduction via these signalling pathways regulate different cellular mechanisms, including cell growth, survival and proliferation. Created with BioRender.com.

1.2.2 EML4-ALK

Another well-established receptor tyrosine kinase known to carry oncogenic driver mutations is *anaplastic lymphoma kinase* (*ALK*). Oncogenic mutations in *ALK* can occur through different types of genetic abnormalities, either as point mutations or chromosomal abnormalities. Oncogenic ALK is known to harbour chromosomal relocation changes, leading to the formation of fusion genes. In NSCLC, a common ALK re-arrangement occurs on the short arm of chromosome 2 between *echinoderm microtubule-associated protein-like 4* (*EML4*) and *ALK*. Different variants of the *EML4-ALK* fusion gene exist, depending on where the break occurs in *EML4*, ranging from

before the HELP domain to different lengths of WD domain (Fig. 1.1B). As the break point in *ALK* remains constant, just before the tyrosine kinase domain, the break point in *EML4* determines which variant of the EML4-ALK fusion protein is formed (Fig. 1.1B). So far, 15 different types of EML4-ALK have been identified. The most prevalent ones are EML4-ALK variant 1 and EML4-ALK variant 3, together representing approximately 80 % of EML4-ALK NSCLC tumours [17]. Similar to oncogenic driver mutations in *EGFR*, the *EML4-ALK* fusion gene results in ligand-independent and constitutively active ALK signalling via the ALK tyrosine kinase domain of the fusion protein. This critically impacts downstream signalling cascades regulated by the ALK pathway, including MAPK/ERK, PI3K/AKT and JAK-STAT/STAT3 signalling [17]. As a result, normal cellular processes are exposed to uncontrolled signal transduction, disrupting essential mechanisms in healthy cells. Thus, EML4-ALK fusion proteins are driving factors strongly promoting uncontrolled cell growth that can lead to tumorigenesis and cancer formation. Both EGFR and EML4-ALK are examples for oncogenic mutations that demonstrate the central role of genome instability and alterations in the formation of cancer cells and illustrate the significance of this characteristic as a hallmark of cancer [18]. Other essential factors that allow tumorigenesis to occur and the formation of established solid tumours is the local tumour microenvironment.

1.3 Components of the tumour microenvironment

The tumour microenvironment (TME) significantly influences tumour growth and development and can promote a favourable environment for cancer cell proliferation. The TME is not only comprised of cancer cells residing in the tissue, but also consists of growth factors, secreted cytokines, blood vessels and various cell types, including the immune cell infiltrate, populating the environment in close proximity to tumour cells. All components of the TME play a role in mediating tumour growth and influence cancer progression [19]. In line with this process, the TME and its components are not static, but subjected to spatial and temporal changes over the course of initial tumorigenesis up to cancer progression and metastasis. One example of the dynamic nature of the TME is the development of vasculature in close proximity to cancer cells.

The adaptation of vasculature in the TME through the formation of new blood vessels from pre-existing vasculature, or angiogenesis, is another key hallmark of cancer [18]. Due to rapid proliferation of cancer cells, higher levels of nutrients and oxygen are

required by the tumour than in normal tissue. This increased supply for the growing tumour is guaranteed by the formation of new blood vessels through angiogenesis. Different cells in the TME, including cancer and some immune cells, mediate the release of pro-angiogenic factors, for example vascular endothelial growth factor (VEGF) or angiopoietin-2 (ANG-2) [20]. These factors stimulate the formation new blood vessels from pre-existing vasculature, thus providing access to nutrients and oxygen to cancer cells that are located further away from already existing vascular system in the tissue, and allows tumours to grow in size without being restricted to the proximity of primary blood vessels. Moreover, the newly formed vessels also provide access for malignant cancer cells to enter the circulation, potentially leading to metastatic spread of the tumour to secondary sites [19,21].

In lung tissue, tumour cells contribute to a tumour-promoting TME by secreting cytokines and growth factors that facilitate a more favourable environment for cancerous cells. This can result in more aggressive tumours leading to extravasation and metastasis. At the same time, cancer cells can emit signals that suppress immune cell activity directed against tumour cells, such as PD-L1, thus preventing an appropriate anti-tumour immune response. Therefore, tumour cells can actively promote an immunosuppressive TME [19,22].

1.4 Immune cell compartment of the tumour microenvironment

As mentioned above, the immune cell compartment of the TME has critical impact on tumorigenesis and cancer progression, which is not only dependent on anti-tumour cell activity, but also determined by levels of immune cell infiltration in the TME. Moreover, immune cells perform different functions, either in a tumour-suppressing manner by actively targeting cancer cells, or contributing to tumour growth by suppressing cancer-directed immune response, thus exhibiting tumour-promoting characteristics. Different types of immune cells are located in the TME (Fig. 1.2). A successful anti-tumour immune response is mediated by the interplay between the innate and the adaptive immune system. It is initially prompted by the detection of tumour cells by innate immune cells, such as natural killer (NK) cells or macrophages, which target the compromised cells, mediating phagocytosis, lysis or apoptosis of tumour cells. Subsequently, the release of cancer cell antigens induces an amplification of the innate immune response and also triggers the adaptive immune response by antigen uptake and presentation by dendritic cells (DCs) in the TME. Upon migration of DCs to a

regional lymph node, antigen processing and presentation prompts priming and activation of tumour cell-specific T-cells, as well as antigen-presenting cells (APCs), to stimulate and maintain a prolonged anti-tumour response. Presentation of cancer antigens primes naïve T-cells in the lymph node, inducing activation and expansion of both tumour-specific helper T-cells (CD4+ T-cells) and cytotoxic T-cells (CD8+ T-cells). Primed T-cells then traffic to the tumour site through blood vessels and infiltrate tumour tissue. There, primed CD8+ T-cells recognize antigens presented by cancer cells, and selectively target and kill compromised cells, resulting in the release of more tumour cell antigens in the TME [19,23,24].

This immune response cascade is a highly complex process, which is subjected to not only stimulating factors, promoting an active immune response, but is also tightly regulated by numerous inhibitory checkpoints and signals to prevent overstimulation of the immune system. Cancer cells can adapt these inhibitory to their advantage, and thus actively contribute to the generation of an immunosuppressive environment that promotes tumour progression. One example is the recruitment of regulatory T-cells (Tregs) to the TME. This subpopulation of T-cells suppresses activation and proliferation of cytotoxic T-cell, thus blocking an active anti-tumour response by the immune system [25]. Similarly, tumour-derived cytokines and growth factors can induce an environment that promotes differentiation and expansion of myeloid-derived suppressor cells (MDSCs), another immune cells type that promotes tumour tolerance by suppressing T-cell function and stimulating tumour angiogenesis (Fig. 1.2) [26]. In NSCLC, the immune cell infiltrate has shown to convey a generally immunosuppressive microenvironment, thereby limiting an active immune response and creating a pro-tumorigenic environment. Presence of Tregs has been detected as an early event in NSCLC [27]. Together with neutrophils, they protect tumours against immune-modulating signals and facilitate immune evasion [28]. Moreover, low infiltration of CD8+ T-cells observed in oncogene-driven NSCLC tumours has been linked to a general lack of immune effector cells, indicating an inactive immune response and further mediating an immunosuppressive TME [29,30]. As illustrated above, immune cells in the TME critically effect the anti-tumour response, and can not only function to combat tumour cells, but can also actively support tumour development. This intricate interplay within the immune cell compartment of the TME is further complicated by changes in the immune landscape that occur during tumour development and progression [31].

Deciphering how specific signalling pathways and crosstalk between different cell types contribute to the modulation of distinct interactions in the TME has been subject of investigation for many years. Increased awareness about the TME improves our understanding of tumour biology, as well as offers opportunities to identify potentially novel therapy approaches in this target-rich environment. This does not only include targeted therapy against cancer cell-specific factors such as receptor tyrosine kinases. With the emergence of immunotherapy, more studies are also focussing on directly modulating the immune response in the TME by attempting to stimulate immune cell activity and induce a change in status of the immune landscape from immunosuppressive to a pro-inflammatory state, resulting in a durable anti-tumour immune response [23,24].

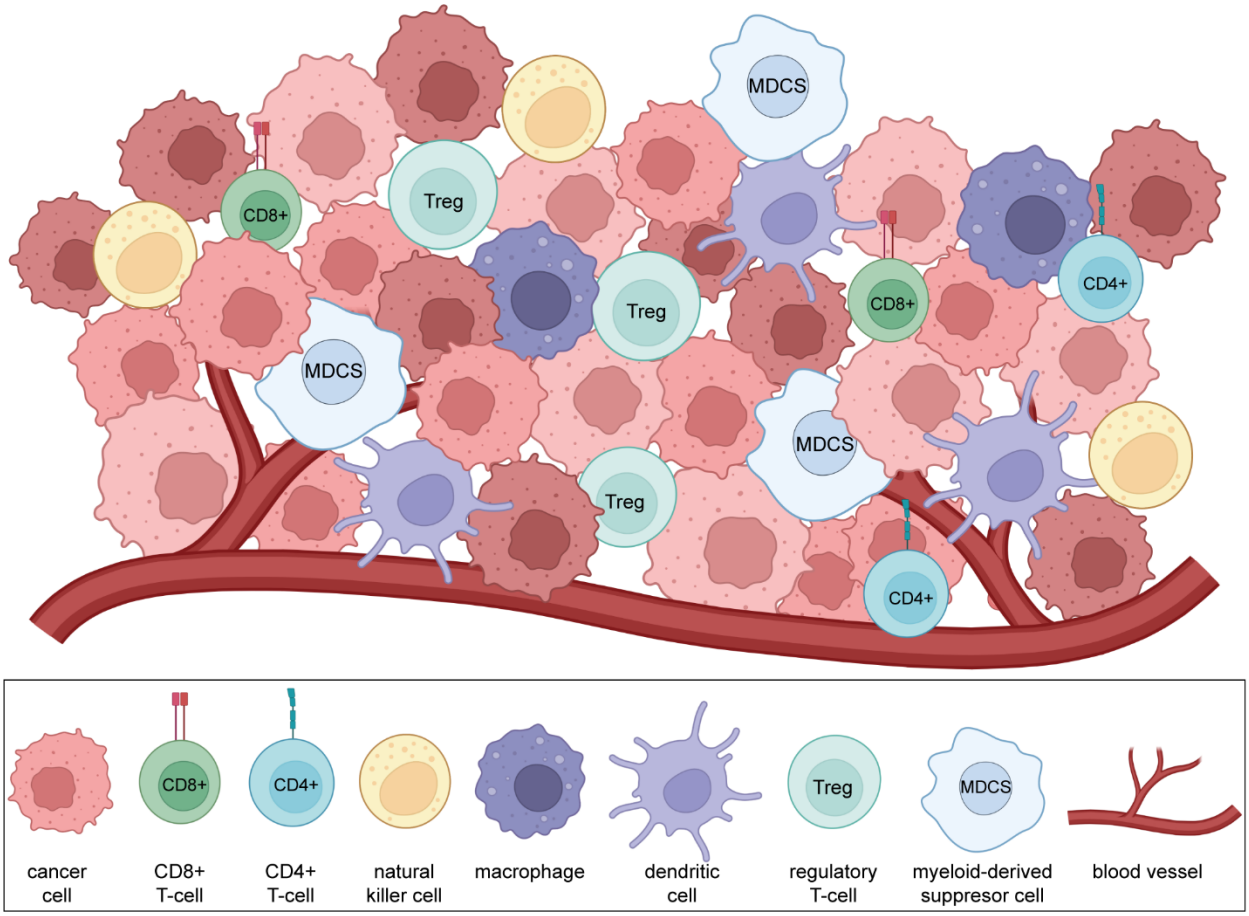

Figure 1.2 The tumour microenvironment (TME). Cancer cells reside in local environment that harbours different types if immune cells, as well as structural and other elements necessary for tumour growth, such as blood vessels that ensure supply of nutrients and oxygen to cancer cells. Immune cell infiltrate can consist of cell types that mediate an active immune response and to fight tumour cells, such as natural killer cells, macrophages, dendritic cells, cytotoxic CD8+ T-cells and helper CD4+ T-cells. Immunosuppressive cell types in the TME include regulatory T-cells and myeloid-derived suppressor cells, that inhibit active immune cell function, for example of cytotoxic CD8+ T-cells. Created with BioRender.com.

1.5 Treatment strategies for NSCLC

Treatment of NSCLC is highly dependent on different factors in regards to the patient, including genetic composition of the cancer and stage of tumour progression [32]. Since the beginning of the current century, treatment of NSCLC has vastly evolved from traditional chemotherapy, and the number of approved therapies for NSCLC have drastically increased. With ever increasing knowledge about the molecular composition of cancers, coupled with new and improved technologies to allow stratification of specific NSCLC subtypes, treatment strategies have become more and more personalised for each patient, thereby improving not only outcome, but also quality of life [33,34]. Especially the identification of different driver gene mutations that lead to oncogenic signalling in cancer cells has offered immense opportunities to develop therapeutic approaches to target specific proteins in tumour cells. Different treatment modalities are currently applied in the clinic for NSCLC patients, depending on specific subtype of cancer [32,34].

1.5.1 Targeted therapy in NSCLC

Targeted therapies are a form of treatment that target and block specific molecular signalling pathways in cancer cells and or the TME, which promote carcinogenesis and tumour growth. Potential targets for this treatment modality are not only expressed by cancer cells themselves, such as mutated oncoproteins, but can also be a part of the microenvironment in close proximity to tumours. Other targets include factors involved in the formation of blood vessels that contribute to the survival of cancer cells, such as VEGF molecules [21]. Due to the high selectivity of targeted therapies to cancer cells and the TME, they offer an alternative treatment approach to chemotherapy, causing less toxicity to healthy cells in the body [34,35]. Anti-angiogenic treatment strategies include the application of targeted therapy, aiming to regulate processes in the TME. As previously mentioned, VEGF and its main receptor VEGFR2 represent key regulators of angiogenesis, the formation of new blood vessels in the TME that enable the delivery of sufficient nutrients and oxygen levels to cancer cells necessary for tumour survival and growth [21]. In 2004, the first angiogenic inhibitor bevacizumab, and anti-VEGF antibody, was approved for use of colorectal cancer patients and introduced in the clinic [36]. Since then, multiple other molecular compounds, such as the VEGFR2 inhibitor vandetanib (ZD6474), have been introduced and approved for

clinical use that block angiogenesis in tumours, thus reducing access to nutrients and oxygen of cancer cells and limiting their survival capacity [37].

A second type of targeted therapy focusses on genetic alterations in tumour and the resulting oncoproteins that are expressed and drive cancer cell growth and proliferation. Many of these oncogenes encode cellular receptors that function as key regulators of signal transduction. Tyrosine kinase inhibitors (TKIs) have been developed that block aberrant receptor signalling caused by oncoproteins. This method has shown particularly successful results in oncogene-driven NSCLC patients harbouring genetic abnormalities in the receptor tyrosine kinases EGFR or ALK. TKIs targeting oncogenic EGFR in NSCLC have been first approved for clinical use in 2003 with gefitinib and erlotinib in 2004 [38,39]. Inhibitors of EGFR signalling function by occupying the ATP-binding site in the tyrosine kinase domain of EGFR, thus blocking ATP-induced autophosphorylation and preventing downstream signalling [40]. While TKI therapy offers good initial response rates in EGFR-driven NSCLC patients, resistance mechanisms eventually emerge after 9-14 months, leading to TKI insensitivity [41]. This most commonly occurs due to the development of secondary mutations in EGFR, such as the point mutations T790M [42]. These so-called “gatekeeper mutations” disrupt interaction between EGFR and the inhibitor and can further increase affinity of the tyrosine kinase domain for ATP binding. To account for this resistance mechanism, more recent generations of EGFR-specific TKIs have been develop that specifically target different gatekeeper mutations, such as T790M-mutated EGFR [43]. Nevertheless, while initial responses to more recent generations of TKIs have been positive, in many cases, tumours eventually progress and become insensitive to the new TKI, due to acquisition of further resistance mechanisms in the tumour [44]. Besides inhibition of aberrant EGFR signalling, TKIs have also been developed for alternative factors involved in mediating oncogenic signalling in other types of NSCLC. For patients harbouring chromosomal rearrangements in ALK, such as EML4-ALK fusion variants, inhibitors of ALK signalling have shown good initial response rates. The first ALK inhibitor approved for clinical use was crizotinib in 2011 [45]. This was followed by development and implementation of second generation TKIs, including alectinib in 2017, that provided improvements in response rates, as well as penetration of the blood brain barrier in patients with advanced NSCLC [46,47]. Similar to EGFR inhibitors, ALK TKI compounds occupy the ATP-binding site in the tyrosine kinase domain of ALK, thus blocking interaction between ATP and ALK. This

prevents ATP-mediated phosphorylation of ALK and the activation of further downstream signalling pathways is abrogated [48]. Unfortunately, secondary and tertiary mutations in the tyrosine kinase domain disrupting interaction between TKI and ALK is a common mechanism of resistance that leads to TKI-resistant tumours in patients [17]. Other factors limiting TKI sensitivity are the occurrence of co-mutations in tumours, such as in *tumour protein p53* (*p53*). This has been shown in patients harbouring both genetic driver mutations and alteration in the tumour suppressor gene *p53*, that indicate poorer clinical outcome compared to patients carrying wildtype *p53* [49].

Due to the highly adaptive nature of cancer cells, other cellular processes can also be activated and adapted to mediate resistance against targeted therapy, such as activation of bypass pathways independent of the original oncogenic signalling cascade [50–53]. Another resistance mechanism in response to targeted therapy can be histological transformation of cancer cells to a lung cancer subtype that is insensitive to TKI treatment, such as small-cell-lung cancer, or undergoing epithelial-to-mesenchymal-transition, which allows tumours to invade the circulatory system and metastasise at secondary sites [54–57]. As illustrated, the mechanisms by which cancer cells can adapt and escape targeted therapy by TKIs are highly diverse and critically increases the complexity of an effective therapy approach that is specifically targeted to the individual tumour cells and cases. To utilise not only cancer cells as therapeutic targets, but also other components of the TME, and attempt to induce a broader, more durable tumour response, other treatment modalities have drawn attention, with particular focus on immunotherapy to enhance the activity of the immune cell infiltrate [23,58].

1.5.2 Immunotherapy in NSCLC

Immunotherapy as a treatment strategy for different types of cancer has been the focus of numerous studies over the last decades and has shown great benefits for some patients in the clinic. As an alternative approach to classical tumour cell-targeted therapy, immunotherapy aims to stimulate the patient's own immune system to actively fight tumour cells, optimally leading to a more effective and durable anti-tumour response by the immune cell infiltrate in the TME [59,60]. The most established strategy in immunotherapy is immune checkpoint blockade (ICB). One prominent target for ICB is the programmed death-1/ programmed death-ligand 1 (PD-1/PD-L1)

signalling axis that transmits inhibitory signals in the TME and contributes to immunosuppression by suppressing cytotoxic function of CD8+ T-cells and increasing levels of anti-inflammatory Tregs in the TME [23,58,61]. While immunotherapy has vastly improved the outcome of NSCLC patients, not only due to lower off-target toxicity compared to traditional chemotherapy, but also due to drastic improvements in anti-tumour response, not all NSCLC cases profit from this type of treatment. In particular, only limited benefits of ICB were observed in oncogene-driven NSCLC tumours, when assessed by retrospective analyses of subgroup data from large clinical trials [62–66]. This illustrates the ongoing demand for further investigation of this approach in the context of driver gene mutations to uncover the responsible mechanisms behind oncogene-mediated insensitivity to ICB. Moreover, studies are also ongoing that examine potential benefits of combining ICB with other treatment regiments, such as targeted therapy via TKI, in oncogene-driven NSCLC [67,68].

Another type of immunotherapy is the procedure of adoptive cellular transfer (ACT), in which lymphocytes are isolated from patients, followed by expansion and different types of stimulation *ex vivo*. Subsequently, activated lymphocytes are re-injected into the patient to mediate a pro-inflammatory immune response and actively combat tumours. Multiple techniques and treatment protocols for ACT have been established, such as transfer of stimulated NK cells, and most prominently transfer of chimeric antigen receptor (CAR) T-cells that are genetically engineered to recognize specific tumour antigens from the patient [59,60]. Factors, such as poor infiltration of immune cells in tumours and lack of surface antigens on tumour cells and generally immunosuppressive TME pose critical challenges for the application of ACT in solid tumours such as NSCLC, illustrating the need for further optimisation of existing cellular approaches or development of novel strategies [69].

1.6 Aims of this work

Targeted therapies for oncogene-driven NSCLC are a well-established treatment approach that has significantly improved outcome for patients over previous alternatives, such as chemotherapy. Targeting specific cellular signalling pathways that drive malignant phenotype of cancer cells has also increased selectivity of treatment with less toxicity to normal cells [34]. However, in the context of cancer biology, cancerous cells represent only one key component for tumour development and progression. Additional factors that are involved in establishment of solid tumours

are other components of the TME, including vasculature and immune cells in close proximity to the tumours [19].

The aims of this work are to investigate targeted therapies as therapeutic approaches in NSCLC and study their broader effect on not only cancer cells, but also other components of the TME. I addressed these goals by first examining targeted therapy in the context of angiogenesis. After investigating the limited efficacy of VEGFR2 inhibition in NSCLC, an EphA2-dependent mechanism responsible for increased invasive phenotype following VEGFR2 inhibition was proposed, identifying EphA2 as a promising therapeutic target. Secondly, I assessed inhibition of oncogenic EGFR signalling in regards to its impact on the immune response in EGFR-driven NSCLC, followed by the analysis of potential benefits of combining EGFR targeted therapy with immunotherapy. Lastly, I established different mouse models to examine ALK+ NSCLC harbouring *EML4-ALK* fusion genes, as well as *EML4-ALK/p53* mutations. These do not only provide appropriate model systems to identify effects of targeted therapy on different aspects of the TME, but also offer suitable platforms to elucidate resistance mechanisms in oncogene-driven NSCLC and alternative treatment strategies.

Chapter 2 – Inhibition of tumour VEGFR2 induces serine 897 EphA2-dependent tumour cell invasion and metastasis in NSCLC

Caroline Volz*, Sara Breid*, **Carolin Selenz ***, Alina Zaplatina, Kristina Golfmann, Lydia Meder, Felix Dietlein, Sven Borchmann, Sampurna Chatterjee, Maike Siobal, Jakob Schöttle, Alexandra Florin, Mirjam Koker, Marieke Nill, Luka Ozretić, Niklas Uhlenbrock, Steven Smith, Reinhard Buettner, Hui Miao, Bingcheng Wang, H. Christian Reinhardt, Daniel Rauh, Michael Hallek, Amparo Acker-Palmer, Lukas C. Heukamp, Roland T. Ullrich

***** shared-first author

Cell Rep. 2020 Apr 28;31(4):107568. doi: 10.1016/j.celrep.2020.107568
NB. Primary literature in American English

Specific author contributions:

- Proximity ligation assays and analyses of NSCLC cell lines H441, H1650, H1975, HCC1359 and A549 upon VEGFR2 inhibition through ZD6474 treatment
- Co-immunoprecipitation experiments with NSCLC cell lines H441, H1650, H1975 and HCC1359
- Western blot analysis of NSCLC cell lines upon VEGFR2 inhibition through treatment with ZD6474
- Spheroid invasion assays of NSCLC cell line HCC1359 upon VEGFR2 inhibition
- Figure editing, generation of graphical abstract
- Manuscript editing, revision and submission

Cell Reports

Article

Inhibition of Tumor VEGFR2 Induces Serine 897 EphA2-Dependent Tumor Cell Invasion and Metastasis in NSCLC

Graphical Abstract

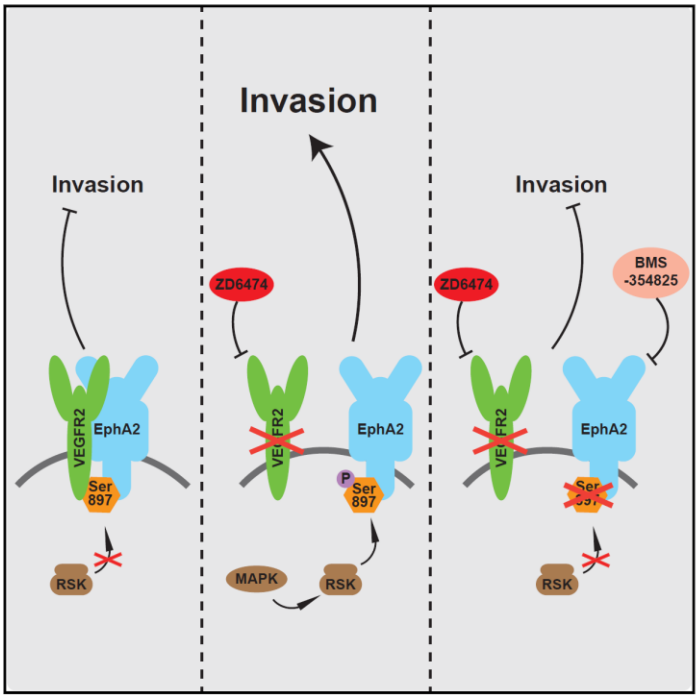

Highlights

- VEGFR2 inhibition in VEGFR2-positive NSCLC tumor cells induces tumor cell invasion
- EphA2-S897 mediates invasive phenotype induced by VEGFR2 inhibition
- These data provide a mechanism for the limited efficacy of VEGFR2-targeted therapy

Authors

Caroline Volz, Sara Breid, Carolin Selenz, ..., Amparo Acker-Palmer, Lukas C. Heukamp, Roland T. Ullrich

Correspondence

roland.ullrich@uk-koeln.de

In Brief

Anti-angiogenic treatment targeting VEGFR2 signaling has shown limited efficacy in lung cancer patients. Volz et al. show that VEGFR2 inhibition leads to a pro-invasive phenotype in VEGFR2-positive non-small cell lung cancer cells, which is mediated by phosphorylation of EphA2-S897.

Volz et al., 2020, Cell Reports *31*, 107568
April 28, 2020
https://doi.org/10.1016/j.celrep.2020.107568

Cell Reports

CellPress
OPEN ACCESS

Article

Inhibition of Tumor VEGFR2 Induces Serine 897 EphA2-Dependent Tumor Cell Invasion and Metastasis in NSCLC

Caroline Volz,[1,9,15] Sara Breid,[1,9,15] Carolin Selenz,[1,9,15] Alina Zaplatina,[1,9] Kristina Golfmann,[1,9] Lydia Meder,[1,9] Felix Dietlein,[1,13,14] Sven Borchmann,[1,9,10,11] Sampurna Chatterjee,[1] Maike Siobal,[1] Jakob Schöttle,[1,2] Alexandra Florin,[3] Mirjam Koker,[1,9] Marieke Nill,[1,9] Luka Ozretić,[12] Niklas Uhlenbrock,[7] Steven Smith,[7] Reinhard Büttner,[3] Hui Miao,[5,6] Bingcheng Wang,[5,6] H. Christian Reinhardt,[1,9] Daniel Rauh,[7] Michael Hallek,[1] Amparo Acker-Palmer,[4] Lukas C. Heukamp,[8] and Roland T. Ullrich[1,9,16,*]

[1]Department I of Internal Medicine, Center for Integrated Oncology Aachen Bonn Cologne Duesseldorf, University of Cologne, Cologne, Germany
[2]Department of Translational Genomics, University of Cologne, Medical Faculty, Cologne, Germany
[3]Institute of Pathology, University Hospital Medical School, Cologne, Germany
[4]Institute for Cell Biology and Neuroscience, University of Frankfurt, Frankfurt, Germany
[5]Rammelkamp Center for Research, MetroHealth Medical Center, Case Western Reserve University School of Medicine, Cleveland, OH, USA
[6]Department of Pharmacology and Oncology, Case Western Reserve University School of Medicine, Cleveland, OH, USA
[7]Faculty of Chemistry and Chemical Biology, TU Dortmund University, Dortmund, Germany
[8]Institute for Hematopathology Hamburg, Hamburg, Germany
[9]Center for Molecular Medicine, Cologne, Germany
[10]University of Cologne, Department I of Internal Medicine, German Hodgkin Study Group (GHSG), Cologne, Germany
[11]University of Cologne, Department I of Internal Medicine, Else Kröner Forschungskolleg Clonal Evolution in Cancer, Cologne, Germany
[12]Department of Cellular Pathology, Royal Free Hospital, London NW3 2QG, UK
[13]Department of Medical Oncology, Dana-Farber Cancer Institute, Boston, MA, USA
[14]Cancer Program, Broad Institute of MIT and Harvard, US Institute for Pathology, Cambridge, MA, USA
[15]These authors contributed equally
[16]Lead Contact
*Correspondence: roland.ullrich@uk-koeln.de
https://doi.org/10.1016/j.celrep.2020.107568

SUMMARY

Anti-angiogenic treatment targeting vascular endothelial growth factor (VEGF)-VEGFR2 signaling has shown limited efficacy in lung cancer patients. Here, we demonstrate that inhibition of VEGFR2 in tumor cells, expressed in ~20% of non-squamous non-small cell lung cancer (NSCLC) patients, leads to a pro-invasive phenotype. Drug-induced inhibition of tumor VEGFR2 interferes with the formation of the EphA2/VEGFR2 heterocomplex, thereby allowing RSK to interact with Serine 897 of EphA2. Inhibition of RSK decreases phosphorylation of Serine 897 EphA2. Selective genetic modeling of Serine 897 of EphA2 or inhibition of EphA2 abrogates the formation of metastases *in vivo* upon VEGFR2 inhibition. In summary, these findings demonstrate that VEGFR2-targeted therapy conditions VEGFR2-positive NSCLC to Serine 897 EphA2-dependent aggressive tumor growth and metastasis. These data shed light on the molecular mechanisms explaining the limited efficacy of VEGFR2-targeted anti-angiogenic treatment in lung cancer patients.

INTRODUCTION

Tumors acquire their blood supply via secretion of angiogenic factors that induce sprouting of new vessels from existing vasculature, a process commonly referred to as "tumor angiogenesis" (Bergers and Benjamin, 2003). The main pro-angiogenic drivers are vascular endothelial growth factor (VEGF) and its receptors VEGFR1–3 (Moens et al., 2014). Over the last decades, several anti-angiogenic agents targeting VEGF or its receptors have been approved for the treatment of various malignant diseases. However, anti-angiogenic treatment either as monotherapy or in combination with chemotherapy showed only modest effects on overall survival in patients (Ebos and Kerbel, 2011). In non-squamous non-small cell lung cancer (NSCLC), the addition of the angiogenesis inhibitor Bevacizumab to chemotherapy slightly improves overall survival (Sandler et al., 2006; Manzo et al., 2017). However, trials with tyrosine kinase inhibitors in combination with chemotherapy still fail to demonstrate efficacy (Tabchi and Blais, 2017). Furthermore, biomarkers that can be used to predict the response to anti-angiogenic therapy have not been found so far. Thus, there is an unmet medical need to decipher potential biomarkers applicable to this context in order to select patients that might profit from anti-angiogenic treatment. Different mechanisms of acquired resistance against anti-angiogenic therapy

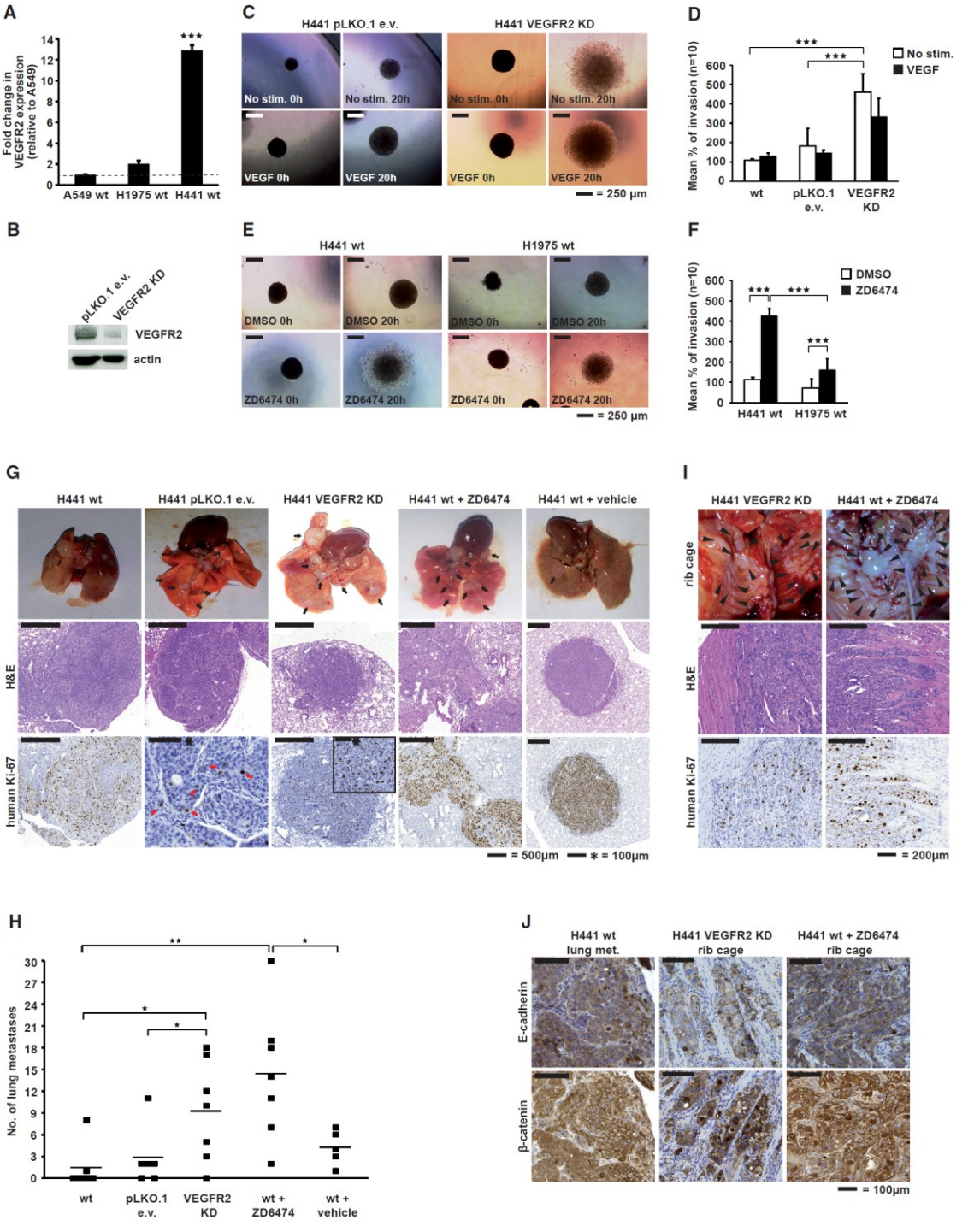

(legend on next page)

have been described, such as the activation of pro-angiogenic pathways, the recruitment of bone marrow-derived cells (e.g., fibrocyte-like cells), infiltration of innate immune cell populations, and activation of invasion and metastasis (Bergers and Hanahan, 2008; Moserle et al., 2014; Mitsuhashi et al., 2015; Rivera and Bergers, 2015). Previous preclinical data even showed that inhibition of tumor angiogenesis by genetic ablation of pro-angiogenic factors (e.g., hypoxia-inducible factor (HIF)-1α, matrix metallopeptidase 9, VEGF) or drug-induced inhibition of VEGF/VEGFR2 signaling (Bevacizumab, Sunitinib, DC101) resulted in increased invasion, formation of secondary satellite structures, or vessel co-option making the tumor more aggressive, especially in models of pancreatic islet cancer (Kuczynski et al., 2019; Pàez-Ribes et al., 2009; Sennino et al., 2012), melanoma, breast cancer (Ebos et al., 2009), and glioblastoma multiforme (GBM) (Du et al., 2008; Gomez-Manzano et al., 2008; Lu et al., 2012). Recent findings also revealed that contributing factors to the invasive phenotype are induced hypoxia (Du et al., 2008; Pàez-Ribes et al., 2009) or increased hepatocyte growth factor (HGF)/c-MET signaling (Lu et al., 2012; Sennino et al., 2012).

Furthermore, the Ephrin receptor signaling pathway has been shown to be involved in tumor cell invasiveness in different types of cancer (Cui et al., 2013a; Gopal et al., 2011; Liu et al., 2012; Miao et al., 2009, 2015; Paraiso et al., 2015). Eph receptor tyrosine kinases comprise the largest receptor tyrosine kinase family in the human genome and are divided into two classes A (EphA 1–9) and B (EphB 1–5) based on their sequence homology of the extracellular domain and their binding preferences for the membrane-anchored Ephrin A (GPI-linked) or Ephrin B (transmembrane domain-containing) ligands (Pasquale, 2010). A unique feature of the Eph/Ephrin pathway is that it can signal in a bidirectional manner (Xi et al., 2012). In addition, EphA2 is able to signal in a ligand-dependent and a ligand-independent manner (Beauchamp and Debinski, 2012). In particular, oncogenic EphA2 signaling seems to be ligand-independent and is mediated by phosphorylation of Serine 897 (S897) of EphA2. Previous studies indicated that S897 of EphA2 is phosphorylated by protein kinase B (AKT) and thereby mediates tumor cell migration and invasion in different cancer types including prostate cancer (Miao et al., 2009), glioma (Gopal et al., 2011; Miao et al., 2009, 2015), melanoma (Paraiso et al., 2015), and cholangiocarcinoma (Cui et al., 2013a). Furthermore, recent studies demonstrated that ribosomal s6 kinase (RSK) phosphorylates S897 of EphA2 in glioblastoma, lung, and breast cancer and promotes cell motility (Zhou et al., 2015) and proliferation (Hamaoka et al., 2016). Besides AKT and RSK, protein kinase A (PKA) has also been described to phosphorylate S897 of EphA2, which blocks cell retraction (Barquilla et al., 2016). These data indicate that non-canonical EphA2 signaling through S897 phosphorylation is regulated by multiple pathways. Therefore, further characterization of the signaling cascade is needed to understand the complex regulation and functions of ligand-independent EphA2 signaling in cancer cells.

In a previous study, we deciphered the role of VEGFR2 signaling in NSCLC. We found that ~20% of NSCLC patients express VEGFR2 on tumor cells. Abrogation of VEGFR2 signaling in these tumor cells resulted in a non-angiogenic phenotype *in vivo* (Chatterjee et al., 2013). As several reports described an invasive phenotype during VEGF/VEGFR2-targeted treatment in different cancer subtypes, we here sought to investigate the impact of VEGFR2 inhibition in NSCLC tumor cells on tumor invasiveness and the formation of metastases.

RESULTS

Knockdown of Tumor VEGFR2 or Drug-Induced Inhibition of VEGFR2 Signaling in NSCLC Cells Induces an Invasive Phenotype *In Vitro* and *In Vivo*

To investigate the impact of knockdown (KD) of VEGFR2 or VEGFR2-targeted treatment on tumor cell invasion *in vitro*, we performed a collagen assay with NSCLC cell lines. We employed the human lung cancer cell lines H441, H1975, and A549, which differentially express VEGFR2 (Figure 1A; Figure S1A) (Chatterjee et al., 2013). Complete KD of VEGFR2 (Figure 1B; Figure S1B) induces an invasive phenotype *in vitro* (Figures 1C and 1D; Figure S1C). In addition, these cell lines were treated with ZD6474, a potent dual inhibitor of VEGFR2 (half maximal inhibitory concentration [IC_{50}] = 40 nM) and the tyrosine kinase epidermal growth factor receptor (EGFR) (IC_{50} = 500 nM). ZD6474 also inhibits the kinase activity of VEGFR3 (IC_{50} = 108 nM), and with less activity against VEGFR1 (IC_{50} = 1,600 nM). Further targets of ZD6467 are platelet-derived growth factor receptor (PDGFR)-β (IC_{50} = 1,100 nM), Tie-2 (IC = 2,500 nM), fibroblast growth factor receptor (FGFR)-1 (IC_{50} = 3,600 nM), c-Kit (IC_{50} < 20 μM), erbB2 (IC > 20 μM), type 1 insulin-like growth factor (IGF-IR) (IC_{50} > 200 μM), and focal adhesion kinase (FAK) (IC_{50} > 200 μM) (Wedge et al., 2002). Our chosen NSCLC cell lines are resistant to EGFR inhibition, due to either a *KRAS*-mutation (H441, A549), or the presence of the T790M gatekeeper mutation in *EGFR* (H1975) (Pao et al., 2005;

Figure 1. Specific KD of Tumor VEGFR2 or Drug-Induced Inhibition of VEGFR2 Signaling in NSCLC Cells Induces an Invasive Phenotype *In Vitro* and *In Vivo*

(A) qRT-PCR for VEGFR2 expression in NSCLC cell lines. Expression was plotted relative to A549 (value of 1).

(B) Western blot analysis of VEGFR2 expression in pLKO.1 e.v. and VEGFR2 KD H441 NSCLC cells.

(C–F) Representative images and corresponding quantification of invasion assay of e.v. and VEGFR2 KD H441 cells with and without VEGF stimulation (C and D), and of H441 and H1975 NSCLC cell lines with ZD6474 and DMSO treatment (E and F). ***$p < 0.001$.

(G) Images and immunohistochemistry (IHC) of resected lungs of orthotopically injected H441 NSCLC cells into nude mice. Mice carrying H441 WT (n = 6), pLKO.1 e.v. (n = 6), or VEGFR2 KD (n = 7) cells received no therapy. Mice with H441 WT cells were treated either with vehicle (n = 5) or ZD6474 (n = 7). Lung metastases are indicated by black arrows. IHC staining of resected lungs for H&E and human Ki-67.

(H) Number of lung metastases of orthotopically injected mice with different cells or treatment, as indicated. Each square represents one mouse and the line indicates the mean. *$p < 0.05$, **$p < 0.01$.

(I) Images of infiltrated rib cages after VEGFR2 inhibition by VEGFR2 KD or ZD6474 treatment with corresponding IHC staining for H&E and human Ki-67.

(J) IHC staining for EMT markers E-cadherin and β-catenin. Rib cages of H441 VEGFR2 KD- and H441 WT-injected animals treated with ZD6474, and as control, H441 WT lung metastases are shown. *$p < 0.05$, **$p < 0.01$, ***$p < 0.001$.

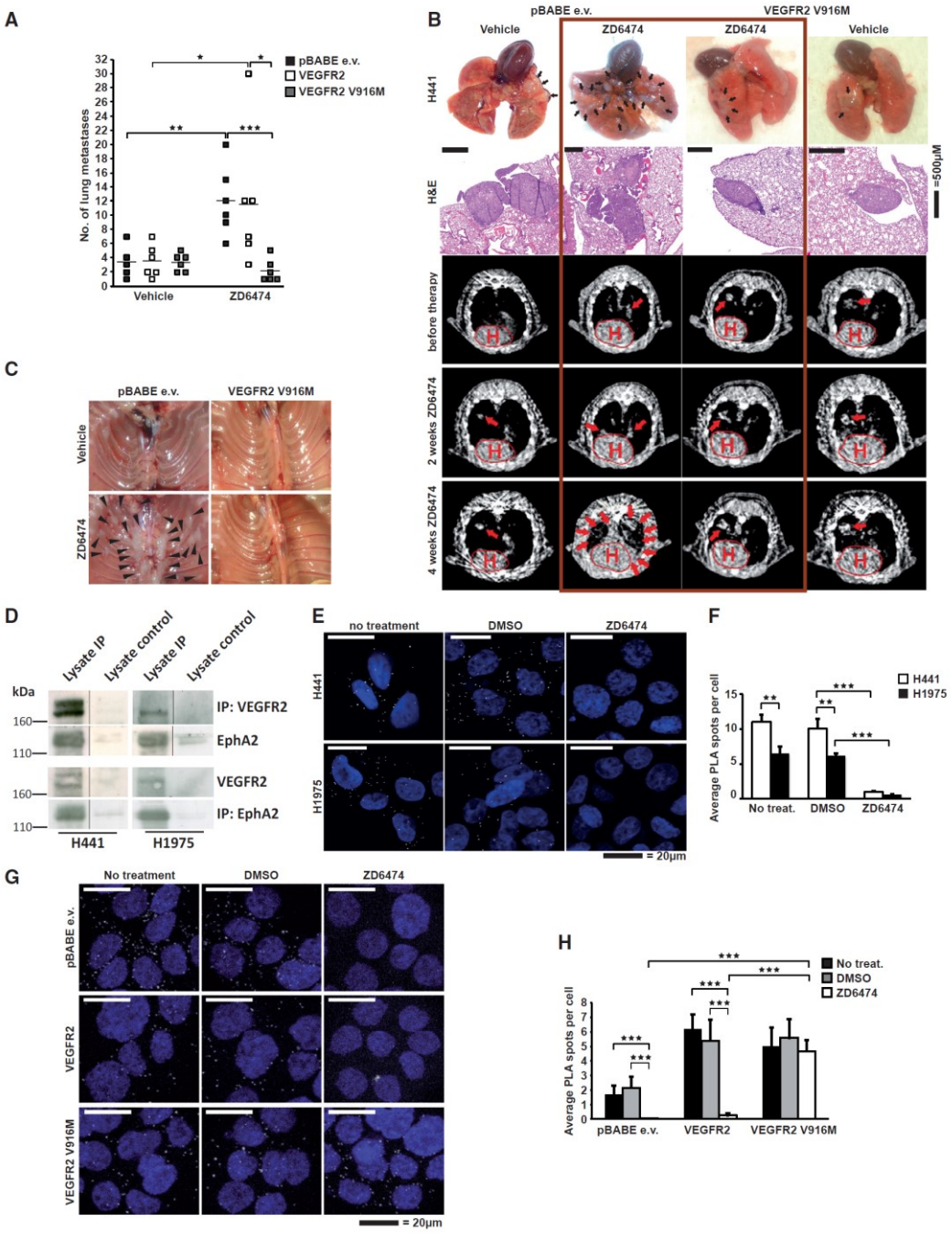

Figure 2. Inhibition of Tumor Cell VEGFR2 Signaling Induces an Invasive Phenotype in NSCLC

(A) Number of lung metastases of orthotopically injected mice with pBABE e.v., VEGFR2, and VEGFR2 V916M gatekeeper mutant cells, treated with either vehicle or ZD6474, as indicated. Each square represents one mouse and the line indicates the mean. *$p < 0.05$, **$p < 0.01$, ***$p < 0.001$.

(B) IHC images of resected lungs and μCT images of orthotopically injected H441 NSCLC cells into nude mice. Mice carrying H441 pBABE e.v. or VEGFR2 V916M gatekeeper cells received vehicle or ZD6474 (n = 6 per group). Lung metastases are indicated by black arrows. IHC staining of resected lungs for H&E.

(legend continued on next page)

Figure S1D). Western blot analysis showed no alteration of EGFR phosphorylation upon ZD6474 treatment (Figure S1E). Therefore, any therapeutic impact on tumor cell invasion in these cell lines can be primarily attributed to inhibition of VEGFR2 and not EGFR. Similar to the VEGFR2 KD, ZD6474 treatment also elicits tumor cell invasion *in vitro* (Figures 1E and 1F; Figures S1F–S1I). To examine the effect of VEGFR2 inhibition *in vivo* we orthotopically injected the NSCLC cell lines into the lungs of nude mice. VEGFR2 wild-type (WT) and empty vector (e.v.) NSCLC cells formed single non-invasive encapsulated tumors (Figure 1G). In contrast, VEGFR2 KD cells induced tumor cell invasion into the ipsilateral and contralateral pulmonary lobes (Figure 1G) as well as increased lung metastases compared to the WT and e.v. cells (Figure 1H). We next treated mice harboring orthotopic VEGFR2 WT tumors with ZD6474. Again, pharmacological targeting of VEGFR2 led to tumor cell invasion with multiple metastases in the ipsilateral and contralateral pulmonary lobes, whereas vehicle-treated tumors only formed single encapsulated tumors (Figures 1G and 1H; Figures S2A and S2B). To exclude that the increased number of lung metastases was due to increased proliferation, lung sections were stained using human Ki-67. Quantifying the Ki-67 positive cells did not show any significant differences in tumor cell proliferation between the groups (Figures S1J and S2D). Most strikingly, we observed an additional infiltration of VEGFR2 KD and WT tumor cells treated with ZD6474 into the rib cage (Figure 1I; Figure S2C). However, quantification of tumor cell proliferation for these settings showed no significant differences (Figures S1K and S2E).

Furthermore, we speculated whether VEGFR2 inhibition or KD of VEGFR2 may induce a switch from epithelial to mesenchymal state, analogous to the classical epithelial-to-mesenchymal transition (EMT) that is highly associated with cancer progression (Lamouille et al., 2014). VEGFR2 KD cells and cells treated with the VEGFR2 inhibitor ZD6474, significantly suppressed the EMT marker E-cadherin and displayed increased nuclear translocation of β-catenin (Figures S2F–S2I). Rib cage metastases of VEGFR2 KD- and ZD6474-treated tumors showed a significant reduction in E-cadherin without significant alteration in nuclear translocation of β-catenin compared to VEGFR2 WT tumors (Figure 1J; Figures S2J and S2K), indicating a partial mesenchymal-to-epithelial transition (MET) at the metastatic site (Aiello et al., 2018; Wykosky et al., 2005). We also analyzed human patient samples and found nuclear β-catenin and reduced E-cadherin in ~2% of the cases indicating a more invasive phenotype, especially in VEGFR2-low-expressing FFPE (formalin-fixed paraffin embedded) samples (Figure S2L).

These findings were further validated in a syngenic and orthotopic mouse model, showing that immunocompetent animals injected with KP938.3 NSCLC tumor cells tend to develop an increased number of metastases in the lung parenchyma and rib cage when VEGFR2 is inhibited by ZD6474 (Figure S2M). However, the effect was not as strong as for H1975 and H441 cells. This is most probably due to the lower expression of VEGFR2 in the murine KP938.3 NSCLC cell line in comparison to high VEGFR2 expression in H441 and H1975 (data not shown).

To validate that the observed results were a consequence of VEGFR2 inhibition on tumor cells, a genetic approach was applied by introducing a gatekeeper resistance mutation against ZD6474-induced VEGFR2 inhibition. The valine-to-methionine substitution of residue 916 (V916M) at the gatekeeper position of VEGFR2 was introduced into H441 cells by site-directed mutagenesis using a pBABE vector. This mutation was able to prevent the interaction between ZD6474 and the VEGFR2 binding pocket, thus abrogating the inhibitory effect of ZD6474 on tumor VEGFR2 phosphorylation (Chatterjee et al., 2013). We then orthotopically injected modified H441 cells (VEGFR2 and VEGFR2 V916M) into the lungs of nude mice. Strikingly, tumors harboring the gatekeeper mutation VEGFR2 V916M that were treated with ZD6474 presented a significantly reduced number of lung metastases compared to control groups (pBABE e.v. versus VEGFR2) (Figure 2A). These tumors were encapsulated and mainly located at one side of the lung. In contrast, ZD6474 treatment in the control groups showed an increase of lung metastases spanning the whole lung (Figure 2B; Figure S3A). In addition, the control settings displayed infiltration of tumor cells into the rib cage, especially upon ZD6474 treatment, which was abolished in tumors harboring the VEGFR2 V916M gatekeeper mutation (Figure 2C; Figure S3A).

These data demonstrate that an invasive phenotype in NSCLC is not mediated by anti-vascular effects via inhibition of VEGFR2 within the tumor microenvironment (e.g., inhibition of VEGFR2 on endothelial cells), but is induced by inhibition of VEGFR2 signaling in tumor cells.

VEGFR2 Forms a Heterocomplex with EphA2 which Is Released upon VEGFR2 Inhibition

In a next step, we aimed to elucidate potential co-receptors that drive tumor cell invasiveness upon VEGFR2 inhibition. EphA2 has been described as a strong mediator of tumor cell invasiveness (Gopal et al., 2011; Miao et al., 2009, 2015; Wykosky et al., 2005). Therefore, we evaluated whether VEGFR2 and EphA2 physically associate with each other by performing reciprocal

Representative μCT images before therapy, after 2 and 4 weeks of ZD6474 or vehicle therapy. The heart is marked in red with a circle and the capital letter H. The tumors are indicated by red arrows.
(C) Images of infiltrated rib cages for pBABE e.v. and VEGFR2 V916M treated with vehicle or ZD6474. The corresponding VEGFR2 control animals are presented in Figure S3A. VEGFR2 forms a heterocomplex with EphA2 that is released upon VEGFR2 inhibition.
(D) Western blot analysis of VEGFR2 and EphA2 immunoprecipitation (IP) in H441 and H1975 WT NSCLC cells (lysate IP samples: cell lysate + antibody + beads, lysate control samples: cell lysate + beads).
(E) Representative images from proximity ligation assays (PLAs) in H441 and H1975 WT NSCLC cells with either no treatment, DMSO-, or ZD6474 treatment. White signals indicate complex formation of VEGFR2 and EphA2.
(F) Quantification of average PLA spots per cell in both cell lines, as indicated. $^{**}p < 0.01$, $^{***}p < 0.001$.
(G) Representative images from PLA assay in H441 pBABE e.v.-, VEGFR2-, and VEGFR2 V916M-transduced NSCLC cells with either no treatment, DMSO-, or ZD6474 treatment. White signals indicate complex formation of VEGFR2 and EphA2.
(H) Quantification of average PLA spots per cell in cell lines, as indicated. $^{***}p < 0.001$.

immunoprecipitation (IP) studies. IP of human NSCLC cells expressing VEGFR2 and EphA2 with a VEGFR2 antibody followed by immunoblotting for EphA2 revealed a physical interaction between these two receptors in the H441 and H1975 cell lines (Figure 2D; Figure S3B). When cells were treated with the VEGFR2 inhibitor ZD6474, the complex formation strongly decreased—as shown in additional IP studies in NSCLC cells with high VEGFR2 expression, namely H441 and HCC1359 (Figure S3B). In line with our IP studies, proximity ligation assays (PLAs) showed an interaction between EphA2 and VEGFR2 that was disrupted by treating the cells with ZD6474 (Figures 2E and 2F). This trend was also observed when inhibiting VEGFR2 in HCC1359 (Figure S3C). Interestingly, we were also able to detect VEGFR2-EphA2 interactions in H1650 cells. This could be explained by increased sensitivity of the PLA technique, enabling us to identify the formation of the heterocomplex on single-cell level, even when VEGFR2 is only very lowly expressed in cells (Figure S3C). Furthermore, the introduction of the gatekeeper mutant V916M *VEGFR2* abrogated the reduction of PLA signals upon ZD6474 treatment (Figures 2G and 2H). This strongly supports our finding that VEGFR2 inhibition in NSCLC tumor cells hinders the VEGFR2/EphA2 heterocomplex formation.

Lu et al. (2012) reported that the invasive phenotype upon anti-angiogenic treatment is due to MET signaling and that both VEGFR2 and MET receptors form a heterocomplex in GBM. However, we could not detect a MET/VEGFR2 heterocomplex using IP in our NSCLC cell lines (data not shown). In addition, stimulation with VEGF had no impact on phosphorylation of MET, indicating that tumor cell invasion is not regulated by MET signaling in these NSCLC cell lines (Figure S3D).

EphA2 KD Prevents VEGFR2 Inhibition-Induced Tumor Cell Invasion *In Vitro* and *In Vivo*

We further sought to investigate whether downregulation of EphA2 might prevent invasion induced by VEGFR2 inhibition in NSCLC. H441 cells with efficient EphA2 KD via lentiviral transduction of three different short hairpin RNAs (shRNAs) were generated, which all reduced EphA2 expression compared to WT, as well as a pLKO.1 e.v. control (Figure 3A). KD of EphA2 in H441 cells did not affect tumor cell viability (Figure S4A). Using these cells, the impact of EphA2 KD on VEGFR2 inhibition-induced tumor cell invasion was tested. Treatment with ZD6474 resulted in increased invasion of the pLKO.1 e.v. H441 cells into the gel, whereas all three EphA2 shRNA-constructs blocked tumor cell invasion (Figures 3B and 3C; Figures S4B and S4C). To confirm the observed effect *in vivo*, we induced orthotopic NSCLC tumors via intrapulmonary injections of H441 EphA2 KD and pLKO.1 e.v. cells. Treatment with ZD6474 significantly increased the number of lung metastases in H441 pLKO.1 e.v. tumors, whereas KD of EphA2 abrogated the formation of metastases in ZD6474-treated mice (Figure 3D).

Of note, in ZD6474-treated NSCLC tumors with the highest initial EphA2 KD efficacy, EphA2 KD nearly completely prevented the formation of lung metastases (Figures 3A and 3D). Vehicle-treated EphA2 KD mice presented encapsulated, mainly local tumors, which were also observed for ZD6474-treated tumors (Figure 3E; Figure S5A). In contrast, ZD6474-treated mice harboring pLKO.1 e.v. NSCLC tumors displayed increased lung metastases that were found throughout the lung tissue (Figures 3D and 3E; Figure S5A). Similarly, drug-induced inhibition of EphA2 through BMS-345825 in combination with ZD6474 also reduced tumor cell invasion. Mice treated with the combination therapy showed decreased numbers of lung metastases when compared to the vehicle- or ZD6474-treated mice (Figures S6A–S6C).

To exclude that reduced proliferation of the EphA2 KD tumors was responsible for this phenotype, Ki-67-positive cells were quantified. We found no significant differences in tumor cell proliferation between EphA2 KD tumors and pLKO.1 e.v control tumors, or between drug-inhibited tumors and control tumors, indicating that EphA2 KD or BMS-345825 do not affect tumor cell proliferation (Figures S5B and S6D).

Since collagen III found in the tumor microenvironment has been described to play a role in regulating tumor progression (Kauppila et al., 1998; Nissen et al., 2019), we performed collagen staining to further support the invasive phenotype of tumors treated with VEGFR2 inhibitor. H441 pLKO.1 e.v. tumors treated with ZD6474 significantly increased collagen III expression with a chaotic shape across the tumor compared to vehicle control (Figures S5C and S5D). In contrast, all EphA2 KD tumors showed minimal expression with well-ordered collagen III fibers in vehicle and ZD6474 treatment conditions (Figures S5C and S5D). As mentioned above, the aggressive phenotype upon VEGFR2 inhibition was additionally characterized by the infiltration of the tumor cells into the rib cages. ZD6474-treated pLKO.1 e.v. mice presented rib cage infiltrations in all cases, displaying an infiltrative phenotype, whereas EphA2 KD prevented the infiltration of tumor cells into the rib cage (Figure 3F; Figure S5E). These results suggest that EphA2 is an essential player driving tumor cell invasion during VEGFR2-targeted treatment.

EphA2 S897 Is Required For Tumor Cell Invasion upon VEGFR2 Inhibition

Next, we aimed to examine the molecular mechanism of EphA2-driven tumor cell invasion upon VEGFR2 inhibition. Miao and colleagues have showed that phosphorylation of S897 on EphA2 is regulated by AKT and required for promoting ligand-independent migration of GBM cells *in vitro* and *in vivo* (Miao et al., 2009, 2015). Therefore, we hypothesized that this specific serine residue might be a key regulator for the invasive phenotype driven by VEGFR2 inhibition. For this purpose, H441, H1975, and HCC1359 cells were stably transduced with either EphA2, EphA2 S897A constructs or the corresponding pBABE e.v. control (Figures S7A and S8A). Strikingly, H441, H1975, and HCC1359 cells containing the EphA2 S897A mutant ceased tumor cell invasion upon VEGFR2 inhibition *in vitro* (Figures 4A and 4B; Figures S7B–S7D, S7G, S8B, and S8C), indicating that S897 of EphA2 is responsible for the induction of tumor cell invasion upon VEGFR2 inhibition. In a next step, H441 and H1975 cells carrying the EphA2 S897A mutant were injected into the lungs of mice. In line with our *in vitro* invasion data, the introduction of the EphA2 S897A mutant in both NSCLC cell lines blocked the formation of tumor metastases upon VEGFR2 inhibition *in vivo* (Figure 4C; Figure S8D) In contrast, EphA2 WT or e.v. NSCLC tumors treated with ZD6474 presented increased tumor infiltrations into the contralateral and ipsilateral lung (Figures 4C

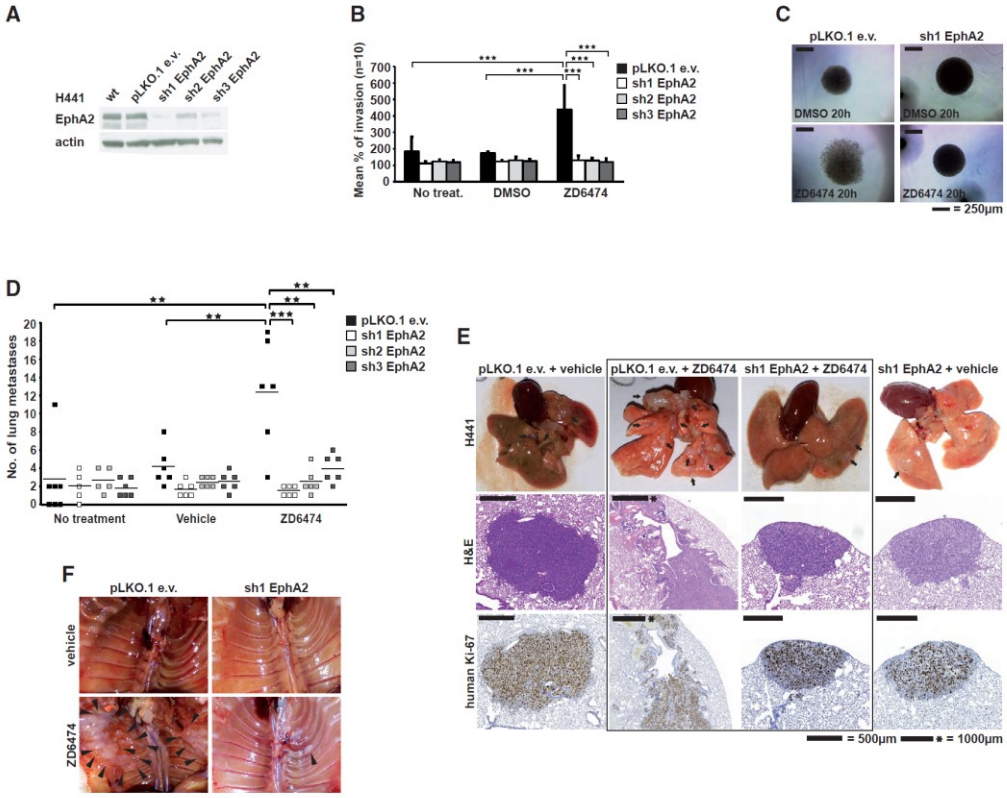

Figure 3. EphA2 KD Prevents VEGFR2 Inhibition-Induced Tumor Cell Invasion *In Vitro* and *In Vivo*

(A) Western blot analysis of EphA2 expression in H441 WT, pLKO.1 e.v., and three different sh-EphA2 cells.

(B) Quantified invasion of H441 pLKO.1 e.v. and sh-EphA2 cells. ***$p < 0.001$.

(C) Representative images of invasion assay of DMSO- and ZD6474-treated H441 pLKO.1 e.v. and sh1 EphA2 spheroids after 20 h. The corresponding 0-h images are shown in Figure S4B. The sh2 and sh3 spheroids are presented in Figure S4C.

(D) Number of lung metastases of mice orthotopically injected with H441 pLKO.1 e.v. and the three sh-EphA2 cells. Each square represents one mouse and the line indicates the mean. Mice were either not treated, were vehicle-treated, or received ZD6474. **$p < 0.01$, ***$p < 0.001$.

(E) Images and IHCs of resected lungs of orthotopically injected H441 pLKO.1 e.v. and sh1-EphA2 NSCLC cells (n = 6 per group [vehicle, ZD6474]). Black arrows indicate lung metastases. IHC staining of resected lungs for H&E and human Ki-67.

(F) Images of rib cages of pLKO.1- and sh1 EphA2 H441-injected mice treated with ZD6474 or vehicle. Black arrows highlight tumors.

and 4D; Figures S7E, S8D, and S8E). This was confirmed by immunohistochemistry (IHC) analysis showing a malignant and invasive phenotype in ZD6474-treated e.v. and EphA2 WT H441 and H1975 tumors represented by a detachment of cell groups at the invasive front. Notably, the S897A mutant tumors remained encapsulated at the injection site of the lung and the formation of metastases was nearly abrogated during ZD6474 treatment (Figures 4C and 4D; Figures S8D and S8E). Again, the proliferation marker Ki-67 was quantified, but did not show significant differences between the conditions (Figures S7F and S8F). Since we observed tumor cell infiltration into the rib cage of mice while inhibiting VEGFR2 in NSCLC tumor cells, the impact of the EphA2 S897A on the formation of metastases into the rib cage was investigated. In contrast to EphA2 WT tumors, H441 and H1975 cells containing the EphA2 S897A mutant strongly reduced rib cage infiltration upon treatment with ZD6474 (Figure 4E; Figure S8G). Furthermore, we examined the impact of ZD6474 treatment on S897 phosphorylation using western blot analysis in H441, H1975, and A549 NSCLC cells. Although we observed initial reduction in serine phosphorylation of EphA2 in H441 and H1975 cells, phosphorylation levels were generally increased in response to ZD6474 treatment over time (Figure S9A).

Taken together, these data demonstrate that in the examined NSCLC cell lines, the S897 position on EphA2 is essential for tumor cell invasion upon VEGFR2-targeted treatment.

RSK Mediates Phosphorylation of S897 EphA2

Phosphorylation of S897-EphA2 has been described to be required for tumor cell motility (Miao et al., 2009). More recent data suggest that EphA2 S897-dependent tumor cell motility is mediated by RSK (Zhou et al., 2015). To test this, we treated

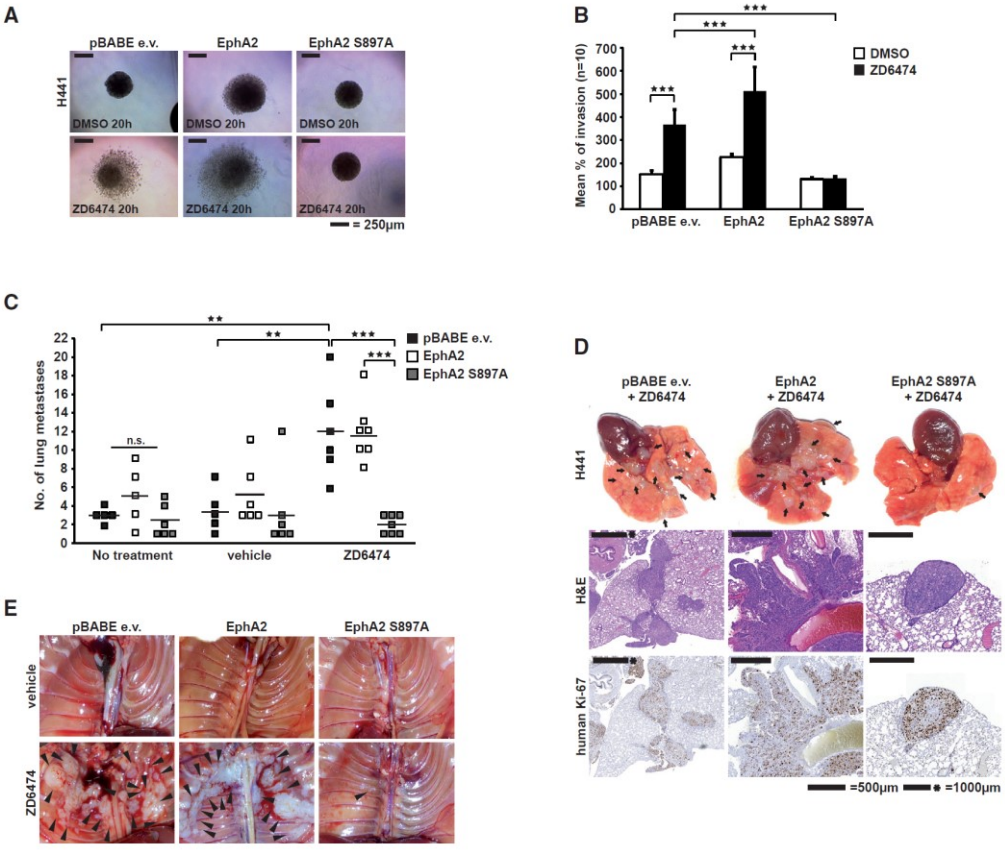

Figure 4. EphA2-S897 Phosphorylation Is Required for Tumor Cell Invasion upon VEGFR2 Inhibition

(A and B) Representative images of invasion assay (A) and the corresponding quantification (B) as mean % of invasion with H441 pBABE e.v.-, EphA2-, and EphA2 S897A-transduced cells. Spheroids were treated with ZD6474. DMSO served as control. The 0-h images are shown in Figure S7B. ***$p < 0.001$.

(C) Number of lung metastases for orthotopically injected H441 pBABE e.v., EphA2, and EphA2 S897A cells. Each square represents one mouse. Mice were either not treated, were vehicle-treated, or received ZD6474 (50 mg/kg) every second day. **$p < 0.01$, ***$p < 0.001$.

(D) Representative images and IHC images of resected lungs of orthotopically injected H441 pBABE e.v. (n = 6), EphA2 (n = 7), and EphA2 S897A (n = 7) NSCLC cells after ZD6474 treatment. Black arrows indicate lung metastases. IHC staining of resected lungs for H&E and human Ki-67. The corresponding vehicle data are presented in Figure S7E.

(E) Images of rib cages of pBABE e.v.-, EphA2-, and EphA2 S897A-injected mice. Black arrows highlight tumors.

NSCLC cells with the commercially available RSK inhibitor BI-D1870 (Sapkota et al., 2007). Treatment with BI-D1870 decreased phosphorylation of S897 EphA2 in a time-dependent manner, indicating that pS897 EphA2 is regulated by RSK (Figure 5A; Figures S9B and S9C). As RSK is known to be regulated by mitogen-activated protein kinase (MAPK) signaling, we subsequently treated NSCLC cells with the MEK Inhibitor PD0325901. We found that inhibition of MAPK kinase (MEK) by PD0325901 reduces phosphorylation of RSK and EphA2 S897 (Figure 5B; Figure S10). Taken together, these results indicate that MAPK signaling regulates phosphorylation of S897 EphA2 via RSK in NSCLC.

Furthermore, EphA2-S897 was identified as substrate for AKT and to be required for cell motility in GBM (Miao et al., 2009). Using IP experiments of EphA2 and blotting with an antibody detecting p-AKT substrate sites, we confirmed that S897 EphA2 is indeed a substrate for AKT in H441 and H1975 NSCLC cells, as the EphA2-S897A mutant cells abolished the substrate detection (Figures S11A and S11B). To functionally dissect the role of AKT for tumor cell invasion, we stably transduced H441 cells with a myristoylated form of AKT (pBABE myr-AKT). H441 with a continuously activated AKT presented a highly invasive phenotype (Figures S11C and S11D). We further aimed to recapitulate the role of AKT in EphA2 S897 phosphorylation by treating NSCLC cells with different AKT inhibitors. However, we found no reduction of S897 EphA2 phosphorylation upon treatment with these inhibitors (Figures S12A and S12B). Thus, our data indicate that phosphorylation of serine 897 of EphA2 is predominantly regulated by the MAPK-RSK signaling axis.

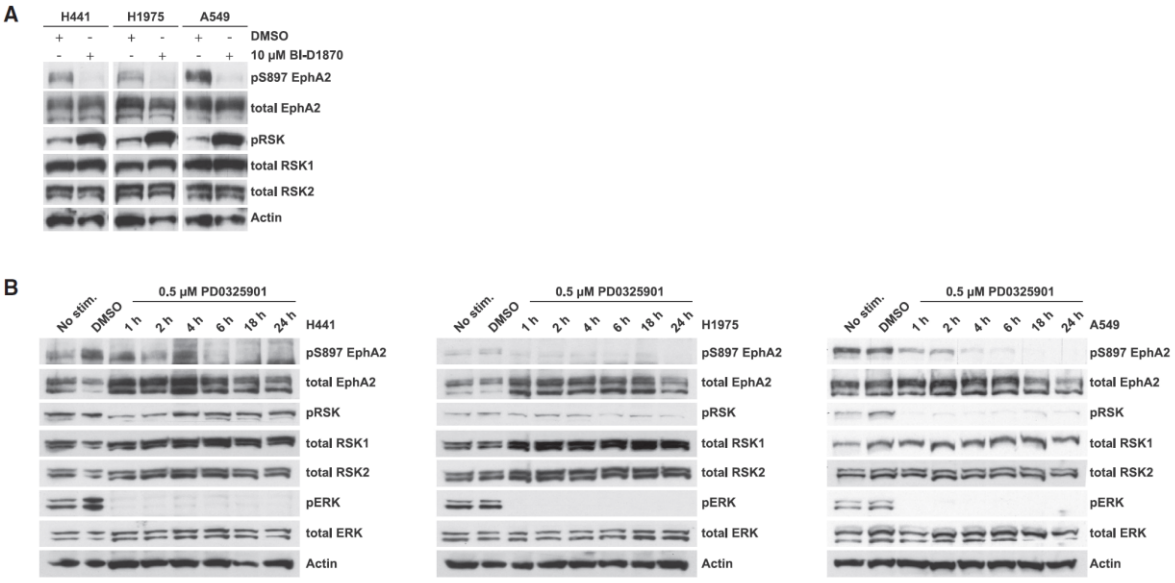

Figure 5. MAPK/RSK Signaling Controls S897 EphA2 Phosphorylation

(A) Western blot analysis of NSCLC cells under 4-h BI-D1870 and DMSO treatment for pS897 EphA2 and phosphorylated RSK (pRSK).

(B) Western blot analysis of H441, H1975, and A549 cells for pS897 EphA2, pRSK, and phosphorylated ERK (pERK) signaling under MEK inhibition with PD0325901 and DMSO control. Lysates were generated at different time points, as indicated.

Furthermore, EphrinA1 has shown to reduce phosphorylation of S897 EphA2 (Miao et al., 2009). To test whether EphrinA1 signaling is active in human xenograft mouse models, we treated our human NSCLC tumor cells with murine EphrinA1. In all cell lines, except for H1650, EphrinA1 reduced S897 EphA2 phosphorylation (Figure S12C). However, phosphorylation of RSK was not altered upon EphrinA1 treatment, indicating regulation of S897 EphA2 phosphorylation by EphrinA1 independent of RSK. EphrinA1 reduced phosphorylated AKT levels in nearly all cell lines, except for A549 and H1581, suggesting that murine EphrinA1 may affect pS897 EphA2 through the PI3K/AKT pathway.

DISCUSSION

In this study, we demonstrate that inhibition of VEGFR2 signaling in NSCLC tumor cells with high VEGFR2 expression induces tumor cell invasiveness and metastasis. While VEGFR2-expressing NSCLC cells present a non-invasive phenotype and form encapsulated tumors *in vivo*, drug-induced inhibition or selective KD of VEGFR2 in these cells results in enhanced aggressiveness with massive tumor cell invasiveness and metastases.

Previous studies described an increased invasive phenotype upon anti-angiogenic therapy mainly targeting the VEGF/VEGFR2 signaling pathway in GBM, melanoma, breast, and pancreatic islet cancer (Du et al., 2008; Ebos et al., 2009; Gomez-Manzano et al., 2008; Lu et al., 2012; Pàez-Ribes et al., 2009; Sennino et al., 2012). We have previously demonstrated that ~20% of patients with NSCLC show high VEGFR2 expression in tumor cells (Chatterjee et al., 2013). Thus, anti-VEGF/VEGFR2-targeted treatment in these patients might enhance tumor cell malignancy through increased invasiveness and occurrence of metastases. Pajares and colleagues found that VEGFR2 expression is associated with the clinical outcome of NSCLC patients (Pajares et al., 2012). Moreover, a previous report described that inhibition of VEGFR2 in chemically induced mouse models of NSCLC leads to divergent effects on tumor progression depending on the histological subtype (Larrayoz et al., 2014).

It has been postulated that VEGF/VEGFR2-targeted treatment impairs the tumor vasculature and thereby triggers tumor hypoxia via activation of the HIF1α pathway. This hypoxic tumor environment selects in favor of malignant invasive cells that start migrating and eventually form metastases (Finger and Giaccia, 2010). However, recent data indicate a distinct role of tumor cell-specific signaling pathways regulating tumor cell invasion independent of tumor hypoxia. Lu et al. (2012) described a functional role of a MET/VEGFR2 heterocomplex for tumor cell invasion and metastasis in GBM. More specifically, VEGF-targeted therapy induced tumor cell invasion via MET signaling in GBM cells in a hypoxia-independent manner. Similar to these findings, we found that the induction of tumor cell invasiveness upon VEGFR2-targeted treatment in NSCLC is regulated by a tumor cell-specific interaction between VEGFR2 and EphA2. In breast cancer, crosstalk between EphA2 and VEGFR2 signaling has already been described in endothelial cells of tumor microvessels, suggesting a regulatory function of EphA2 and VEGFR2 for tumor angiogenesis (Brantley et al., 2002). EphA2 is also differentially expressed in patients with NSCLC and associated with smoking history and poor prognosis (Brannan et al., 2009;

Faoro et al., 2010). Furthermore, inhibition of EphA2 leads to impaired tumor development and reduced metastasis in GBM (Miao et al., 2015), ovarian (Landen et al., 2005), and breast cancer (Brantley-Sieders et al., 2005). In line with these findings, we observed that EphA2 KD reduced lung metastasis and rib cage infiltration upon VEGFR2 inhibition, thus confirming EphA2 as an essential mediator for the observed invasive phenotype. In murine *KRAS*- and *EGFR*-driven NSCLC models, the loss of EphA2 has been associated with reduced tumor growth and increased apoptosis (Amato et al., 2014, 2016). Moreover, another report described a tumor-suppressive function for EphA2 in *KRAS*-mutated lung adenocarcinoma (Yeddula et al., 2015). In contrast, we found that KD of EphA2 abrogated tumor metastasis upon VEGFR2 inhibition without affecting tumor cell viability.

Recent studies described that EphA2 phosphorylation at S897 mediates a ligand-independent promotion of migration and invasion in different cancer types (Cui et al., 2013; Gopal et al., 2011; Miao et al., 2009, 2015; Paraiso et al., 2015; Zhou et al., 2015). In nasopharyngeal cancer, the S897 phosphorylation of EphA2 has even been described to be indispensable for invasion and metastasis (Li et al., 2019). Our study is in accordance with these previous findings, as selective genetic alteration of EphA2 S897 completely abrogates the invasive phenotype induced by VEGFR2 inhibition. Moreover, our data confirm previous findings demonstrating that RSK induces S897 EphA2 phosphorylation (Zhou et al., 2015). In line with this, inhibition of MAPK reduced phosphorylation of S897 EphA2 and RSK, providing evidence that MAPK/RSK signaling controls S897 EphA2 phosphorylation. Other studies also suggested S897 EphA2 to be a substrate of AKT (Cui et al., 2013b; Gopal et al., 2011; Miao et al., 2009, 2015; Paraiso et al., 2015). This was only partially confirmed by our IP experiments, as we did observe S897 EphA2 substrate specificity for AKT in NSCLC cell lines. However, inhibition of AKT did not reduce S897 EphA2 phosphorylation levels. To further unravel this interaction, single-cell RNA sequencing from patients' biopsies before VEGF/VEGFR2-targeted treatment and re-biopsies with progressive disease would be an appropriate method to consider for future plans. This approach could provide more detailed information on a single-cell level to identify sub-populations of tumor cells that drive cancer growth and metastasis.

With regard to clinical applications, our data support a selection of lung cancer patients upfront by evaluating expression levels of VEGFR2 and EphA2 on the tumor cells to determine who may likely develop metastases during VEGFR2-targeted treatment. We further propose that patients with VEGFR2-positive NSCLC might benefit from a combined VEGFR2/EphA2-targeted treatment.

In summary, we have identified a potential mechanism explaining the divergent effects of anti-angiogenic treatment. In NSCLC tumor cells that express VEGFR2, inhibition of the receptor interferes with the formation of the VEGFR2-EphA2 heterocomplex, thus promoting invasion. Selective genetic modeling of S897 completely abrogates the invasive phenotype induced by VEGFR2 inhibition. Concordantly, stable KD of EphA2 blocks tumor cell invasion during VEGFR2-targeted treatment. These results suggest that the invasive phenotype observed upon VEGFR2 inhibition is mediated by EphA2 signaling, and provides valuable insights into the mechanisms responsible for the limited efficacy of VEGFR2-targeted therapy in lung cancer patients.

STAR★METHODS

Detailed methods are provided in the online version of this paper and include the following:

- KEY RESOURCES TABLE
- RESOURCE AVAILABILITY
  - Lead Contact
  - Materials Availability
  - Data and code availability
- EXPERIMENTAL MODEL AND SUBJECT DETAILS
  - Cell lines and reagents
  - Animals and orthotopic implantation
- METHOD DETAILS
  - Knockdown and constructs for retroviral expression and stable transduction
  - Cell treatment and lysates
  - 3D spheroid invasion assay
  - Western blotting and co-immunoprecipitation
  - Viability assay and CTG® assay
  - RNA isolation and quantitative RT-PCR
  - Proximity ligation assay (PLA)®
  - Tumor samples and immunohistochemistry
- QUANTIFICATION AND STATISTICAL ANALYSIS
  - Statistical analysis

SUPPLEMENTAL INFORMATION

Supplemental Information can be found online at https://doi.org/10.1016/j.celrep.2020.107568.

ACKNOWLEDGMENTS

This work was supported by the Deutsche Forschungsgemeinschaft (DFG) (grant no. UL379/1-1 to R.T.U.); by the Thyssen Foundation (grant no. 10.16.1.028MN to R.T.U.); through SFB832 (Z2 to R.T.U.; TP6 to R.T.U.; TP5 to L.C.H.; and Z1 to L.C.H.); and by the Nachwuchsforschungsgruppen-NRW (grant no. 1411ng005 to R.T.U.).

AUTHOR CONTRIBUTIONS

C.V., S.B., and C.S. designed the research study, conducted experiments, acquired data, analyzed data, and wrote the manuscript. K.G., A.Z., L.M., F.D., S.B., S.C., M.S., J.S., A.F., M.K., M.N., L.O., N.U., and S.S. conducted experiments and acquired data. R.T.U., R.B., H.M., B.W., H.C.R., D.R., M.H., A.A.P., and L.C.H. designed the research study and edited the manuscript. All authors read the manuscript and provided feedback.

DECLARATION OF INTERESTS

The authors declare no competing interests.

Received: April 4, 2019
Revised: March 11, 2020
Accepted: April 3, 2020
Published: April 28, 2020

REFERENCES

Aiello, N.M., Maddipati, R., Norgard, R.J., Balli, D., Li, J., Yuan, S., Yamazoe, T., Black, T., Sahmoud, A., Furth, E.E., et al. (2018). EMT subtype influences epithelial plasticity and mode of cell migration. Dev. Cell *45*, 681–695.e4.

Amato, K.R., Wang, S., Hastings, A.K., Youngblood, V.M., Santapuram, P.R., Chen, H., Cates, J.M., Colvin, D.C., Ye, F., Brantley-Sieders, D.M., et al. (2014). Genetic and pharmacologic inhibition of EPHA2 promotes apoptosis in NSCLC. J. Clin. Invest. *124*, 2037–2049.

Amato, K.R., Wang, S., Tan, L., Hastings, A.K., Song, W., Lovly, C.M., Meador, C.B., Ye, F., Lu, P., Balko, J.M., et al. (2016). EPHA2 blockade overcomes acquired resistance to EGFR kinase inhibitors in lung cancer. Cancer Res. *76*, 305–318.

Barquilla, A., Lamberto, I., Noberini, R., Heynen-Genel, S., Brill, L.M., and Pasquale, E.B. (2016). Protein kinase A can block EphA2 receptor-mediated cell repulsion by increasing EphA2 S897 phosphorylation. Mol. Biol. Cell *27*, 2757–2770.

Beauchamp, A., and Debinski, W. (2012). Ephs and ephrins in cancer: ephrin-A1 signalling. Semin. Cell Dev. Biol. *23*, 109–115.

Bergers, G., and Benjamin, L.E. (2003). Tumorigenesis and the angiogenic switch. Nat. Rev. Cancer *3*, 401–410.

Bergers, G., and Hanahan, D. (2008). Modes of resistance to anti-angiogenic therapy. Nat. Rev. Cancer *8*, 592–603.

Brannan, J.M., Dong, W., Prudkin, L., Behrens, C., Lotan, R., Bekele, B.N., Wistuba, I., and Johnson, F.M. (2009). Expression of the receptor tyrosine kinase EphA2 is increased in smokers and predicts poor survival in non-small cell lung cancer. Clin. Cancer Res. *15*, 4423–4430.

Brantley, D.M., Cheng, N., Thompson, E.J., Lin, Q., Brekken, R.A., Thorpe, P.E., Muraoka, R.S., Cerretti, D.P., Pozzi, A., Jackson, D., et al. (2002). Soluble Eph A receptors inhibit tumor angiogenesis and progression in vivo. Oncogene *21*, 7011–7026.

Chatterjee, S., Heukamp, L.C., Siobal, M., Schöttle, J., Wieczorek, C., Peifer, M., Frasca, D., Koker, M., König, K., Meder, L., et al. (2013). Tumor VEGF:-VEGFR2 autocrine feed-forward loop triggers angiogenesis in lung cancer. J. Clin. Invest. *123*, 1732–1740.

Brantley-Sieders, D.M., Fang, W.B., Hicks, D.J., Zhuang, G., Shyr, Y., and Chen, J. (2005). Impaired tumor microenvironment in EphA2-deficient mice inhibits tumor angiogenesis and metastatic progression. FASEB J. *19*, 1884–1886.

Cui, X.-D., Lee, M.-J., Kim, J.-H., Hao, P.-P., Liu, L., Yu, G.-R., and Kim, D.-G. (2013a). Activation of mammalian target of rapamycin complex 1 (mTORC1) and Raf/Pyk2 by growth factor-mediated Eph receptor 2 (EphA2) is required for cholangiocarcinoma growth and metastasis. Hepatology *57*, 2248–2260.

Del Duca, D., Werbowetski, T., and Del Maestro, R.F. (2004). Spheroid preparation from hanging drops: characterization of a model of brain tumor invasion. J. Neurooncol. *67*, 295–303.

Doki, Y., Murakami, K., Yamaura, T., Sugiyama, S., Misaki, T., and Saiki, I. (1999). Mediastinal lymph node metastasis model by orthotopic intrapulmonary implantation of Lewis lung carcinoma cells in mice. Br. J. Cancer *79*, 1121–1126.

Du, R., Lu, K.V., Petritsch, C., Liu, P., Ganss, R., Passegué, E., Song, H., Vandenberg, S., Johnson, R.S., Werb, Z., and Bergers, G. (2008). HIF1α induces the recruitment of bone marrow-derived vascular modulatory cells to regulate tumor angiogenesis and invasion. Cancer Cell *13*, 206–220.

Ebos, J.M.L., and Kerbel, R.S. (2011). Antiangiogenic therapy: impact on invasion, disease progression, and metastasis. Nat. Rev. Clin. Oncol. *8*, 210–221.

Ebos, J.M.L., Lee, C.R., Cruz-Munoz, W., Bjarnason, G.A., Christensen, J.G., and Kerbel, R.S. (2009). Accelerated metastasis after short-term treatment with a potent inhibitor of tumor angiogenesis. Cancer Cell *15*, 232–239.

Faoro, L., Singleton, P.A., Cervantes, G.M., Lennon, F.E., Choong, N.W., Kanteti, R., Ferguson, B.D., Husain, A.N., Tretiakova, M.S., Ramnath, N., et al. (2010). EphA2 mutation in lung squamous cell carcinoma promotes increased cell survival, cell invasion, focal adhesions, and mammalian target of rapamycin activation. J. Biol. Chem. *285*, 18575–18585.

Finger, E.C., and Giaccia, A.J. (2010). Hypoxia, inflammation, and the tumor microenvironment in metastatic disease. Cancer Metastasis Rev. *29*, 285–293.

Gomez-Manzano, C., Holash, J., Fueyo, J., Xu, J., Conrad, C.A., Aldape, K.D., de Groot, J.F., Bekele, B.N., and Yung, W.K.A. (2008). VEGF Trap induces antiglioma effect at different stages of disease. Neuro-oncol. *10*, 940–945.

Gopal, U., Bohonowych, J.E., Lema-Tome, C., Liu, A., Garrett-Mayer, E., Wang, B., and Isaacs, J.S. (2011). A novel extracellular Hsp90 mediated co-receptor function for LRP1 regulates EphA2 dependent glioblastoma cell invasion. PLoS ONE *6*, e17649.

Hamaoka, Y., Negishi, M., and Katoh, H. (2016). EphA2 is a key effector of the MEK/ERK/RSK pathway regulating glioblastoma cell proliferation. Cell. Signal. *28*, 937–945.

Kauppila, S., Stenbäck, F., Risteli, J., Jukkola, A., and Risteli, L. (1998). Aberrant type I and type III collagen gene expression in human breast cancer in vivo. J. Pathol. *186*, 262–268.

Kuczynski, E.A., Vermeulen, P.B., Pezzella, F., Kerbel, R.S., and Reynolds, A.R. (2019). Vessel co-option in cancer. Nat. Rev. Clin. Oncol. *16*, 469–493.

Lamouille, S., Xu, J., and Derynck, R. (2014). Molecular mechanisms of epithelial-mesenchymal transition. Nat. Rev. Mol. Cell Biol. *15*, 178–196.

Landen, C.N., Jr., Chavez-Reyes, A., Bucana, C., Schmandt, R., Deavers, M.T., Lopez-Berestein, G., and Sood, A.K. (2005). Therapeutic EphA2 gene targeting in vivo using neutral liposomal small interfering RNA delivery. Cancer Res. *65*, 6910–6918.

Larrayoz, M., Pio, R., Pajares, M.J., Zudaire, I., Ajona, D., Casanovas, O., Montuenga, L.M., and Agorreta, J. (2014). Contrasting responses of non-small cell lung cancer to antiangiogenic therapies depend on histological subtype. EMBO Mol. Med. *6*, 539–550.

Li, J.Y., Xiao, T., Yi, H.M., Yi, H., Feng, J., Zhu, J.F., Huang, W., Lu, S.S., Zhou, Y.H., Li, X.H., and Xiao, Z.Q. (2019). S897 phosphorylation of EphA2 is indispensable for EphA2-dependent nasopharyngeal carcinoma cell invasion, metastasis and stem properties. Cancer Lett. *444*, 162–174.

Liu, P., Morrison, C., Wang, L., Xiong, D., Vedell, P., Cui, P., Hua, X., Ding, F., Lu, Y., James, M., et al. (2012). Identification of somatic mutations in non-small cell lung carcinomas using whole-exome sequencing. Carcinogenesis *33*, 1270–1276.

Livak, K.J., and Schmittgen, T.D. (2001). Analysis of Relative Gene Expression Data Using Real-Time Quantitative PCR and the $2^{-\Delta\Delta C_T}$ Method. Methods *25*, 402–408.

Lu, K.V., Chang, J.P., Parachoniak, C.A., Pandika, M.M., Aghi, M.K., Meyronet, D., Isachenko, N., Fouse, S.D., Phillips, J.J., Cheresh, D.A., et al. (2012). VEGF inhibits tumor cell invasion and mesenchymal transition through a MET/VEGFR2 complex. Cancer Cell *22*, 21–35.

Manzo, A., Montanino, A., Carillio, G., Costanzo, R., Sandomenico, C., Normanno, N., Piccirillo, M.C., Daniele, G., Perrone, F., Rocco, G., and Morabito, A. (2017). Angiogenesis inhibitors in NSCLC. Int. J. Mol. Sci. *18*, 1–17.

Miao, H., Li, D.Q., Mukherjee, A., Guo, H., Petty, A., Cutter, J., Basilion, J.P., Sedor, J., Wu, J., Danielpour, D., et al. (2009). EphA2 mediates ligand-dependent inhibition and ligand-independent promotion of cell migration and invasion via a reciprocal regulatory loop with Akt. Cancer Cell *16*, 9–20.

Miao, H., Gale, N.W., Guo, H., Qian, J., Petty, A., Kaspar, J., Murphy, A.J., Valenzuela, D.M., Yancopoulos, G., Hambardzumyan, D., et al. (2015). EphA2 promotes infiltrative invasion of glioma stem cells in vivo through cross-talk with Akt and regulates stem cell properties. Oncogene *34*, 558–567.

Mitsuhashi, A., Goto, H., Saijo, A., Trung, V.T., Aono, Y., Ogino, H., Kuramoto, T., Tabata, S., Uehara, H., Izumi, K., et al. (2015). Fibrocyte-like cells mediate acquired resistance to anti-angiogenic therapy with bevacizumab. Nat. Commun. *6*, 8792.

Moens, S., Goveia, J., Stapor, P.C., Cantelmo, A.R., and Carmeliet, P. (2014). The multifaceted activity of VEGF in angiogenesis—implications for therapy responses. Cytokine Growth Factor Rev. *25*, 473–482.

Moffat, J., Grueneberg, D.A., Yang, X., Kim, S.Y., Kloepfer, A.M., Hinkle, G., Piqani, B., Eisenhaure, T.M., Luo, B., Grenier, J.K., et al. (2006). A lentiviral RNAi library for human and mouse genes applied to an arrayed viral high-content screen. Cell *124*, 1283–1298.

Morgenstern, J.P., and Land, H. (1990). Advanced mammalian gene transfer: high titre retroviral vectors with multiple drug selection markers and a complementary helper-free packaging cell line. Nucleic. Acid Research *18*, 3587–3596.

Moserle, L., Jiménez-Valerio, G., and Casanovas, O. (2014). Antiangiogenic therapies: going beyond their limits. Cancer Discov. *4*, 31–41.

Nissen, N.I., Karsdal, M., and Willumsen, N. (2019). Collagens and cancer associated fibroblasts in the reactive stroma and its relation to cancer biology. J. Exp. Clin. Cancer Res. *38*, 115.

Pàez-Ribes, M., Allen, E., Hudock, J., Takeda, T., Okuyama, H., Viñals, F., Inoue, M., Bergers, G., Hanahan, D., and Casanovas, O. (2009). Antiangiogenic therapy elicits malignant progression of tumors to increased local invasion and distant metastasis. Cancer Cell *15*, 220–231.

Pajares, M.J., Agorreta, J., Larrayoz, M., Vesin, A., Ezponda, T., Zudaire, I., Torre, W., Lozano, M.D., Brambilla, E., Brambilla, C., et al. (2012). Expression of tumor-derived vascular endothelial growth factor and its receptors is associated with outcome in early squamous cell carcinoma of the lung. J. Clin. Oncol. *30*, 1129–1136.

Pao, W., Miller, V.A., Politi, K.A., Riely, G.J., Somwar, R., Zakowski, M.F., Kris, M.G., and Varmus, H. (2005). Acquired resistance of lung adenocarcinomas to gefitinib or erlotinib is associated with a second mutation in the EGFR kinase domain. PLoS Med. *2*, e73.

Paraiso, K.H.T., Das Thakur, M., Fang, B., Koomen, J.M., Fedorenko, I.V., John, J.K., Tsao, H., Flaherty, K.T., Sondak, V.K., Messina, J.L., et al. (2015). Ligand-independent EPHA2 signaling drives the adoption of a targeted therapy-mediated metastatic melanoma phenotype. Cancer Discov. *5*, 264–273.

Pasquale, E.B. (2010). Eph receptors and ephrins in cancer: bidirectional signalling and beyond. Nat. Rev. Cancer *10*, 165–180.

Rivera, L.B., and Bergers, G. (2015). Intertwined regulation of angiogenesis and immunity by myeloid cells. Trends Immunol. *36*, 240–249.

Sandler, A., Gray, R., Perry, M.C., Brahmer, J., Schiller, J.H., Dowlati, A., Lilenbaum, R., and Johnson, D.H. (2006). Paclitaxel-carboplatin alone or with bevacizumab for non-small-cell lung cancer. N. Engl. J. Med. *355*, 2542–2550.

Sapkota, G.P., Cummings, L., Newell, F.S., Armstrong, C., Bain, J., Frodin, M., Grauert, M., Hoffmann, M., Schnapp, G., Steegmaier, M., et al. (2007). BI-D1870 is a specific inhibitor of the p90 RSK (ribosomal S6 kinase) isoforms in vitro and in vivo. Biochem. J. *401*, 29–38.

Sennino, B., Ishiguro-Oonuma, T., Wei, Y., Naylor, R.M., Williamson, C.W., Bhagwandin, V., Tabruyn, S.P., You, W.K., Chapman, H.A., Christensen, J.G., et al. (2012). Suppression of tumor invasion and metastasis by concurrent inhibition of c-Met and VEGF signaling in pancreatic neuroendocrine tumors. Cancer Discov. *2*, 270–287.

Stewart, S.A., Dykxhoorn, D.M., Palliser, D., Mizuno, H., Yu, E.Y., An, D.S., Sabatini, D.M., Chen, I.S., Hahn, W.C., Sharp, P.A., et al. (2003). Lentivirus-delivered stable gene silencing by RNAi in primary cells. RNA *9*, 493–501.

Tabchi, S., and Blais, N. (2017). Antiangiogenesis for advanced non-small-cell lung cancer in the era of immunotherapy and personalized medicine. Front. Oncol. *7*, 52.

Wedge, S.R., Ogilvie, D.J., Dukes, M., Kendrew, J., Chester, R., Jackson, J.A., Boffey, S.J., Valentine, P.J., Curwen, J.O., Musgrove, H.L., et al. (2002). ZD6474 inhibits vascular endothelial growth factor signaling, angiogenesis, and tumor growth following oral administration. (2015). Cancer Res. *62*, 4645–4655.

Wykosky, J., Gibo, D.M., Stanton, C., and Debinski, W. (2005). EphA2 as a novel molecular marker and target in glioblastoma multiforme. Mol. Cancer Res. *3*, 541–551.

Xi, H.Q., Wu, X.S., Wei, B., and Chen, L. (2012). Eph receptors and ephrins as targets for cancer therapy. J. Cell. Mol. Med. *16*, 2894–2909.

Yeddula, N., Xia, Y., Ke, E., Beumer, J., and Verma, I.M. (2015). Screening for tumor suppressors: loss of ephrin receptor A2 cooperates with oncogenic *KRas* in promoting lung adenocarcinoma. Proc. Natl. Acad. Sci. USA *112*, E6476–E6485.

Zhou, Y., Yamada, N., Tanaka, T., Hori, T., Yokoyama, S., Hayakawa, Y., Yano, S., Fukuoka, J., Koizumi, K., Saiki, I., and Sakurai, H. (2015). Crucial roles of RSK in cell motility by catalysing serine phosphorylation of EphA2. Nat. Commun. *9*, 7679.

STAR★METHODS

KEY RESOURCES TABLE

REAGENT or RESOURCE	SOURCE	IDENTIFIER
Antibodies		
β-actin (clone C4)	MP Biomedicals LLC	Cat# SKU 08691001; RRID: AB_2335127
VEGFR2	Cell Signaling	Cat# 2479L; RRID: AB_2212507
pMet (Y1234/1235)	Cell Signaling	Cat# 3077; RRID: AB_2143884
Met	Cell Signaling	Cat# 8198; RRID: AB_10858224
p(Ser/Thr) AKT Substrate	Cell Signaling	Cat# 9611; RRID: AB_330302
pS6 ribosomal protein (S235/236)	Cell Signaling	Cat# 2211; RRID: AB_331679
S6 ribosomal protein	Cell Signaling	Cat# 2217; RRID: AB_331355
pEGFR (Y1068)	Cell Signaling	Cat# 3777; RRID: AB_2096270
EGFR	Cell Signaling	Cat# 4267; RRID: AB_2246311
pERK (T202/Y204)	Cell Signaling	Cat# 9101; RRID: AB_331646
ERK	Cell Signaling	Cat# 4695; RRID: AB_390779
pRSK (S380)	Cell Signaling	Cat# 11989; RRID: AB_2687613
RSK1	Cell Signaling	Cat# 8408; RRID: AB_10828594
RSK2	Cell Signaling	Cat# 5528; RRID: AB_10860075
EphA2 (for IP and WB)	Santa Cruz	Cat# sc-398832
EphA2 (for PLA)	Cell Signaling	Cat# 12927; RRID: AB_2798063
pS897 EphA2 (I)	Cell Signaling	Cat# 6347; RRID: AB_11220420
pS897 EphA2 (II)	Bingcheng Wang & Hui Miao	N/A
anti-rabbit-HRP	Merck	Cat# 12-348; RRID: AB_390191
anti-mouse-HRP	Merck	Cat# 12-349; RRID: AB_390192
human Ki-67	Thermo Fisher Scientific	Cat# RM-9106; RRID: AB_2335745
β-catenin	Thermo Fisher Scientific	Cat# RB-9035; RRID: AB_149843
E- cadherin	Dako	Cat# M3612; RRID: AB_2341210
Collagen III	Southern Biotech	Cat# 1330-01; RRID: AB_2794734
Biological Samples		
Patient samples	University Hospital Cologne, Cologne, Germany	Local ethics committee ref # 10-242
Chemicals, Peptides, and Recombinant Proteins		
Fetal Bovine Serum	Sigma Aldrich	Cat# F9665
Penicillin/Streptomycin	Life Technologies	Cat# 15070063
RPMI 1640 Medium	Life Technologies	Cat# 61870044
DMEM/F12 Medium	Life Technologies	Cat# 31330095
Recombinant human $VEGF_{165}$	Tebu-bio	Cat# 100-20-B
Recombinant human HGF	R&D Systems	Cat# 294-HG
Recombinant Ephrin-A1 FC chimera	R&D Systems	Cat# 6417-A1
Recombinant human IgG_1Fc	R&D Systems	Cat# 110-HG
ZD6474 (Zactima)	from LC Laboratories	Cat# V-9402
BMS-354825 (Dasatinib)	from LC Laboratories	Cat# D-3307
PD0325901	from LC Laboratories	Cat# P-9688
AKT inhibitor RL1784	Daniel Rauh	N/A
AKT inhibitor RL1785	Daniel Rauh	N/A
AKT inhibitor MK2206	Daniel Rauh	N/A
RSK inhibitor BI-D1870	Roman K. Thomas	N/A
Polybrene	Santa Cruz	Cat# Sc-134220

(*Continued on next page*)

Continued

REAGENT or RESOURCE	SOURCE	IDENTIFIER
Puromycin	Sigma-Aldrich	Cat# P9620-10ML
DMSO	Applichem	Cat# a3672,0100
Cell lysis buffer (10x)	Cell Signaling	Cat# 9803
Complete protease inhibitor cocktail mini tablet (1x)	Sigma Aldrich	Cat# 11873580001
PMSF	Sigma Aldrich	Cat# 93482-50ML-F
Phosphatase inhibitor cocktail set III	Sigma Aldrich	Cat# P5726
NuPage LDS buffer (4x)	Life Technologies	Cat# B0007
Sample reducing agent (10x)	Life Technologies	Cat# b0009
NuPage Bis-Tris Gels	Life Technologies	Cat# np0322box
Protein A-Agarose Beads	Santa Cruz	Cat# sc-2001
Rat Tail Collagen High Concentration	Corning	Cat# 354249
HEPES	Sigma Aldrich	Cat# h0887
$NaHCO_3$	Sigma Aldrich	Cat# S8761
NaOH	Sigma Aldrich	Cat# s2770
RPMI (10x)	Sigma Aldrich	Cat# R1145-500ML
PBS (10x)	Carl Roth	Cat# 9150.1
Trypan Blue Solution, 0.4%	Life Technologies	Cat# 15250061
Formaldehyde	Sigma Aldrich	Cat# F8775
Saponin	Sigma Aldrich	Cat# 47036-50G-F
Ketamine	Henry Schein	Cat# 12467832
Xylazine (Rompun)	Henry Schein	Cat# 1320422
Carprofen	Henry Schein	Cat# 110208
Isoflurane	PCC	Cat# 9714675
Critical Commercial Assays		
TRANS-IT	Mirus	Cat# MIR2300
QuickChange II XL Site-Directed Mutagenesis Kit	Agilent	Cat# 200521
Lipofectamine LTX with Plus Reagent	Life Technologies	Cat# 15338030
BCA Protein Assay	Thermo Fisher Scientific	Cat# 23227
CellTiter-Glo Luminescent Cell Viability Assay	Promega	Cat# G7570
TRIZOL	Invitrogen	Cat# 15596026
Power SYBR Green PCR Master Mix	Thermo Fisher Scientific	Cat# 4368577
SuperScript VILO cDNA Synthesis Kit	Invitrogen	Cat# 11754050
Hs_GAPDH_2_SG QuantiTect Primer Assay	QIAGEN	Cat# QT01192646
Duolink PLA Probes PLUS	Sigma Aldrich	Cat# DUO92002-100RXN
Duolink PLA Probes MINUS	Sigma Aldrich	Cat# DUO92004-100RXN
Duolink Detection Reagents Red	Sigma Aldrich	Cat# DUO92101-1KT
Histofine Simple Stain Mouse MAX PO	Medac	Cat# 414311F
Histofine Mouse Stain Kit	Medac	Cat# 414341F
Experimental Models: Cell Lines		
H441	ATCC	HTB-174
H1975	ATCC	CRL-5908
A549	ATCC	CCL-185
HCC1359	ATCC	N/A
HCC827	ATCC	CRL-2868
PC9	Sigma Aldrich	90071810-1VL

(*Continued on next page*)

Continued

REAGENT or RESOURCE	SOURCE	IDENTIFIER
H1650	ATCC	CRL-5883
H1581	ATCC	CRL-5878
H441 VEGFR2 KD	Chatterjee et al., 2013	N/A
H441 VEGFR2	Chatterjee et al., 2013	N/A
H441 VEGFR2 V916M	Chatterjee et al., 2013	N/A
HEK293T	ATCC	CRL-11268
Experimental Models: Organisms/Strains		
NMRI Nude Mouse	Janvier Labs	Rj:NMRI-Foxn1nu/nu
BL6 Mouse	Internal U.H.C. Breeding Facility	N/A
Oligonucleotides		
Sh1: CGGACAGACATATAGGATATTCTC GAGAATATCCTATATGTCTGTCCG	Sigma Aldrich	N/A
Sh2: GATAAGTTTCTATTCTGTCAGCTCG AGCTGACAGAATAGAAACTTATC	Sigma Aldrich	N/A
Sh3: TCGGACAGACATATAGGATATCTCG AGATATCCTATATGTCTGTCCGA	Sigma Aldrich	N/A
KDR primer I: 5′-CATCGAGCTCTCATGTCTGAAC-3′	This paper	N/A
KDR primer II: 5′-TCCTCAGGTAAGTGGACAGGTT-3′	This paper	N/A
β-catenin primer I: 5′-GCTACTCAAGCTGATTTGATGGA-3′	This paper	N/A
β-catenin primer II: 5′-GGTAGTGGCACCAGAATGGAT-3′	This paper	N/A
E-cadherin primer I: 5′-CGGGAATGCAGTTGAGGATC-3′,	This paper	N/A
E-cadherin primer II: 5′-AGGATGGTGTAAGCGATGGC-3′	This paper	N/A
Recombinant DNA		
pLKO.1 – TRC lentiviral vector	David Root	Addgene #10878
Δ8.9	Roman K. Thomas	N/A
pCMV-VSV-G	Bob Weinberg	Addgene #8454
pBABE-puro retroviral vector	Hartmut Land, Jay Morgenstern & Bob Weinberg	Addgene #1764
pCL Ampho plasmid	Novus Biological	Cat# NBP2-29541
Software and Algorithms		
InVesalius 3.0	Online download	https://www.cti.gov.br/en/invesalius
ImageJ	Online download	https://imagej.net
SPSS	Online download	https://www.ibm.com/products/spss-statistics
GraphPad Prism 7	Online download	https://www.graphpad.com/scientific-software/prism/

RESOURCE AVAILABILITY

Lead Contact

Further information and requests for resources and reagents should be directed to and will be fulfilled by the Lead Contact, Roland Ullrich (roland.ullrich@uk-koeln.de).

Materials Availability

This study did not generate new unique reagents.

Data and code availability

This study did not generate datasets.

EXPERIMENTAL MODEL AND SUBJECT DETAILS

Cell lines and reagents

NSCLC cell lines, H441 (papillary adenocarcinoma, epithelial, adherent, *KRAS* V12D-mutated), H1975 (adenocarcinoma, epithelial, adherent, *EGFR*-mutated L858R+T790M), A549 (carcinoma, epithelial, adherent, wt *EGFR*-, *KRAS*-mutated G12S), HCC1359 (adenocarcinoma, epithelial, adherent), HCC827 (adenocarcinoma, epithelial, adherent, *EGFR*-mutated), PC9 (adenocarcinoma, epithelial, adherent. *EGFR*-mutated), H1650 (adenocarcinoma, epithelial, adherent, *EGFR*-mutated, *PTEN* loss) and H1581 (adenocarcinoma, adherent, *FGFR1* amplified) were purchased from LGC Standards GmbH. With the exception of HCC1359 cells, which were cultivated in DMEM/F12 medium, all cell lines were maintained in RPMI 1640 medium with 10% fetal bovine serum (FBS) and 1% antibiotics (penicillin and streptomycin). VEGF was purchased from Tebu-bio, recombinant human HGF, recombinant Ephrin-A1 FC chimera and recombinant human IgG_1Fc were purchased from R&D Systems, ZD6474 (Zactima), BMS-354825 (Dasatinib) and PD0325901 were purchased from LC Laboratories. AKT inhibitors RL1784, RL1785 and MK2206 were kindly provided by the laboratory of Prof. Dr. Daniel Rauh, TU Dortmund, Germany. RSK inhibitor BI-D1870 was kindly provided by the laboratory of Prof. Dr. Roman K. Thomas, University of Cologne, Germany. Compound stocks (in DMSO) were stored at –20°C or in vehicle solution (sterile, deionized water with 1% Tween 80) at 4°C for animal therapy.

Animals and orthotopic implantation

All animal procedures were in accordance with the German Laws for Animal Protection and were approved by the local animal care committee and local governmental authorities (Recklinghausen, Germany).

All experiments were performed in 10 to 15 week old male athymic NMRI nude mice (Janvier, Europe) or immunocompetent BL6 mice. The orthotopic intrapulmonary injections of NSCLC cells were performed as previously described (Doki et al., 1999). Animals were anesthetized with i.p. injection of Ketamine/Xylazine. A cell suspension of $5x10^6$ cells in PBS was injected into the lung parenchyma. After surgery animals were treated with analgesic (5mg/kg i.p. Carprofen (Sigma Aldrich)). One week after implantation animals were treated for four weeks every second day by oral gavage of ZD6474 (50mg/kg), BMS-354825 (30mg/kg), the combination of ZD6474 (50mg/kg) and BMS-354825 (30mg/kg) or vehicle solution. After treatment, lungs with primary tumor nodules and part of infiltrated rib cages were excised for histological examination.

For the VEGFR2, VEGFR2 V916M and KP938.3 injected cells, additional μCT imaging was performed. Animals were scanned under isoflurane anesthesia using a LaTheta LCT-100 small animal μCT (Aloka Instruments, Tokyo, Japan). CT-images were taken from the whole lung at 0.3 mm intervals. First scan was performed one week after injection and continued every week until ZD6474 therapy was ended. Representative CT-images were analyzed via the InVesalius 3.0 software.

METHOD DETAILS

Knockdown and constructs for retroviral expression and stable transduction

Generation of H441 VEGFR2 KD, VEGFR2 and VEGFR2 V916M have been previously described (Chatterjee et al., 2013). Stable KD of EphA2 in H441 cells was achieved by lentiviral transduction of shRNA sequence targeting human EphA2 using the pLKO.1 lentiviral vector (pLKO.1 - TRC cloning vector was a gift from David Root (Addgene plasmid #10878) (www.broad.mit.edu/genome_bio/trc/rnai.html) (Moffat et al., 2006). Virus was produced by co-transfection with Δ8.9 and pCMV-VSV-G (pCMV-VSV-G was a gift from Bob Weinberg (Addgene plasmid #8454)) (Stewart et al., 2003) in HEK293T cells (www.broadinstitute.org/rnai/trc/lib) using TRANS-IT (Mirus). Cells were transduced in the presence of polybrene (Santa Cruz). After transduction, cells were selected with puromycin. Hairpins were ordered from Sigma Aldrich (sh1:CGGACAGACATATAGGATATTCTCGAGAATATCCTATATGTCTGTCCG,

sh2: GATAAGTTTCTATTCTGTCAGCTCGAGCTGACAGAATAGAAACTTATC,
sh3: TCGGACAGACATATAGGATATCTCGAGATATCCTATATGTCTGTCCGA) and

cloned into pLKO.1. The EphA2 S897A mutation was generated using QuickChange II XL Site-Directed Mutagenesis Kit (Agilent). Stable expression of S897A EphA2, EphA2 wt and myr-AKT was achieved by retroviral transduction using the pBABE vector (pBABE-puro was a gift from Hartmut Land & Jay Morgenstern & Bob Weinberg (Addgene plasmid #1764)) (Morgenstern and Land, 1990). Of note, the used VEGFR2 V916M cell lines in part still endogenously express WT VEGFR2. Corresponding viruses were produced by co-transfection with the pCL Ampho plasmid in HEK293T cells (Orbigen) using Lipofectamine® LTX with Plus Reagent (Life Technologies).

Cell treatment and lysates

Cells were plated and starved for 20h (growth media with 0.25% FBS and 1% PS). Cells were treated as follows: 1μM ZD6474 for indicated time points (1h-24h) followed by 25min 40ng/ml $VEGF_{165}$ (human recombinant) (Tebu-bio) treatment; single treatment

with recombinant Ephrin-A1 FC chimera or control IgG_1-FC (R&D Systems) (1μg/ml, 25min); $VEGF_{165}$ was added in increasing concentrations from 20ng/ml to 100ng/ml (3h) followed by human recombinant HGF (R&D Systems) in concentrations from 10ng/ml to 100ng/ml (25min); single stimulation with VEGF (50ng/ml, 3h) or HGF (10ng/ml HGF, 25 min); AKT inhibitors were used at 1μM for the indicated time points. BI-D1870 was added either in the concentration of 1μM or 10μM for the indicated time points (1-24h). PD0325901 was used at 0.5μM for 1h-24h as indicated. DMSO served as control and was added in the highest concentration of the compound used in the experiment and incubated for the corresponding time. After stimulation, cell lysates were prepared. Cells were washed with cold PBS, lysis buffer was added (1ml of cell lysis buffer (10x) (Cell Signaling), 1x complete protease inhibitor cocktail mini tablet (Roche), 1mM PMSF (Carl Roth), 200μl phosphatase inhibitor cocktail set III (Calbiochem)); for 10ml of 1x lysis buffer, incubated on ice (5min), scraped, transferred to a tube (15min, ice), centrifuged (14000rpm, 15min, 4°C) and the supernatant was collected. Protein concentrations were determined using BCA Protein Assay (Thermo Fisher Scientific). 25μg cell lysates were mixed with 4x NuPage LDS buffer and 10x sample reducing agent (both Life Technologies), boiled (80°C, 10 min) and loaded on NuPage Bis-Tris Gels (Invitrogen, Life Technologies). Each lysate was prepared at least three times.

3D spheroid invasion assay

Spheroids were generated by the modified hanging drop method (Del Duca et al., 2004). A concentration of $2x10^5$ cells/ml was prepared. Drops of cell suspension (25μl) were placed onto lids of 10cm dishes which were then placed over dishes containing 10ml sterile water. Hanging drop cultures were incubated between 3 (H441), 6 (H1975, A549) and 8 (HCC1359) days. Single spheroids were embedded into 100μl collagen gel in a 96-well plate (2mg/ml Rat Tail Collagen High Concentration Type I (Corning), 136mM HEPES, 1,8% $NaHCO_3$ (7,5%), 0,05mM NaOH (1M), 10x RPMI (1X end concentration) (all from Sigma Aldrich) and 10X PBS (GIBCO) (1X end concentration). ZD6474 (5μM), DMSO and VEGF (100ng/ml) were directly added to the embedding solution. ZD6474 (1μM), DMSO and VEGF (40ng/ml) were additionally pipetted on the spheroids before covering with gel-mixture to guarantee appropriate concentration of inhibitor or stimulant on the spheroid. Pictures were taken (Zeiss, Axiovert 135, 10x magnification) at 0h and 20h after embedding and invasion was quantified by measuring the area occupied by cells using ImageJ software. Invasion was calculated in percentage relative to the starting point (0h).

Western blotting and co-immunoprecipitation

Western blotting was performed using the following antibodies: β-actin (clone C4) (MP Biomedicals LLC), VEGFR2, pMet (Y1234/1235), Met, p(Ser/Thr) AKT Substrate, pS6 ribosomal protein (S235/236), S6 ribosomal protein, pEGFR (Y1068), EGFR, pERK (T202/Y204), ERK, pRSK (S380), RSK1, RSK2 (Cell Signaling), EphA2 (Santa Cruz), anti-rabbit-HRP and anti-mouse-HRP antibodies (both from Millipore). pS897 staining in Figures S7A and S8A were performed with pS897 EphA2-antibody from the lab of Prof. Bingcheng Wang and Hui Miao, Case Western Reserve University School of Medicine, Cleveland, Ohio, USA; all other pS897 stainings were done with pS897 EphA2 antibody from Cell Signaling. For EphA2 immunoprecipitation (IP) and VEGFR2/EphA2 co-IP, 500μg (H441 cells) or 1000μg (H1975 cells) of clarified lysate was incubated with anti-EphA2 (Santa Cruz) or anti-VEGFR2 antibody (Cell Signaling), Protein A-Agarose Beads (Santa Cruz) and 500μl PBS overnight at 4°C with constant gentle rocking. Internal controls were lysate controls (lysate + beads incubated without any antibodies) in 500μl PBS. IPs and lysate controls were washed 3 times with ice-cold PBS (1000 g, 5min, 4°C), eluted with 4x NuPage LDS buffer and 10x reducing agent (both Life Technologies), heated (80°C, 10min) and loaded on a NuPage Bis-Tris Gel (Invitrogen, Life Technologies) followed by procedures for western blotting according to the manufacturer's instructions (Life Technologies). Each IP and western blot analysis was performed at least three times.

Viability assay and CTG® assay

Cells were plated in triplicates and incubated overnight. Next day, media was replaced by compound dilutions (dissolved in DMSO, diluted with appropriate media) with increasing concentrations from 0.01μM to 30μM. DMSO served as control and was added in the highest dilution used in the assay. Cell viability was determined after 96h via trypan blue staining (0.4% trypan blue solution) and cells were counted with a Luna™ automated cell counter (Logos Biosystems). Each experiment was performed three times. For ZD6474 viability curves, CellTiter-Glo® Luminescent Cell Viability Assay (Promega) was performed after 96h according to the manufacturer's instructions.

RNA isolation and quantitative RT-PCR

Total RNA was isolated from cell culture with TRIZOL® Reagent (Invitrogen) according to the manufacturer's instructions. First strand cDNA synthesis was generated using the SuperScript® VILO cDNA Synthesis Kit (Invitrogen). First strand cDNA (2μl) was then used for quantitative PCR using Power SYBR® Green PCR Master Mix (Applied Biosystems®). Each sample was prepared in triplicates. Data are reported as mean expression values of three replicates per sample evaluated via the comparative C_T method (Livak and Schmittgen, 2001). Primer sequences for gene products were: *KDR* 5′-CATCGAGCTCTCATGTCTGAAC-3′, 5′-TCCTCAGG TAAGTGGACAGGTT-3′; *β-catenin* 5′-GCTACTCAAGCTGATTTGATGGA-3′, 5′-GGTAGTGGCACCAGAATGGAT-3′; *E-cadherin* 5′-CGGGAATGCAGTTGAGGATC-3′, 5′-AGGATGGTGTAAGCGATGGC-3′, GAPDH (Hs_GAPDH_2_SG QuantiTect Primer Assay (QIAGEN) Order no. QT01192646) served as internal reference.

Proximity ligation assay (PLA)®

Cells were seeded in 12-well plates, starved overnight and treated with ZD6474 (1μM) or DMSO. Cells were fixed (4% formaldehyde, 10min), permeabilized (0.1% Saponin (Sigma-Aldrich), 15min), blocked with Duolink® blocking solution (30min, 37°C) and incubated with anti-rabbit VEGFR2 (1:200, Cell Signaling) in conjunction with anti-mouse EphA2 (1:200, Cell Signaling) at 4°C overnight. The proximity ligation reaction and visualization of the signal was performed according to the manufacturer's protocol using the Duolink® Detection Kit (red) with PLA PLUS and MINUS probes for rabbit and mouse antibodies (Sigma Aldrich). Images were generated with an Olympus Fluoview FV 1000 confocal microscope using an oil-based 40x objective. Each experiment was performed at least three times. For PLA with cell lines HCC1359 and H1650, a Leica TCS SP8 gSTED confocal microscope was used to obtain images with an oil-based 63x objective. Experiments were performed in duplicates. PLA signals were analyzed and quantified using ImageJ software.

Tumor samples and immunohistochemistry

Resected lungs, rib cages and human samples were processed within the diagnostics pipeline of the Institute of Pathology, University Hospital Cologne with approval of the local ethics committee (ref no. 10-242). Tissue was fixed in 4% formaldehyde for 24h, transferred to PBS and embedded in paraffin. Rib cages were additionally decalcified. 3μm sections were stained with primary antibodies (human Ki-67 (Thermo Fisher Scientific, RM-9106) (1:50, pretreatment pH 6, 20min), β-catenin (Thermo Fisher Scientific, RB-9035) (1:50, citrate (pH 6) overnight), E- cadherin (Dako, M3612) (1:50, EDTA (pH 9) overnight), Collagen III (Southern Biotech 1330-01) (1:50, EDTA (pH 9) overnight), VEGFR2 (Cell Signaling, 2479) (1:50, EDTA (pH 9) overnight)) by standard protocol of the Institute for Pathology, University Hospital Cologne. For reduced background on murine tissue, corresponding secondary antibody detection kits were used (Histofine Simple Stain Mouse MAX PO and Histofine-mouse-stain kit, Medac) and stained on an automated stainer (LabVisionAutostainer480S, Thermo Scientific).

Quantification of Ki-67 was performed by choosing 3 regions with 100 cells per sample and counting positive cells. The mean of the 3 regions was calculated and taken as value for one IHC sample. For each animal group, the mean was calculated from all sample values. Quantification of E-cadherin, β-catenin and collagen III was performed as for Ki-67 staining. The mean of positive cells in 3 regions was calculated and taken as value for one IHC sample. For each animal group, the mean was calculated from all sample values as before. In addition, quantification of E-cadherin, β-catenin and collagen III was performed by scoring the signal intensity of each section in 1 (low), 2 (medium) and 3 (strong).

QUANTIFICATION AND STATISTICAL ANALYSIS

Statistical analysis

Fisher's exact tests were performed using SPSS software. A level of significance of $p < 0.05$ was chosen. Data are presented as mean with standard error of the mean (±SEM) in all figures in which error bars are shown. Graphs were generated using GraphPad Prism 7 software.

Chapter 3 – EGFR inhibition strongly modulates the tumour immune microenvironment in EGFR-driven non-small-cell lung cancer

Carolin Selenz, Anik Compes, Marieke Nill, Sven Borchmann, Margarete Odenthal, Alexandra Florin, Johannes Brägelmann, Reinhard Büttner, Lydia Meder, and Roland T. Ullrich

Cancers (Basel). 2022 Aug 16;14(16):3943. doi: 10.3390/cancers14163943

Specific author contributions:

- Experimental design of EGFR-driven NSCLC cohorts
- Therapy administration and monitoring of mice
- Data acquisition during experiment and in follow-up analyses, e.g. by flow cytometry
- Formal analyses of data, concerning tumour growth, RNAseq and flow cytometry data
- Establishment of transgenic EGFR-driven mouse model in group
- Breeding and maintenance of mice
- Design and generation of graphs and manuscript figures
- Manuscript writing, editing and submission

cancers

MDPI

Article

EGFR Inhibition Strongly Modulates the Tumour Immune Microenvironment in EGFR-Driven Non-Small-Cell Lung Cancer

Carolin Selenz [1,2], Anik Compes [1,2,3], Marieke Nill [1,2], Sven Borchmann [1], Margarete Odenthal [4], Alexandra Florin [4], Johannes Brägelmann [2,3,5], Reinhard Büttner [4], Lydia Meder [1,2,3,*] and Roland T. Ullrich [1,2,*]

1 Department I of Internal Medicine, Center for Integrated Oncology Aachen Bonn Cologne Duesseldorf, Faculty of Medicine and University Hospital Cologne, University of Cologne, 50931 Cologne, Germany
2 Center for Molecular Medicine Cologne, Faculty of Medicine and University Hospital Cologne, University of Cologne, 50931 Cologne, Germany
3 Mildred Scheel School of Oncology Cologne, Faculty of Medicine and University Hospital Cologne, University of Cologne, 50931 Cologne, Germany
4 Institute of Pathology, Faculty of Medicine and University Hospital Cologne, University of Cologne, 50931 Cologne, Germany
5 Department of Translational Genomics, Faculty of Medicine and University Hospital Cologne, University of Cologne, 50931 Cologne, Germany
* Correspondence: lydia.meder@uk-koeln.de (L.M.); roland.ullrich@uk-koeln.de (R.T.U.); Tel.: +49-221-478-96815 (L.M.); +49-221-478-89771 (R.T.U.)

Simple Summary: Lung cancer that is driven by mutations in the epidermal growth factor receptor (EGFR) is currently treated with tyrosine kinase inhibitors (TKIs). Although patients initially respond well to TKI treatment, drug resistance against EGFR-targeted therapy emerges. Attempts to combine immunotherapy with EGFR-targeted treatment to prolong response rates or prevent the development of resistances have been limited due to insufficient knowledge about the effects of targeted therapy on the tumour microenvironment (TME) in EGFR-driven tumours and tumour-infiltrating immune cells. The aims of this study were to improve our understanding on the impact of EGFR inhibition on the immune response in EGFR-driven lung cancer and, furthermore, to gain insights into the impact of combining targeted therapy with immunotherapy on the TME.

Abstract: EGFR-driven non-small-cell lung cancer (NSCLC) patients are currently treated with TKIs targeting EGFR, such as erlotinib or osimertinib. Despite a promising initial response to TKI treatment, most patients gain resistance to oncogene-targeted therapy, and tumours progress. With the development of inhibitors against immune checkpoints, such as PD-1, that mediate an immunosuppressive microenvironment, immunotherapy approaches attempt to restore a proinflammatory immune response in tumours. However, this strategy has shown only limited benefits in EGFR-driven NSCLC. Approaches combining EGFR inhibition with immunotherapy to stimulate the immune response and overcome resistance to therapy have been limited due to insufficient understanding about the effect of EGFR-targeting treatment on the immune cells in the TME. Here, we investigate the impact of EGFR inhibition by erlotinib on the TME and its effect on the antitumour response of the immune cell infiltrate. For this purpose, we used a transgenic conditional mouse model to study the immunological profile in EGFR-driven NSCLC tumours. We found that EGFR inhibition mediated a higher infiltration of immune cells and increased local proliferation of T-cells in the tumours. Moreover, inhibiting EGFR signalling led to increased activation of immune cells in the TME. Most strikingly, combined simultaneous blockade of EGFR and anti-PD-1 (aPD-1) enhanced tumour treatment response in a transgenic mouse model of EGFR-driven NSCLC. Thus, our findings show that EGFR inhibition promotes an active and proinflammatory immune cell infiltrate in the TME while improving response to immune checkpoint inhibitors in EGFR-driven NSCLC.

check for updates

Citation: Selenz, C.; Compes, A.; Nill, M.; Borchmann, S.; Odenthal, M.; Florin, A.; Brägelmann, J.; Büttner, R.; Meder, L.; Ullrich, R.T. EGFR Inhibition Strongly Modulates the Tumour Immune Microenvironment in EGFR-Driven Non-Small-Cell Lung Cancer. *Cancers* **2022**, *14*, 3943. https://doi.org/10.3390/cancers14163943

Academic Editor: Samuel C. Mok

Received: 21 July 2022
Accepted: 13 August 2022
Published: 16 August 2022

Publisher's Note: MDPI stays neutral with regard to jurisdictional claims in published maps and institutional affiliations.

Keywords: NSCLC; EGFR; tyrosine kinase inhibitors; immune checkpoint blockade; anti-PD-1; erlotinib; tumour microenvironment; immune cell infiltrate; immune response

1. Introduction

Lung cancer is responsible for the most cancer-related deaths worldwide, with NSCLC accounting for nearly 80% of all cases [1,2]. Different subclassifications of NSCLC are identified by specific genetic alterations present in tumours, such as oncogenic driver mutations in the *epidermal growth factor receptor* (*EGFR*) gene. Targeted therapies against driver gene mutations have been developed and successfully established in the clinic in the form of EGFR TKIs, including erlotinib. TKI therapy has replaced standard chemotherapy as first-line treatment in EGFR-driven NSCLC due to promising initial response rates and prolonged progression-free survival of patients [3]. However, patients successfully treated with TKIs often become resistant to therapy after 9–14 months, most commonly by acquiring secondary EGFR mutations and, therefore, diminishing TKI efficacy [4,5]. Thus, novel therapy approaches are urgently required.

Increasing evidence demonstrates that, in NSCLC, the TME is generally characterised by noninflamed tumours with poor immune cell infiltrate mediated by immunosuppressive signals. This is attributed to different factors, such increased levels of inhibitory checkpoints on immune cells and their ligands that suppress antitumour activity [6,7]. This limits immunological surveillance and allows the tumour to progress and evade an active immune response [8]. In recent years, immunotherapy as an alternative treatment strategy has demonstrated beneficial antitumour responses in patients by mobilising the immune system to actively combat tumour cells that have previously escaped an immune response. By blocking key receptors facilitating inhibitory signalling pathways of the immune system, such as programmed cell death-1 (PD-1) and programmed cell death-ligand 1 (PD-L1), immune checkpoint blockade (ICB) has demonstrated encouraging responses in NSCLC patients [9,10]. However, when examining the response of EGFR-driven NSCLC patients specifically, ICB shows only limited benefits, for which the exact underlying mechanism still needs to be elucidated [9,11,12].

Different efforts have been made to boost efficacy of ICB in EGFR-driven NSCLC by combining it with target therapy. While a phase I clinical trial with advanced EGFR-driven NSCLC patients indicated durable tumour response rates upon combining ICB with erlotinib [13], the benefit of using this combination therapy approach is still not conclusively proven. This is illustrated by contrasting findings from preclinical studies investigating EGFR-driven NSCLC in mice. While Sugiyama and colleagues did observe an improved response upon application of both ICB and TKI treatment [14], implying potential benefits for combining ICB and EGFR inhibition, another study did not yield the same improved results after a four week period of simultaneous ICB and erlotinib therapy [15]. It should be noted that the administration of the therapy regimes, as well as the models used to mimic EGFR-driven NSCLC in vivo, varied between each study. These aspects should be taken into consideration when evaluating and comparing previous findings on the effect of ICB and targeted therapy on EGFR-driven tumours and the TME. Similarly, findings about the effect of EGFR inhibition on the immune cell infiltrate in these tumours have also displayed variability and remain to be conclusively established, with one study observing a decrease in regulatory T-cell (Tregs) levels after erlotinib therapy [14], whereas another did not notice any difference in tumour-infiltrating Tregs [15]. These contrasting findings not only illustrate the increasing need to further explore combinatorial approaches with ICB and TKI treatment, and their effect on EGFR-driven tumours, but also demonstrate how much is yet to be determined about the impact of targeted therapy alone on the TME and specifically on the immune cell infiltrate [16]. Therefore, to advance the understanding of the effects of TKI treatment on the immune cell infiltrate and improve upon existing therapy strategies, we investigate how EGFR inhibition modulates the TME in EGFR-driven NSCLC.

2. Materials and Methods

2.1. In Vivo Experiments

Experiments were performed in accordance with FELASA recommendations. The protocol was approved by the local ethics committee. Mice were housed and all experiments were performed in a sterile environment. Mice were fed, given water, and monitored daily for health, and cages were changed weekly.

2.2. Autochthonous $EGFR^{L858R}$ NSCLC Model

We used a previously described EGFR-driven NSCLC mouse model [17,18]. *CCSP-rtTA; TetO-*$EGFR^{L858R}$ mice aged 8–16 weeks were fed ad libitum with doxycycline-containing feed (1000 ppm; ssniff Spezialdiäten GmbH) for the duration of the experiments. Four weeks after starting doxycycline feed, mice were scanned by µCT to confirm tumour formation. Tumour progression was monitored by weekly µCT scans using a LaTheta LCT-100 small animal µCT (Hitachi Aloka Instruments, Tokyo, Japan). CT images of the whole lung were taken at 0.3 mm intervals and analysed using Onis 2.5 Free Edition software (Digital Core Co., Ltd., Tokyo, Japan). Tumour progress and response were assessed by mouse-adapted RECIST criteria v1.1, as previously published [19]. The average of two tumour lesions per mouse was calculated and used to analyse tumour size fold change after therapy start. Tumour and spleen tissues were harvested at end of experiment and flash-frozen for subsequent RNA isolation, as well as further treated to obtain flow cytometry data. Overall survival of mice was assessed using Kaplan–Meier analysis.

2.3. Therapy Administration

Erlotinib (LC Laboratories, Woburn, MA, USA) was solved in 6% Captisol solution and orally administered at a concentration of 50 mg/kg body weight (BW) twice per week. Anti-mouse PD-1 antibody (clone RMP1-14, BioXCell, Lebanon, NH, USA) was administered at 10 mg/kg BW intraperitoneal twice per week [20,21]. Vehicle mice were treated twice per week with 6% Captisol given orally in combination with intraperitoneal administration of the appropriate murine aPD-1 IgG control (Isotype control rat IgG2a, κ; BioXCell, Lebanon, NH, USA). Mice were randomly assigned to the different therapy groups before start of treatment.

2.4. RNA Sequencing

RNA was extracted from flash-frozen tumour tissue by homogenisation using sterile 1.5 mL tissue homogenizers and subsequent isolation using Qiagen RNeasy Mini Kit, according to manufacturer's protocol (Qiagen, Germantown, MD, USA). Corresponding to the manufacturer's requirements, 20–30 mg of tissue was used from each sample. Libraries of 3'mRNA were obtained from total RNA using the Lexogen QuantSeq kit according to standard protocol. After validation and quantification (2200 TapeStation, Agilent Technologies, Santa Clara, CA, USA and Qubit System, Invitrogen, Carlsbad, California, CA, USA respectively), pools of cDNA libraries were generated. Pools were quantified using the KAPA Library Quantification kit (Peqlab, Radnor, PA, USA) and the 7900HT Sequence Detection System (Applied Biosystems, Foster City, PA, USA) and lastly sequenced on an Illumina HiSeq4000 or NovaSeq6000 sequencer using a 1 × 50 base pair protocol.

2.5. RNA Analysis

FASTQ files of 3′ UTR RNA-sequencing were checked for quality using FastQC (version 0.11.4), and reads were mapped to the mouse reference genome GRCm38 (p6) using the STAR aligner (version 2.7.0). Prior to downstream analysis, expression was quantified with RSEM (version 1.3.1). Analyses were run on the computing cluster of the Regional Computing Centre of the University of Cologne (RRZK). Gene set enrichment analysis (GSEA) was performed using GSEA software (version 4.0.2, Broad Institute, Cambridge, MA, USA). The *z*-scores of counts per million (CPM) were used as input, and all erlotinib-treated samples (namely, erlotinib and aPD-1 + erlotinib samples) were analysed against

all other samples (vehicle and aPD-1 samples). To focus on gene sets relevant for certain aspects of immune function in the context of cancer, we used curated gene sets based on the ncounter Mouse PanCancer Immune Profiling Panel (Nanostring, Seattle, WA, USA), as previously established in our lab (Borchmann et al., under revision). Analyses were run with 1000 permutations, excluding gene sets smaller than five genes. Otherwise, standard settings were applied. Volcano plots of protein-coding transcripts were obtained after running multiple-comparison *t*-tests on sample *z*-scores from each treatment group against vehicle group samples.

2.6. Inference of TME Based on Differential Gene Expression

To interpret the composition of the tumour immune infiltrate on the basis of gene expression, we created a curated list of immune cell subtype-specific transcripts (Table S1). We started with a list of immune cell subtype enriched genes as defined in the Nanostring Vantage 3D RNA: Protein Immune Cell Profiling Assay (Nanostring, Seattle, WA, USA). This list was simplified by omitting transcripts enriched in multiple immune cell subtypes, only keeping transcripts unique to a specific immune cell subtype (Table S1). For each experiment, *z*-scores of CPM were calculated for all transcripts. The *z*-scores for all transcripts unique to a specific immune cell subtype from each sample were compared between groups to identify differences in the cellular composition of the tumour immune infiltrate.

2.7. Flow Cytometry

Single-cell suspensions of tumour and spleen tissues were generated via mechanical dissociation using 40 µm filters and taking up the cells in PBS. After pelleting cells, they were resuspended in 1 mL of ACK lysis buffer and incubated at room temperature for 5 min. Cells were washed once with PBS before proceeding with extracellular antibody staining and applying the viability dye Zombie UV (Biolegend, San Diego, CA, USA) for 30 min at 4 °C in FACS buffer (PBS containing 2% FBS and 1 mM EDTA). After incubation with antibodies, cells were washed with FACS buffer and fixed using 1% formaldehyde in FACS buffer for 15 min at room temperature. Permeabilisation of cells was performed using 0.1% Triton-X100-containing FACS buffer while incubating for 20 min at 4 °C. Subsequently, cells were stained with intracellular antibodies diluted in FACS buffer and incubated for 30 min at 4 °C. Before final analysis, cells were washed and resuspended in FACS buffer. The following extracellular antibodies (Biolegend, San Diego, CA, USA) were used for the analysis of cells: anti-CD45-PerCP-Cy5.5 (clone 30-F11), anti-CD3-PE-Cy7 (clone 145-2C11), anti-NK1.1-AF700 (clone PK136), anti-γδTCR-APC-Fire750 (clone GL3), anti-CD8a-BV421 (clone 53–6.7), anti-CD279 (PD-1)-BV510 (clone 29F.1A12), and anti-CD4-BV785 (clone GK1.5). The following intracellular antibodies (Biolegend, San Diego, CA, USA) were used: anti-IFNγ-PE-Dazzle594 (clone XMG1.2) and anti-Ki67-BV605 (clone 16A8). Flow cytometry of stained cells was performed on the Cytoflex LX Flow Cytometer (Beckmann Coulter, Krefeld, Germany). Results were analysed using Kaluza Software (version 2.1, Beckmann Coulter). Cells were initially gated to include alive singlet cells and then further selected using the following gating strategies. $CD4^+$ T-cells were defined as $CD45^+CD3^+CD4^+$ cells, while $CD8^+$ T-cells were identified as $CD45^+CD3^+CD8^+$ cells. NK T-cells were defined as $CD45^+CD3^+NK1.1^+$ cells, and γδT-cells were defined as $CD45^+CD3^+TCR\gamma/\delta^+$ cells. IFNγ and Ki67 expression was assessed and reported as mean fluorescent intensity.

2.8. Cytokine Analysis

Serum samples were separated by centrifugation and stored at −80 °C until use. Levels of 32 murine biomarkers were quantified using a Mouse Cytokine/Chemokine 31-Plex Discovery Assay® Array (Milipore, Darmstadt, Germany), according to the manufacturer's protocol, and measured using the Luminex™ 100 system (Luminex, Austin, TX, USA) by Eve Technologies Corporation (Calgary, AB, Canada). The biomarkers measured include Eotaxin, G-CSF, GM-CSF, IFNγ, IL-1α, IL-1β, IL-2, IL-3, IL-4, IL-5, IL-6, IL-7, IL-9, IL-10, IL-12p40, IL-12p70, IL-13, IL-15, IL-17A, IP-10, KC, LIF, LIX, MCP-1, M-CSF, MIG, MIP-1α,

MIP-1β, MIP-2, RANTES, TNFα, and VEGF-A. All samples were measured in duplicate. Rarely, a detected marker was below the limit of quantification. In these instances, the value was set to half of the minimum quantification level. To generate a heatmap with Morpheus (Broad Institute, Cambridge, MA, USA), z-scores of the $\log_{10}$ of raw biomarker levels were calculated for each biomarker, and the heatmap was created using hierarchical clustering with the metric of $1 -$ Pearson correlation.

2.9. Immunohistochemistry

Lung tissue was harvested and fixed in 4% formaldehyde for 24 h, transferred to PBS, and embedded in paraffin (FFPE) using established routine protocols of the Pathology Department, University Hospital Cologne. Three micrometre lung sections were deparaffinised, and immunohistochemistry was performed on the LabVision Autostainer 480S (Thermo Fisher Scientific, Waltham, MA, USA). Staining was performed using haematoxylin and eosin (H&E), as well as primary antibodies against $EGFR^{L858R}$ (Cell Signaling Technologies, 3197, Leiden, The Netherlands), CD3 (Thermo Fisher, RM-9107-S, Waltham, MA, USA), CD4 (Abcam, EPR19514, Cambidge, UK), CD8 (Abcam polyclonal, ab203035, Cambidge, UK), and CD45R (BD Biosciences, 550286, Franklin Lakes, NJ, USA). Subsequently, primary antibodies were detected using secondary Histofine Simple Stain (SHSS) detection kits (Medac, Wedel, Germany). Slides were scanned on the Leica SCN400 Slidescanner (Leica Biosystems, Deer Park, IL, USA).

2.10. Statistics

Statistical analyses and data graphs were carried out using GraphPad Prism (version 8.4.3), unless stated otherwise. Statistical tests were performed as described in figure legends.

3. Results

3.1. Inhibition of EGFR Mediates Higher Immune Cell Infiltration in the TME of EGFR-Driven Tumours

To investigate the changes in the TME occurring after EGFR inhibition via TKI therapy, we treated autochthonous $EGFR^{L858R}$-driven NSCLC mice with vehicle, aPD-1, erlotinib, or aPD-1 + erlotinib to assess and compare the effects of both immunotherapy and targeted therapy approaches (Figure 1A). To distinguish the effect of EGFR inhibition on the TME, we applied immune cell deconvolution via 3′ mRNA-sequencing. Comparing lesions treated with erlotinib to vehicle- or aPD-1-treated tumour samples, we observed a significant increase in intratumoural T-cell levels in the erlotinib and aPD-1 + erlotinib group (Figure 1B). Upon investigating different subtypes of T-cells, we specifically detected higher infiltration of not only cytotoxic $CD8^+$ T-cells, but also of Th1, Th2, and Tfh cells upon EGFR inhibition (Figure 1C,D). Interestingly, we also observed increased levels regulatory T-cells (Tregs) in the TME of tumours treated with erlotinib and aPD-1 + erlotinib (Figure 1C). In addition to higher levels of intratumoural T-cells, we further detected overall increased infiltration of natural killer (NK) cells, mast cells, and eosinophils upon EGFR inhibition, as well as higher levels of intratumoural B cells and dendritic cells (DCs), thus increasing antigen capabilities of the TME (Figure 1E–I). Greater infiltration of T-cells in general, as well as $CD8^+$ T-cells and B cells, in the TME upon EGFR inhibition was further observed in immunohistochemistry staining of tumour sections from samples treated with either erlotinib or aPD-1 + erlotinib (Figure S1). Taken together, these data demonstrate an overall greater infiltration of immune cells into the TME facilitated by EGFR inhibition.

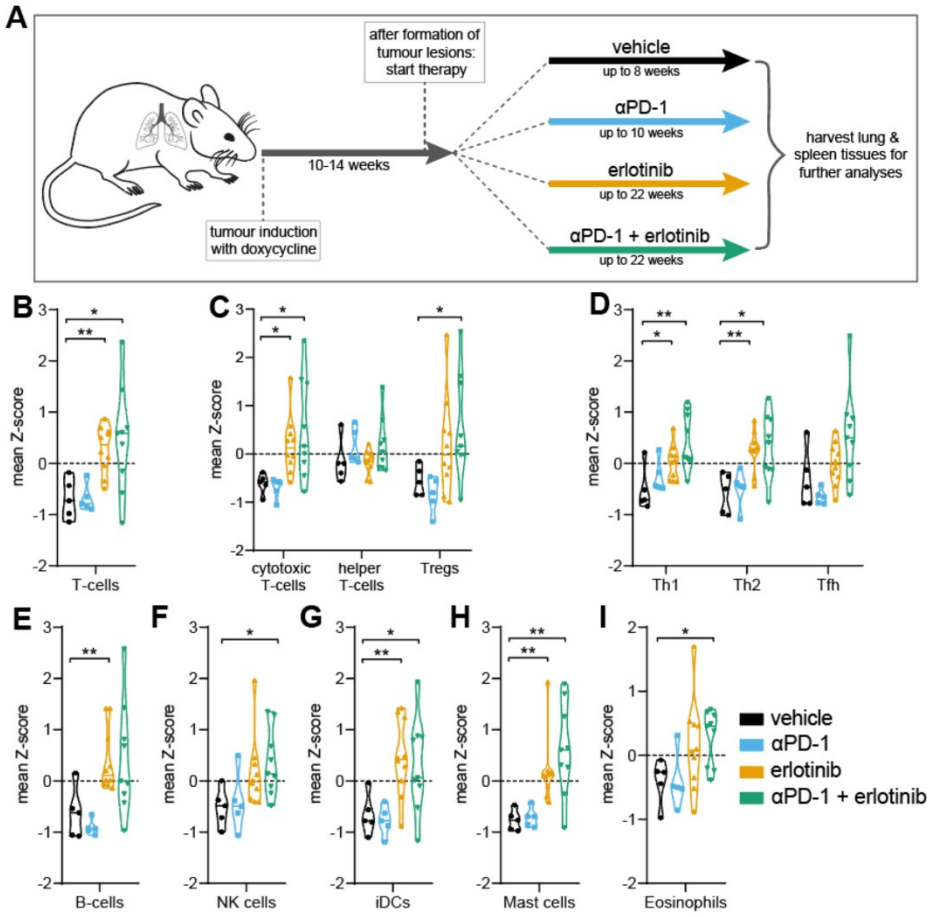

Figure 1. Inhibition of EGFR mediates higher immune cell infiltration in the TME of EGFR-driven tumours. (**A**) Experimental setup of tumour induction and treatment strategies using $EGFR^{L858R}$-NSCLC mice on a continuous doxycycline diet. Mice were divided into different therapy cohorts: vehicle, αPD−1, erlotinib, or αPD−1 + erlotinib. After up to 22 weeks under therapy, lung tumours and spleens were harvested for further analysis, including RNA isolation or flow cytometry. (**B**–**D**) Immune cell deconvolution illustrating mean gene expression *z*-scores of T-cell-specific transcripts (n = 5–12 mice per group). (**E**–**I**) Immune cell deconvolution illustrating mean gene expression *z*-scores of immune cell-specific transcripts (n = 5–12 mice per group). (**B**–**I**) Data are shown as violin plots; the statistical test used was Student's *t*-test (statistically significant changes are indicated as follows: * $p < 0.05$; ** $p < 0.01$).

3.2. EGFR Inhibition Enhances Proliferation and Activation of T-Cells in TME

After detecting increased levels of immune cells in the TME, we further explored the functional dynamics of the immune cell infiltrate to ascertain the effect of EGFR inhibition on the inflammatory status of the TME. To assess T-cell activity and proliferative capacity, single-cell suspensions of lung tumour tissue were analysed by flow cytometry. Notably, we observed that Ki67 expression levels of all T-cell subtypes were increased in tumours that were treated with erlotinib (Figure 2A). A similar trend was detected for the combination group treated with ICB and erlotinib. In contrast, we observed a slight decrease in Ki67 expression for ICB-treated mice compared to the vehicle group, indicating lower

proliferation of T-cells upon aPD-1 monotherapy (Figure 2A). Regarding IFNγ expression, we noticed similar trends of increasing levels in tumour tissue upon EGFR inhibition in the erlotinib-treated mice. Again, this trend was not only observed in the erlotinib monotherapy group, but also when combined with aPD-1, indicating increased activation in T-cells, especially in the NK T-cell and γδT-cell populations, of the TME. Similar to Ki67 expression, IFNγ levels in tumours treated with ICB exhibited a slight decrease compared to vehicle tumours (Figure 2B). Concerning PD-1 expression, no changes in PD-1 levels were observed on the different T-cell subtypes, except for increased levels of PD-1 after ICB in $CD8^+$ T-cells (Figure S2A). To ascertain whether the observed shifts in Ki67 and IFNγ expression in $CD4^+$, $CD8^+$, NK, and γδT-cells were locally specific to the TME, flow cytometry was performed using single-cell suspensions of spleen tissue from the treated mice. In contrast to our findings from the tumour immune infiltrate, we found that Ki67 levels were not altered upon EGFR inhibition compared to vehicle control in spleen tissues (Figure 2C). Moreover, we did not detect consistent changes in IFNγ expression in $CD4^+$ and $CD8^+$ T-cells after erlotinib treatment, as well as only a slight increase of IFNγ levels in NK and γδT-cells (Figure 2D). This suggests that increased proliferation and activation of T-cells in response to EGFR inhibition are specific to the TME. Notably, reduced expression of both Ki67 and IFNγ in aPD-1-treated mice compared to the vehicle group was more pronounced in the spleen than in tumour tissue (Figure 2C,D). These data suggest that ICB therapy alone, targeting the PD-1 signalling axis, conveys an immunosuppressive phenotype in T-cells, affecting T-cells not only in the TME, but also in other tissues. This was further confirmed after analyses of circulating cytokine signatures, which illustrated more pronounced changes in cytokine levels upon ICB treatment compared to vehicle control (Figure S3A–C). In contrast, circulating cytokine levels from mice treated with either erlotinib or aPD-1 + erlotinib did not indicate notable changes (Figure S3A–C). Together, these data reveal that EGFR inhibition appears to modulate T-cells specifically in the TME towards an enhanced proliferative and inflammatory phenotype, thus facilitating an improved T-cell response against the tumours.

3.3. Inhibition of EGFR Increases Active Phenotype of Immune Cell Infiltrate in EGFR-Driven Tumours

Following our results of an increased inflammatory T-cell phenotype in the TME, we were prompted to examine the general activation status of the TME using 3′ mRNA-sequencing data. To determine, whether similar trends could be observed for the overall immune response in the TME, *z*-scores of transcripts increasingly expressed upon immune cell activation were examined. These transcripts included Gzma, Il2ra, Tnfrsf4, encoding granzyme A, IL-2, and OX40, as well as CD29 and CD69 (Figure 3A). These markers are not only known to be upregulated in active T-cells, but are also associated with proliferation and activation of other immune cell types, such as B cells and NK cells [22–26]. Interestingly, increased levels of activation-specific gene expression were observed in both erlotinib monotherapy and aPD-1 + erlotinib groups (Figure 3A), suggesting that EGFR inhibition mediates a shift towards a more inflammatory immune cell infiltrate. To further investigate which signatures of immune response are promoted by EGFR inhibition, gene set enrichment analysis (GSEA) was performed comparing all tumours undergoing EGFR inhibition (namely, erlotinib monotherapy and aPD-1 + erlotinib) against vehicle and aPD-1 tumours. After GSEA analysis, significant enrichment was detected in signatures promoting an active immune response (Figure 3B), including signatures of the TNF superfamily, which is known to promote a proinflammatory immune response and mediates signalling responsible for proliferation, differentiation, and effector functions of immune cells (Figure 3B) [27,28]. Moreover, the complement pathway has been implicated enhancing T-cell function and proliferation [29,30], and NK cells play a crucial role in antitumour response [31,32], illustrating the importance of enrichment in NK cell functions (Figure 3B). These observations further strengthen our findings that EGFR inhibition not only affects T-cell activity, but also stimulates an increased response of the immune cell infiltrate overall.

To investigate potential mechanisms of how the modulation of oncogenic EGFR signalling in tumour cells facilitates changes in the immune response, we next examined the expression of the transcription factor, IRF1, a known tumour suppressor gene. Previously, IRF1 has been implicated not only in the regulation of CD274 (PD-L1) expression [33], but also in playing a role in suppressing tumour proliferation and stimulating an active immune response in tumours [34,35]. Moreover, IRF1 has been shown to be negatively regulated by oncogenic EGFR signalling in NSCLC [14]. In line with previous studies, IRF1 expression was increased in tumours, displaying a proinflammatory immune phenotype upon EGFR inhibition (Figure 3C). Increases in PD-L1 or PD-L2 levels were not observed, presumably due to the high spread of transcript expression in the vehicle group (Figure S2B). In contrast, expression of CCL21 was also elevated upon blocking oncogenic EGFR signalling (Figure 3D). CCL21 is a chemotactic cytokine known to recruit T-cells to the TME, thus promoting increased immune activity [36,37].

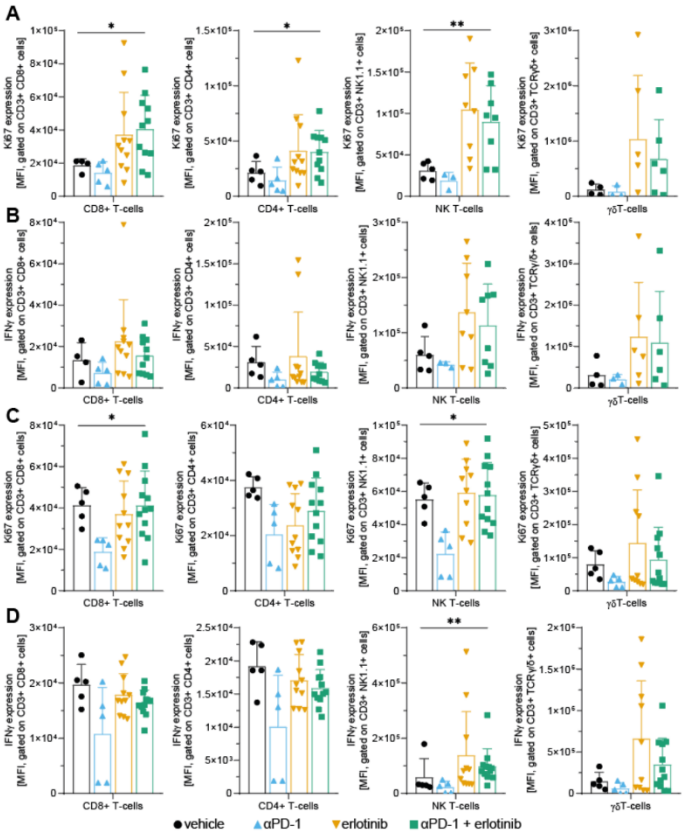

Figure 2. EGFR inhibition enhances proliferation and activation of T-cells in TME. (**A**,**B**) Mean fluorescence intensity data of (**A**) intracellular Ki67 and (**B**) intracellular IFNγ expression, illustrating proliferation and activation status, respectively. Data shown for cytotoxic $CD8^+$ T-cells, helper $CD4^+$ T-cells, NK T-cells, and γδT-cells from lung tumour tissue. (**C**,**D**) Mean fluorescence intensity data of (**C**) intracellular Ki67 and (**D**) intracellular IFNγ expression, illustrating proliferation and activation status, respectively. Data shown for cytotoxic $CD8^+$ T-cells, helper $CD4^+$ T-cells, NK T-cells, and γδT-cells from spleen tissue (n = 5–12 mice per group). (**A**–**D**) Data are shown as the mean with SD; the statistical test used was the Kruskal–Wallis test to compare all therapy groups (statistically significant changes are indicated across all groups as follows: * $p < 0.05$; ** $p < 0.01$).

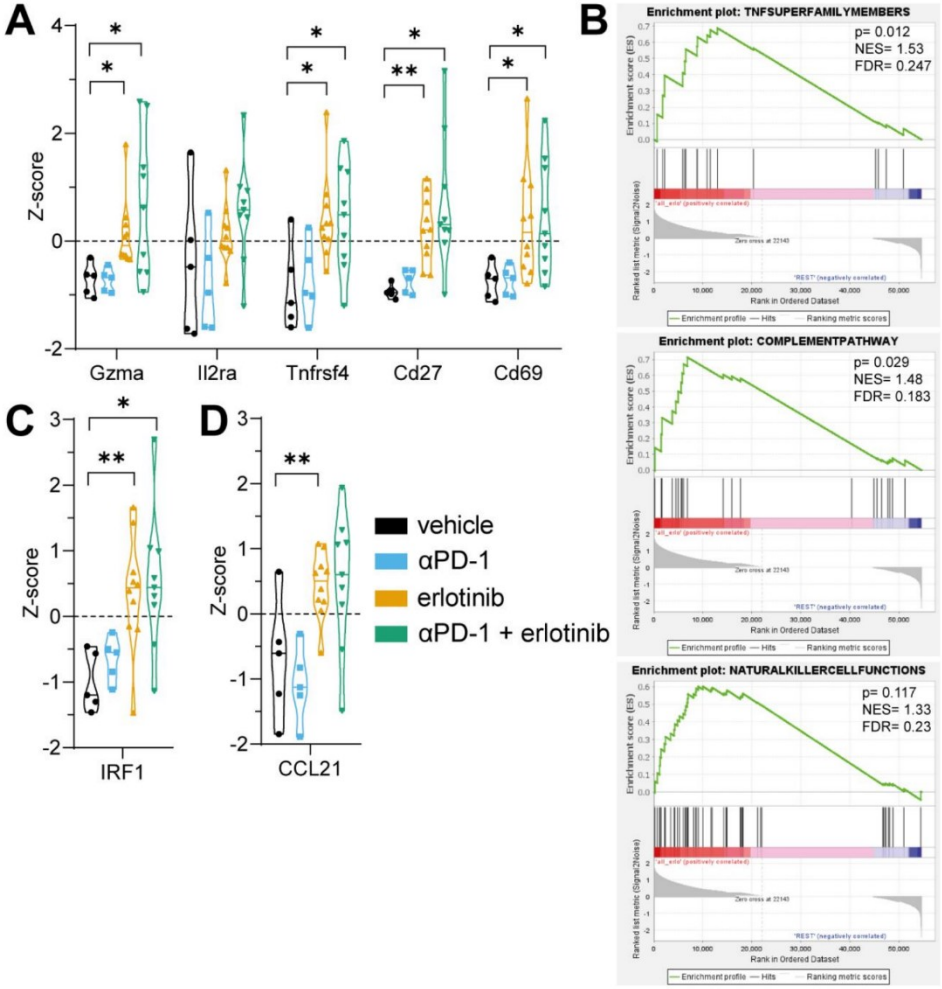

Figure 3. Inhibition of EGFR increases active phenotype of immune cell infiltrate in EGFR-driven tumours. (**A**) Mean gene expression *z*-scores of immune cell activation markers (n = 5–10 mice per group). (**B**) Gene set enrichment analysis for different gene sets from any erlotinib-treated mice (namely, erlotinib and aPD−1 + erlotinib groups) against the others (vehicle and aPD−1 groups). (**C**,**D**) Mean gene expression *z*-score of transcription factor mediating tumour-suppressive functions and intratumoural chemokines, respectively (n = 5–12 mice per group). (**A**,**C**,**D**) Data are shown as violin plots; the statistical test used was Student's *t*-test (statistically significant changes are indicated as follows: * $p < 0.05$; ** $p < 0.01$).

Furthermore, analysis of the most differentially expressed transcripts by multiple-comparison *t*-tests of sample *z*-scores revealed multiple significantly upregulated transcripts in both erlotinib (Figure 4A) and aPD-1+erlotinib groups (Figure 4B) compared to vehicle. These include Ccnb1 and Tpx2, which have been previously associated with higher immune cell infiltration [38,39] and antitumour activity of $CD8^+$ T-cells [40]. Interestingly, expression of Ddr2, a collagen receptor playing a key role in cell interaction, was significantly downregulated in the erlotinib-treated samples compared to control. Depletion of Ddr2 has been previously associated with higher $CD8^+$ T-cell infiltration, as well as

increasing sensitivity towards ICB [41]. Taken together, these data illustrate that blocking oncogenic EGFR signalling in tumours increased the immune cell infiltration in the TME and stimulated a proinflammatory immune response against tumours.

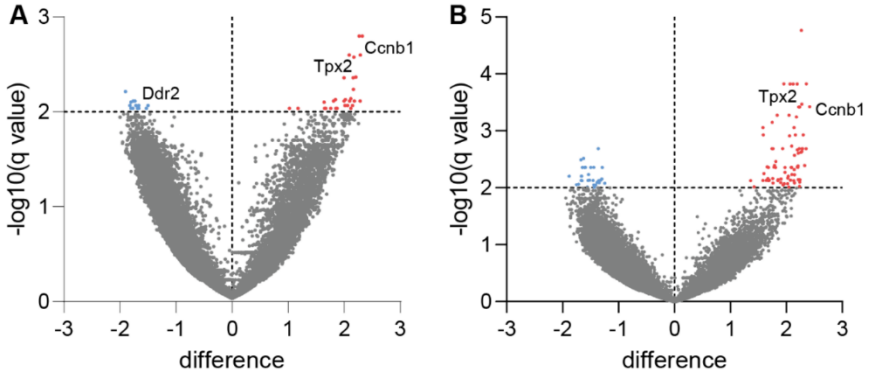

Figure 4. EGFR inhibition leads to increase in transcripts associated with higher immune cell infiltration. (**A**) Volcano plot showing transcripts detected at significantly altered levels in lung tumour tissue from erlotinib-treated mice compared to vehicle control group. (**B**) Volcano plot showing transcripts detected at significantly altered levels in lung tumour tissue from aPD−1 + erlotinib-treated mice compared to vehicle control group. (**A**,**B**) Blue points illustrate significantly downregulated transcripts, while red points indicate significantly upregulated transcripts.

3.4. Simultaneous EGFR Inhibition and ICB Indicate Slower Tumour Growth and Improved Antitumour Response over EGFR Inhibition Alone in EGFR-Driven NSCLC Model

On the basis of our observations that blocking EGFR signalling in oncogene-driven NSCLC alters the TME towards a proinflammatory status, thus promoting an enhanced immune response, we next examined tumour growth rates by analysing target lesion size to assess tumour response. Mice treated with aPD-1 alone showed no treatment response (Figure 5A,B), underlining the limited efficacy of ICB in EGFR-driven tumours [9,42]. In line with our previous results, EGFR inhibition improved antitumour response compared to vehicle (Figure 5A,B) and significantly increased overall survival of mice treated with erlotinib over both vehicle and aPD-1 groups (Figure S3D). Furthermore, combined treatment with aPD-1 + erlotinib also prolonged overall survival and improved tumour response to therapy compared to the vehicle and aPD-1 control groups (Figures 5A,B and S3D). When analysing the best response rates, similar results for mice treated with erlotinib monotherapy or combining ICB with EGFR inhibition were observed (Figure 5C). Interestingly, we were able to detect a trend towards improvement of antitumour response in the combination group when considering target lesion data. This was indicated by not only a faster reduction in tumour size upon aPD-1 + erlotinib therapy compared to EGFR inhibition alone, but also by tumours remaining in a partial response (PR) state until the end of the experiments, in contrast to the erlotinib group (Figure 5A). To summarise, we observed compelling antitumour responses upon blocking oncogenic EGFR signalling with prolonged survival over vehicle tumours. When combining EGFR inhibition with ICB, we observed a trend to faster antitumour response and slower outgrowth of tumours after relapse, compared to EGFR inhibition alone.

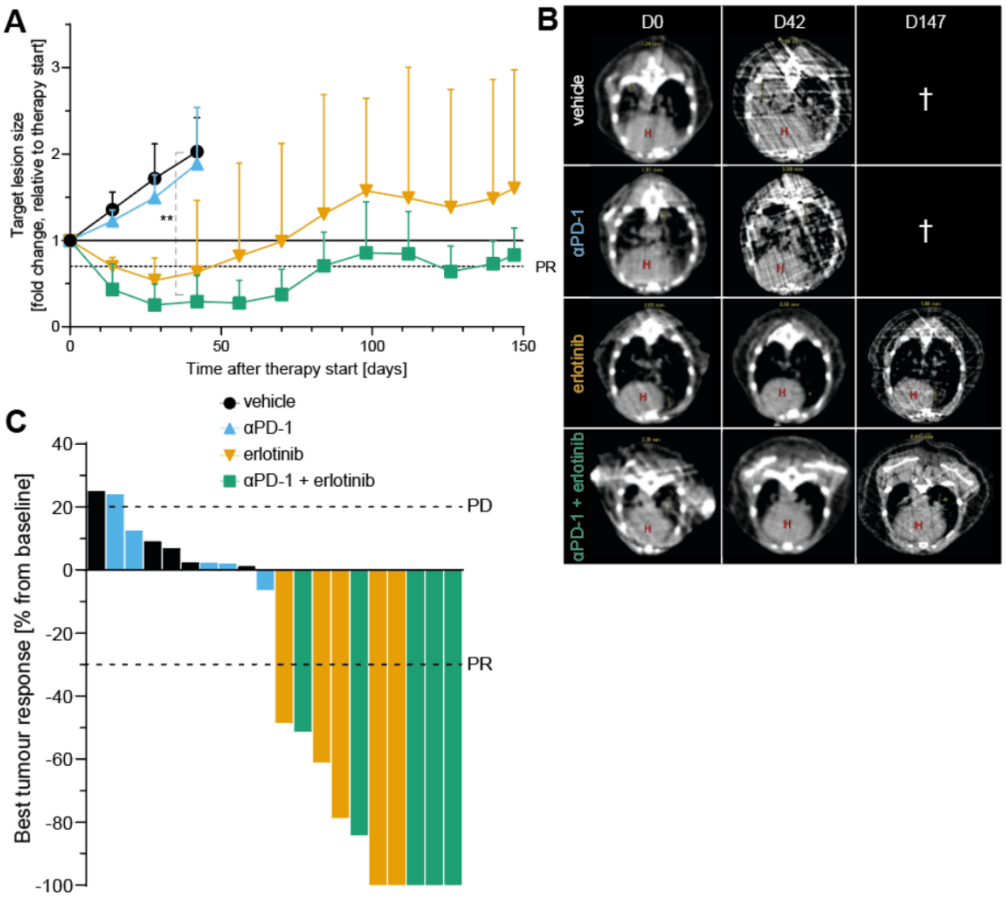

Figure 5. Simultaneous EGFR inhibition and ICB indicate slower tumour growth and improved antitumour response over EGFR inhibition alone in EGFR-driven NSCLC model. (**A**) Mean fold change of EGFR-driven target lesion growth over time in indicated treatment groups. Data are shown as the mean with SD; the statistical test used was Student's *t*-test of individual groups at the endpoint of vehicle and aPD−1 groups (day 42; statistically significant changes are indicated as follows: ** $p < 0.01$). (**B**) Representative µCT images taken prior to therapy start (D0) and on days 42 (D42) and 147 (D147) after therapy start of $EGFR^{L858R}$-driven mice; the red H indicates the heart; † indicates that no mice from treatment group reached the indicated time point. (**C**) Best response to therapy from beginning of treatment (baseline) for individual mice. (**A**,**C**) PR, partial response; PD, progressive disease.

4. Discussion

In this study, we aimed to improve our understanding of the limited efficacy of immune checkpoint inhibitors in EGFR-driven NSCLC patients and the role of oncogenic EGFR signalling for the immunosuppressive composition of the TME. This was approached by investigating the effect of EGFR inhibition through TKI erlotinib in an oncogene-dependent mouse model and examining different aspects of the corresponding immune response. It has been reported that oncogene-driven tumours are characterised by the establishment of a noninflamed TME, thus facilitating the evasion of an active immune response by tumours [8]. Major factors promoting an immunosuppressive TME include low infiltration of immune cells into the tumour, lack of proliferation to achieve an

appropriate antitumour response, and/or reduced activation of tumour-infiltrated immune cells [43,44]. Previous studies have shown that, although immunotherapy approaches such as targeting immune checkpoint by ICB are beneficial in many cancer entities to promote a proinflammatory TME, EGFR-driven NSCLC tumours do not respond to this type of therapy [9,11,12]. Given the increasing interest in applying immunotherapy in combination with targeted therapies to try and circumvent this issue and increase efficacy of ICB in EGFR-driven NSCLC, different efforts have been made to investigate combination therapy regimes [13–15]. However, due to varying results on the effect of combining ICB with targeted therapy, no final conclusion on potential benefits of this therapy regime can be drawn to date. To appropriately assess the implication of combining immunotherapy with targeted therapy on the TME, it is also critical to consider how targeted therapy alone impacts not only tumour cells, but also other components of the TME. This question has gained more attention in recent years, but has not yet yielded a comprehensive answer, in part also due to varying results on the subject, such as differences between infiltrating immune cell populations [14–16]. This illustrates the need for further investigation in this field and validation of previous findings. In our study, we found that, in unresponsive tumours, where oncogenic EGFR signalling remained constitutively active, levels of immune cells in the TME were reduced compared to tumours that exhibited an active tumour response to therapy (Figure 1B–I), aligning with previous evidence that untreated EGFR-driven NSCLC mediates an immunosuppressive TME. In turn, we observed that, upon EGFR inhibition, immune cell infiltration was elevated in the TME (Figure 1B–I), confirming previous findings after erlotinib treatment in NSCLC mouse models [15,45]. Moreover, EGFR inhibition in tumour cells induced T-cell proliferation and activation, thus promoting an enhanced immune response in tumours treated with the TKI erlotinib (Figure 2A). This further confirms observations that erlotinib increases cytokine-producing T-cells in the TME [15]. As previously mentioned, aPD-1 therapy does not induce beneficial responses in patients with EGFR-driven tumours [9,11,12]. This corresponds with our findings, which did not indicate improvements in tumour response upon ICB treatment compared to vehicle control (Figure 5A–C). An explanation for these results could be the downregulation of PD-L1 on tumour cells, mediated indirectly by oncogenic EGFR signalling via IRF1. In previous studies, transcription factor IRF1 was shown to be negatively impacted by EGFR signalling [14,35]. This corresponds to our own data that illustrate an increase in IRF1 expression levels upon EGFR inhibition (Figure 3C). Additionally, IRF1 has also been implicated in the regulation of $CD8^+$ T-cell infiltration in tumours by mediating the expression of the chemokine CXCL10 [14]. This could be one mechanism underlying how EGFR inhibition increases $CD8^+$ T-cell infiltration in EGFR-driven tumours that we observed (Figure 1B and Figure S1). Another chemokine that has been linked to EGFR signalling is CCL21, previously shown to be involved in the recruitment and infiltration of tumour-specific T-cells into the TME [37]. CCL21 has been previously shown to be downregulated in EGFR-driven tumours and contribute to an immunosuppressive TME [14], which can be confirmed by our data (Figure 3D). Moreover, in hepatic cell cancer (HCC), expression of *Ccnb1* and *Tpx2* was positively associated with higher immune cell infiltration in tumours, suggesting potential immune-regulatory roles for the proteins [38,39]. This is line with recent results indicating that Tpx2 overexpression increased antitumour activity of $CD8^+$ T-cells in HCC in a CXCR5-dependent manner [40]. Lastly, treatment with ICB in combination with EGFR inhibition induced an antitumour immune response, when considering levels of immune cell infiltrate (Figure 1B–I) and immune cell activation in the TME (Figure 3A). Despite similar immune cell infiltrate signatures between ICB combined with EGFR inhibition and EGFR inhibition alone, growth data suggest an improved antitumour response in aPD-1 + erlotinib mice, resulting in a faster reduction in tumour size and slower tumour progression until the end of the experiments (Figure 5A). However, this observation remains to be confirmed in future studies.

In this study, we examined the immune-modulating effect of targeted therapy in EGFR-driven NSCLC on the TME using an $EGFR^{L858R}$-dependent mouse model. Moreover,

we provided insights into the changes to the TME after long-term exposure to continuous targeted therapy using erlotinib, as well as after ongoing simultaneous long-term administration of targeted therapy and ICB in EGFR-driven NSCLC. We observed that EGFR inhibition induces a proinflammatory immune response with increased proliferation and activation of tumour-infiltrated T-cells. Thus, our results suggest that oncogenic EGFR signalling modulates the TME to evade the immune response by promoting an immunosuppressive microenvironment. Future studies should provide more insights into the underlying cellular mechanisms involved in this process.

5. Conclusions

In summary, our findings shed more light on the impact of targeted therapy on the TME, as well as improve our understanding of how the immune cell infiltrate is altered upon continuous long-term exposure to TKI treatment and simultaneous administration of TKIs and ICB in EGFR-driven tumours. These aspects are not only critical for improving current targeted therapy approaches, but also provide important and clinically relevant information for future investigations on combining immunotherapy with TKIs to further stimulate and improve the antitumour immune response in EGFR-driven NSCLC.

Supplementary Materials: The following supporting information can be downloaded at https://www.mdpi.com/article/10.3390/cancers14163943/s1: Figure S1. Infiltration of immune cells in $EGFR^{L585R}$-driven tumours is elevated upon EGFR inhibition; Figure S2. EGFR inhibition does not increase PD-1 levels; Figure S3. EGFR inhibition does not increase circulating cytokines; Table S1. Immune cell-specific transcripts.

Author Contributions: Conceptualisation, C.S. and R.T.U.; methodology, C.S., L.M. and R.T.U.; software, C.S.; validation, C.S., A.C. and R.T.U.; formal analysis, C.S.; investigation, C.S., A.C., M.N. and A.F.; resources, S.B., M.O., J.B., R.B. and L.M.; data curation, C.S., A.C. and J.B.; writing—original draft preparation, C.S.; writing—review and editing, C.S., L.M. and R.T.U.; visualisation, C.S. and A.C.; supervision, L.M. and R.T.U.; project administration, C.S., L.M. and R.T.U.; funding acquisition, L.M. and R.T.U. All authors have read and agreed to the published version of the manuscript.

Funding: This research was funded by Deutsche Krebshilfe (70113009 to R.T.U.), Nachwuchsforschungsgruppen NRW grant (1411ng005 to R.T.U.), Deutsche Forschungsgemeinschaft (SFB-1530-B05 to R.T.U., UL 379/5-1 to R.T.U.), Fritz Thyssen Foundation (10.21.1.026MN to L.M.), and Mildred Scheel Nachwuchszentrum grant (70113307 to J.B.).

Institutional Review Board Statement: The animal study protocol was approved by the local Ethics Committee of Animal experiments (84-02.04.2015.A199; 81-02.04.2020.A026).

Informed Consent Statement: The data presented in this study are available in this article.

Data Availability Statement: The RNA sequencing data presented in this study are openly available in the NCBI Sequence Read Archive under the accession code PRJNA860558 (https://www.ncbi.nlm.nih.gov/sra/PRJNA860558, accessed on 20 July 2022).

Acknowledgments: We would like to thank Kerstin Wennhold, Martin Thelen, and Hans A. Schlößer, who provided support concerning flow cytometry experiments. We also thank Priya S. Dalvi for her support in animal care.

Conflicts of Interest: The authors declare no conflict of interest.

References

1. Torre, L.A.; Bray, F.; Siegel, R.L.; Ferlay, J.; Lortet-Tieulent, J.; Jemal, A. Global Cancer Statistics, 2012. *CA Cancer J. Clin.* **2015**, *65*, 87–108. [CrossRef] [PubMed]
2. Miller, K.D.; Siegel, R.L.; Lin, C.C.; Mariotto, A.B.; Kramer, J.L.; Rowland, J.H.; Stein, K.D.; Alteri, R.; Jemal, A. Cancer Treatment and Survivorship Statistics, 2016. *CA Cancer J. Clin.* **2016**, *66*, 271–289. [CrossRef] [PubMed]
3. Ohashi, K.; Maruvka, Y.E.; Michor, F.; Pao, W. Epidermal Growth Factor Receptor Tyrosine Kinase Inhibitor-Resistant Disease. *J. Clin. Oncol.* **2013**, *31*, 1070–1080. [CrossRef] [PubMed]

4. Cross, D.A.E.; Ashton, S.E.; Ghiorghiu, S.; Eberlein, C.; Nebhan, C.A.; Spitzler, P.J.; Orme, J.P.; Finlay, M.R.V.; Ward, R.A.; Mellor, M.J.; et al. AZD9291, an Irreversible EGFR TKI, Overcomes T790M-Mediated Resistance to EGFR Inhibitors in Lung Cancer. *Cancer Discov.* **2014**, *4*, 1046–1061. [CrossRef]
5. Thress, K.S.; Paweletz, C.P.; Felip, E.; Cho, B.C.; Stetson, D.; Dougherty, B.; Lai, Z.; Markovets, A.; Vivancos, A.; Kuang, Y.; et al. Acquired EGFR C797S Mutation Mediates Resistance to AZD9291 in Non-Small Cell Lung Cancer Harboring EGFR T790M. *Nat. Med.* **2015**, *21*, 560–562. [CrossRef]
6. Akbay, E.A.; Koyama, S.; Carretero, J.; Altabef, A.; Tchaicha, J.H.; Christensen, C.L.; Mikse, O.R.; Cherniack, A.D.; Beauchamp, E.M.; Pugh, T.J.; et al. Activation of the PD-1 Pathway Contributes to Immune Escape in EGFR-Driven Lung Tumors. *Cancer Discov.* **2013**, *3*, 1355–1363. [CrossRef]
7. Chen, N.; Fang, W.; Zhan, J.; Hong, S.; Tang, Y.; Kang, S.; Zhang, Y.; He, X.; Zhou, T.; Qin, T.; et al. Upregulation of PD-L1 by EGFR Activation Mediates the Immune Escape in EGFR-Driven NSCLC: Implication for Optional Immune Targeted Therapy for NSCLC Patients with EGFR Mutation. *J. Thorac. Oncol.* **2015**, *10*, 910–923. [CrossRef]
8. Taube, J.M.; Galon, J.; Sholl, L.M.; Rodig, S.J.; Cottrell, T.R.; Giraldo, N.A.; Baras, A.S.; Patel, S.S.; Anders, R.A.; Rimm, D.L.; et al. Implications of the Tumor Immune Microenvironment for Staging and Therapeutics. *Mod. Pathol.* **2018**, *31*, 214–234. [CrossRef]
9. Borghaei, H.; Paz-Ares, L.; Horn, L.; Spigel, D.R.; Steins, M.; Ready, N.E.; Chow, L.Q.; Vokes, E.E.; Felip, E.; Holgado, E.; et al. Nivolumab versus Docetaxel in Advanced Nonsquamous Non–Small-Cell Lung Cancer. *N. Engl. J. Med.* **2015**, *373*, 1627–1639. [CrossRef]
10. Reck, M.; Rodríguez-Abreu, D.; Robinson, A.G.; Hui, R.; Csőszi, T.; Fülöp, A.; Gottfried, M.; Peled, N.; Tafreshi, A.; Cuffe, S.; et al. Pembrolizumab versus Chemotherapy for PD-L1–Positive Non–Small-Cell Lung Cancer. *N. Engl. J. Med.* **2016**, *375*, 1823–1833. [CrossRef]
11. Gainor, J.F.; Shaw, A.T.; Sequist, L.V.; Fu, X.; Azzoli, C.G.; Piotrowska, Z.; Huynh, T.G.; Zhao, L.; Fulton, L.; Schultz, K.R.; et al. EGFR Mutations and ALK Rearrangements Are Associated with Low Response Rates to PD-1 Pathway Blockade in Non-Small Cell Lung Cancer: A Retrospective Analysis. *Clin. Cancer Res.* **2016**, *22*, 4585–4593. [CrossRef] [PubMed]
12. Lee, C.K.; Man, J.; Lord, S.; Links, M.; Gebski, V.; Mok, T.; Yang, J.C.H. Checkpoint Inhibitors in Metastatic EGFR-Mutated Non–Small Cell Lung Cancer—A Meta-Analysis. *J. Thorac. Oncol.* **2017**, *12*, 403–407. [CrossRef]
13. Gettinger, S.; Hellmann, M.D.; Chow, L.Q.M.; Borghaei, H.; Antonia, S.; Brahmer, J.R.; Goldman, J.W.; Gerber, D.E.; Juergens, R.A.; Shepherd, F.A.; et al. Nivolumab Plus Erlotinib in Patients With EGFR-Mutant Advanced NSCLC. *J. Thorac. Oncol.* **2018**, *13*, 1363–1372. [CrossRef] [PubMed]
14. Sugiyama, E.; Togashi, Y.; Takeuchi, Y.; Shinya, S.; Tada, Y.; Kataoka, K.; Tane, K.; Sato, E.; Ishii, G.; Goto, K.; et al. Blockade of EGFR Improves Responsiveness to PD-1 Blockade in EGFR -Mutated Non—Small Cell Lung Cancer. *Sci. Immunol.* **2020**, *5*, 3937. [CrossRef] [PubMed]
15. Ayeni, D.; Miller, B.; Kuhlmann, A.; Ho, P.C.; Robles-Oteiza, C.; Gaefele, M.; Levy, S.; De Miguel, F.J.; Perry, C.; Guan, T.; et al. Tumor Regression Mediated by Oncogene Withdrawal or Erlotinib Stimulates Infiltration of Inflammatory Immune Cells in EGFR Mutant Lung Tumors. *J. Immunother. Cancer* **2019**, *7*, 172. [CrossRef]
16. Gotwals, P.; Cameron, S.; Cipolletta, D.; Cremasco, V.; Crystal, A.; Hewes, B.; Mueller, B.; Quaratino, S.; Sabatos-Peyton, C.; Petruzzelli, L.; et al. Prospects for Combining Targeted and Conventional Cancer Therapy with Immunotherapy. *Nat. Rev. Cancer* **2017**, *17*, 286–301. [CrossRef]
17. Politi, K.; Zakowski, M.F.; Fan, P.D.; Schonfeld, E.A.; Pao, W.; Varmus, H.E. Lung Adenocarcinomas Induced in Mice by Mutant EGF Receptors Found in Human Lung Cancers Respond to a Tyrosine Kinase Inhibitor or to Down-Regulation of the Receptors. *Genes Dev.* **2006**, *20*, 1496–1510. [CrossRef]
18. Macheleidt, I.F.; Dalvi, P.S.; Lim, S.Y.; Meemboor, S.; Meder, L.; Käsgen, O.; Müller, M.; Kleemann, K.; Wang, L.; Nürnberg, P.; et al. Preclinical Studies Reveal That LSD1 Inhibition Results in Tumor Growth Arrest in Lung Adenocarcinoma Independently of Driver Mutations. *Mol. Oncol.* **2018**, *12*, 1965–1979. [CrossRef]
19. Meder, L.; Schuldt, P.; Thelen, M.; Schmitt, A.; Dietlein, F.; Klein, S.; Borchmann, S.; Wennhold, K.; Vlasic, I.; Oberbeck, S.; et al. Combined VEGF and PD-L1 Blockade Displays Synergistic Treatment Effects in an Autochthonous Mouse Model of Small Cell Lung Cancer. *Cancer Res.* **2018**, *78*, 4270–4281. [CrossRef]
20. Moynihan, K.D.; Opel, C.F.; Szeto, G.L.; Tzeng, A.; Zhu, E.F.; Engreitz, J.M.; Williams, R.T.; Rakhra, K.; Zhang, M.H.; Rothschilds, A.M.; et al. Eradication of Large Established Tumors in Mice by Combination Immunotherapy That Engages Innate and Adaptive Immune Responses. *Nat. Med.* **2016**, *22*, 1402–1410. [CrossRef]
21. Triplett, T.A.; Garrison, K.C.; Marshall, N.; Donkor, M.; Blazeck, J.; Lamb, C.; Qerqez, A.; Dekker, J.D.; Tanno, Y.; Lu, W.C.; et al. Reversal of Indoleamine 2,3-Dioxygenase–Mediated Cancer Immune Suppression by Systemic Kynurenine Depletion with a Therapeutic Enzyme. *Nat. Biotechnol.* **2018**, *36*, 758–764. [CrossRef]
22. Hay, Z.L.Z.; Slansky, J.E. Granzymes: The Molecular Executors of Immune-Mediated Cytotoxicity. *Int. J. Mol. Sci.* **2022**, *23*, 1833. [CrossRef] [PubMed]
23. Mullins, G.N.; Valentine, K.M.; Al-Kuhlani, M.; Davini, D.; Jensen, K.D.C.; Hoyer, K.K. T Cell Signaling and Treg Dysfunction Correlate to Disease Kinetics in IL-2Rα-KO Autoimmune Mice. *Sci. Rep.* **2020**, *10*, 21994. [CrossRef] [PubMed]
24. Croft, M.; So, T.; Duan, W.; Soroosh, P. The Significance of OX40 and OX40L to T Cell Biology and Immune Disease OX40 and OX40L Are Induced on Lymphoid and Non-Lymphoid Cells. *Immunol. Rev.* **2009**, *229*, 173–191. [CrossRef] [PubMed]

25. Buchan, S.L.; Rogel, A.; Al-Shamkhani, A. The Immunobiology of CD27 and OX40 and Their Potential as Targets for Cancer Immunotherapy. *Blood* **2018**, *131*, 39–48. [CrossRef] [PubMed]
26. Cibrián, D.; Sánchez-Madrid, F. Europe PMC Funders Group CD69: From Activation Marker to Metabolic Gatekeeper. *Eur. J. Immunol.* **2017**, *47*, 946–953. [CrossRef]
27. Croft, M.; Benedict, C.A.; Ware, C.F. Clinical Targeting of the TNF and TNFR Superfamilies. *Nat. Rev. Drug Discov.* **2013**, *12*, 147–168. [CrossRef]
28. Dostert, C.; Grusdat, M.; Letellier, E.; Brenner, D. The TNF Family of Ligands and Receptors: Communication Modules in the Immune System and Beyond. *Physiol. Rev.* **2019**, *99*, 115–160. [CrossRef]
29. Noris, M.; Remuzzi, G. Overview of Complement Activation and Regulation. *Semin. Nephrol.* **2013**, *33*, 479–492. [CrossRef]
30. Strainic, M.G.; Liu, J.; Huang, D.; An, F.; Lalli, P.N.; Muqim, N.; Shapiro, V.S.; Dubyak, G.R.R.; Heeger, P.S.; Medof, M.E. Locally Produced Complement Fragments C5a and C3a Provide Both Costimulatory and Survival Signals to Naive CD4+ T Cells. *Immunity* **2008**, *28*, 425–435. [CrossRef]
31. Russell, É.; Conroy, M.J.; Barr, M.P. Harnessing Natural Killer Cells in Non-Small Cell Lung Cancer. *Cells* **2022**, *11*, 605. [CrossRef] [PubMed]
32. Du, N.; Guo, F.; Wang, Y.; Cui, J. Nk Cell Therapy: A Rising Star in Cancer Treatment. *Cancers* **2021**, *13*, 4129. [CrossRef] [PubMed]
33. Garcia-Diaz, A.; Shin, D.S.; Moreno, B.H.; Saco, J.; Escuin-Ordinas, H.; Rodriguez, G.A.; Zaretsky, J.M.; Sun, L.; Hugo, W.; Wang, X.; et al. Interferon Receptor Signaling Pathways Regulating PD-L1 and PD-L2 Expression. *Cell Rep.* **2017**, *19*, 1189–1201. [CrossRef] [PubMed]
34. Xu, X.; Wu, Y.; Yi, K.; Hu, Y.; Ding, W.; Xing, C. IRF1 Regulates the Progression of Colorectal Cancer via Interferon-Induced Proteins. *Int. J. Mol. Med.* **2021**, *47*, 104. [CrossRef]
35. Brägelmann, J.; Lorenz, C.; Borchmann, S.; Nishii, K.; Wegner, J.; Meder, L.; Ostendorp, J.; Ast, D.F.; Heimsoeth, A.; Nakasuka, T.; et al. MAPK-Pathway Inhibition Mediates Inflammatory Reprogramming and Sensitizes Tumors to Targeted Activation of Innate Immunity Sensor RIG-I. *Nat. Commun.* **2021**, *12*, 5505. [CrossRef]
36. Flanagan, K.; Moroziewicz, D.; Kwak, H.; Hörig, H.; Kaufman, H.L. The Lymphoid Chemokine CCL21 Costimulates Naïve T Cell Expansion and Th1 Polarization of Non-Regulatory CD4+ T Cells. *Cell. Immunol.* **2004**, *231*, 75–84. [CrossRef]
37. Phan-Lai, V.; Kievit, F.; Florczyk, S.; Wang, K.; Disis, M.; Zhang, M. CCL21 and IFNγ Recruit and Activate Tumor Specific T Cells in 3D Scaffold Model of Breast Cancer. *Anticancer Agents Med. Chem.* **2014**, *14*, 204–210. [CrossRef]
38. Zhu, H.; Liu, J.; Feng, J.; Zhang, Q.; Bian, T.; Li, X.; Sun, H.; Zhang, J.; Liu, Y. Overexpression of TPX2 Predicts Poor Clinical Outcome and Is Associated with Immune Infiltration in Hepatic Cell Cancer. *Medicine (Baltimore)* **2020**, *99*, e23554. [CrossRef]
39. Zou, Y.; Ruan, S.; Liang, J.; Chen, Z.; Han, H.; Zhang, Y.; Jian, Z.; Lin, Y.; Shi, N.; Jin, H. CDK1, CCNB1, and CCNB2 Are Prognostic Biomarkers and Correlated with Immune Infiltration in Hepatocellular Carcinoma. *Med. Sci. Monit.* **2020**, *26*, e925289-1–e925289-14. [CrossRef]
40. Wang, X.; Wang, J.; Shen, H.; Luo, Z.; Lu, X. Downregulation of TPX2 Impairs the Antitumor Activity of CD8+ T Cells in Hepatocellular Carcinoma. *Cell Death Dis.* **2022**, *13*, 223. [CrossRef]
41. Tu, M.M.; Lee, F.Y.F.; Jones, R.T.; Kimball, A.K.; Saravia, E.; Graziano, R.F.; Coleman, B.; Menard, K.; Yan, J.; Michaud, E.; et al. Targeting DDR2 Enhances Tumor Response to Anti–PD-1 Immunotherapy. *Sci. Adv.* **2019**, *5*, eaav2437. [CrossRef] [PubMed]
42. Lee, C.K.; Man, J.; Lord, S.; Cooper, W.; Links, M.; Gebski, V.; Herbst, R.S.; Gralla, R.J.; Mok, T.; Yang, J.C.H. Clinical and Molecular Characteristics Associated with Survival among Patients Treated with Checkpoint Inhibitors for Advanced Non-Small Cell Lung Carcinoma: A Systematic Review and Meta-Analysis. *JAMA Oncol.* **2018**, *4*, 210–216. [CrossRef] [PubMed]
43. Ahmadzadeh, M.; Johnson, L.A.; Heemskerk, B.; Wunderlich, J.R.; Dudley, M.E.; White, D.E.; Rosenberg, S.A. Tumor Antigen-Specific CD8 T Cells Infiltrating the Tumor Express High Levels of PD-1 and Are Functionally Impaired. *Blood* **2009**, *114*, 1537–1544. [CrossRef] [PubMed]
44. Vinay, D.S.; Ryan, E.P.; Pawelec, G.; Talib, W.H.; Stagg, J.; Elkord, E.; Lichtor, T.; Decker, W.K.; Whelan, R.L.; Kumara, H.M.C.S.; et al. Immune Evasion in Cancer: Mechanistic Basis and Therapeutic Strategies. *Semin. Cancer Biol.* **2015**, *35*, S185–S198. [CrossRef] [PubMed]
45. Jia, Y.; Zhao, S.; Jiang, T.; Li, X.; Zhao, C.; Liu, Y.; Han, R. Lung Cancer Impact of EGFR-TKIs Combined with PD-L1 Antibody on the Lung Tissue of EGFR -Driven Tumor-Bearing Mice. *Lung Cancer* **2019**, *137*, 85–93. [CrossRef]

Chapter 4 – Establishment of multiple EML4-ALK-driven NSCLC mouse models

4.1 Introduction

Lung cancer is the leading cause of cancer-related deaths worldwide, while non-small cell lung cancer accounts for approximately 80 % cases, making it the most prevalent type of lung cancer [2,3]. Rearrangement between the *anaplastic lymphoma kinase* (*ALK*) and the *echinoderm microtubule-associated protein-like 4* (*EML4*) genes, resulting in the *EML4-ALK* fusion gene, are identified in 3-7 % of NSCLC cases [70]. Depending on the breakpoint on the *EML4* gene, different variants have been identified, the most common ones being EML4-ALK variant 1 and EML4-ALK variant 3 [70,71]. While the *EML4* part of the fusion gene may vary in length, the *ALK* segment remains the same in all variants and includes its intracellular tyrosine kinase domain, that mediates oncogenic ALK signalling [71,72]. To combat this ALK-mediated oncogenic signalling, targeted therapies have been developed in the form of ALK tyrosine kinase inhibitors (TKIs), such as alectinib, and are currently used as first-line treatment in the clinic [73,74]. However, although initial response to TKI treatment shows beneficial responses in patients, resistance towards targeted therapy eventually develops, leading to tumour progression and limiting clinical benefits of ALK inhibition through TKIs [75].

Increasing evidence demonstrates that oncogene-driven NSCLC tumours generally display a non-inflamed tumour microenvironment (TME) characterised by poor immune cell infiltration and immunosuppressive signals, thus limiting the anti-tumour immune response and enabling tumour progression [76]. To improve therapeutic strategies for EML4-ALK-driven NSCLC, approaches with immune checkpoint inhibitors haven been investigated to induce a pro-inflammatory tumour microenvironment. However, results of past studies using only checkpoint inhibitors have reported lack of efficacy in ALK-rearranged NSCLC patients [77]. Moreover, combination therapies administering ALK TKIs and checkpoint inhibitors have not only demonstrated lack of beneficial tumour response, but also increased toxicity in patients [78,79]. These results highlight the necessity to improve existing therapy strategies for EML4-ALK-driven NSCLC patients, especially after the development of resistances to first-line targeted therapy using ALK TKIs. We have established two different *in vivo* EML4-ALK-driven NSCLC models in

our group to be able to study potential therapy approaches following acquired resistance to TKI treatment.

4.2 Materials & Methods

4.2.1 Cell lines

Murine NSCLC cell lines carrying either *EML4-ALK variant 1/ p53-null* (EAv1.1 and EAv1.2) or *EML3-ALK variant 3/ p53-null* (EA v3.1 and EAv3.2) mutations were kindly provided by Rocio Sotillo (University of Heidelberg, Germany). Human NSCLC cell line H3122 was kindly provided by Martin Sos (University Hospital Cologne, Germany). Murine cell lines were culture in DMEM high glucose, GlutaMAX, pyruvate media (Gibco) supplemented with 10 % fetal bovine serum (FBS) and 100 U/ml penicillin, 100 µg/ml streptomycin and 300 µg/ml L-glutamine (all by Gibco). H3122 cells were cultured in RPMI-1640 media (Gibco) containing 10 % fetal bovine serum (FBS) and 100 U/ml penicillin, 100 µg/ml streptomycin (all Gibco). All cells were cultured at 37°C and 5 % CO_2.

4.2.2 Cell viability assay

Murine NSCLC cells were plated in triplicates and incubated in regular DMEM media containing supplements, as described above. After 24 hours, compound dilutions and DMSO control were added to wells. Final concentrations of alectinib (dissolved in DMSO) in wells ranged from 0.002 to 10 µM. Cell viability was determined after 72 hours using the CellTiter-Glo Luminescent Cell Viability Assay (Promega, WI, USA), following the manufacturer's protocol.

4.2.3 Alectinib assay

EA v1 and EA v3 cell were seeded in a 6-well containing 250,000 cells/well in starving conditions, namely DMEM-GlutaMAX, pyruvate media containing 100 units/ml penicillin (Gibco), 100 µg/ml streptomycin (Gibco) and µg/ml L-glutamine (Gibco). Cells were left in starving media for 24 hours before removing starving media, replacing it with fresh regular media and adding either DMSO or alectinib dissolved in DMSO in the appropriate concentration. Cells were incubated as before, and at 4-hour 24-hour time points, cell culture supernatant was collected, centrifuged at 3000 *xg* and stored at -80°C for later cytokine analysis.

4.2.4 Cytokine analysis

Cell culture supernatant samples were cleared of debris by centrifugation and stored at -80 °C until use. Levels of 32 murine biomarkers were quantified using a Mouse Cytokine/Chemokine 31-Plex Discovery Assay® Array (Milipore), according to the manufacturer's protocol, and measured using the LuminexTM 100 system (Luminex, Austin, TX) by Eve Technologies Corporation (Calgary, Alberta). The biomarkers measured include Eotaxin, G-CSF, GM-CSF, IFNγ, IL-1α, IL-1β, IL-2, IL-3, IL-4, IL-5, IL-6, IL-7, IL-9, IL-10, IL-12p40, IL-12p70, IL-13, IL-15, IL-17A, IP-10, KC, LIF, LIX, MCP-1, M-CSF, MIG, MIP-1α, MIP-1β, MIP-2, RANTES, TNFα, VEGF-A. All samples were measured in duplicates. Raw values were normalised to the average of DMSO control samples for each time point.

4.2.5 In vivo experiments

Experiments were performed in accordance with FELASA recommendations. The protocol was approved by the local ethics committee. Mice were housed and all experiments performed in a sterile environment. Mice were fed, given water and monitored daily for health, and cages were changed weekly.

4.2.6 Autochthonous EML4-ALK NSCLC mouse model

We used a previously established EML4-ALK-driven NSCLC mouse model (Madallo et al., 2014). To establish autochthonous lung tumour in mice, 8-16 weeks old male and female wild-type C57BL/6J mice were anaesthetised by intraperitoneal (i.p.) injection of ketamine /xylazine (with a concentration of 100 mg/kg body weight (BW) and 0.5 mg/kg BW, respectively) and 3 x 10^8 p.f.u. of EML4-ALK-Cas9-adeonivirus (Ad-EA) was applied via intranasal application as previously described (Madallo et al., 2014, Meder et al., 2018). Viral vectors were obtained from ViraQuest Inc. (ViraQuest Inc., Iowa, USA). Serial MRI scans were performed to confirm tumour induction and monitor progression, starting after four weeks of viral induction. MRI scans were performed on a 3.0T MRI (Philips) using a dedicated small animal coil with an integrated heating coil (diameter: 40 mm; Philips Research). For duration of MRI scan, mice were anaesthetised using 1.5-2.3 % isoflurane and monitored closely. MRI scans of the whole lung were analysed using Onis 2.5 software.

4.2.7 Subcutaneous EML4-ALK/p53 NSCLC mouse model

For the syngeneic EML4-ALK lung cancer model, 8-16 weeks old FVB/N mice were anaesthetised by isoflurane and injected subcutaneously (s.c.) with 5 x 10^6 EAv1.1 or EAv3.2 cells suspended in 100 in each flank in 100 µl PBS in each flank. Start of therapy occurred when tumours reached the size of 50 mm^3. Tumour growth was measured twice per week by caliper measurement measuring tumour length (l) and width (w). Volume of tumours were calculated using the following formula: (w^2x l)/2. Fold changes were calculated according to tumour volume at start of therapy.

4.2.8 Therapy administration

Alectinib (LC Laboratories) was solved in 6 % Captisol (Ligand, San Diego, USA) solution and orally administered at a concentration of either 6 mg/ kg body weight (BW) or 20 mg/kg BW five times per week. Vehicle mice were treated five times per week with 6 % Captisol. For lymphodepletion, 200 mg/kg BW cyclophosphamide (HEXAL, Holzkirchen, Germany) and 40 mg/kg BW fludarabine (Sanofi Genzyme, Paris, France) in PBS were administered once via i.p. injection. For adoptive cellular transfer (ACT) therapy, lymphodepletion was conducted 24 hours before injection of cells. On day of therapy start, the four cellular components of ACT, described in more detail below, were harvested and suspended in PBS. A mix of 2.5 x 10^6 cells/ cell type was injected i.p., resulting in 1 x 10^7 cells, in a total of 200 µl suspension volume per mouse. To support engraftment of ACT cells, daily doses of 1 x 10^5 units of recombinant interleukin-2 (IL-2; Aldesleukin, Novartis, Basel, Switzerland) were given s.c. for five consecutive days after therapy start.

4.2.9 Histochemistry

Lung tissue was harvested and incubated in 4 % formalin for fixation over 24 hours at room temperature, transferred to PBS and embedded in paraffin. The resulting formalin-fixed, paraffin-embedded (FFPE) tissue samples were cut in three micrometre lung sections and deparaffinised. Haematoxylin and eosin (HE) staining was performed on the LabVision Autostainer 480S (Thermo Fisher Scientific, Waltham, USA). Embedding of samples and subsequent staining was conducted by the Pathology Department of the University Hospital Cologne, following standard protocols. Slides were scanned on the Leica SCN400 Slidescanner (Leica Biosystems, IL, USA).

4.2.10 Flow cytometry analysis

Single cell suspensions of tumour tissues were generated by mechanically meshing the tissue through a 40 µm filter and taking up the cells in PBS. After pelleting cells, they were re-suspended in 1 ml ACK lysis buffer and incubated at room temperature for five minutes. Cells were washed once with PBS before proceeding with the extracellular staining and applying the viability dye Zombie UV (Biolegend, San Diego, USA) for 30 minutes at 4°C in FACS buffer (PBS containing 2 % FBS and 1 mM EDTA). After incubation with antibodies, cells were washed with FACS buffer and fixed using 1 % formaldehyde in FACS buffer for 15 minutes at room temperature. After subsequent wash using FACS buffer, cells were permeabilised in 0.1 % Triton-X100-containing FACS buffer for 20 minutes at 4°C. After another wash with FACS buffer, cells were re-suspended with intracellular antibodies diluted in FACS buffer and incubated for 30 minutes at 4°C. Before final analysis, cells were washed once and re-suspended in FACS buffer. The following extracellular anti-mouse antibodies were used for the analysis of murine cells: anti-CD45-PerCP-Cy5.5 (clone 30-F11), anti-CD3-PE-Cy7 (clone 145-2C11), anti-PD1-APC (clone 29F.1A12), anti-CD49b-PE-Dazzle594, anti-γδTCR-APC-Fire750 (clone GL3), anti-CD8-BV421 (clone 53-6.7), anti-CD4-BV785 (clone GK1.5) and anti-CD69-BUV737 (clone H1.2F3, BD). The following intracellular anti-mouse antibodies were used: anti-FoxP3-PE (clone 150D), anti-IFN-γ-AF700 (clone XMG1.2) and anti-Ki67-BV605 (clone 16A8). Flow cytometry of stained cells was performed on the Cytoflex LX Flow Cytometer (Beckmann Coulter). Results were analysed using Kaluza Software (version 2.1, Beckmann Coulter). For analysis, gates were initially set to select alive cells of the correct size and multiples were excluded.

4.2.11 Differentiation of adoptive cellular therapy

For the adoptive cellular therapy approach, cells used for *ex vivo* differentiation and culture originated from splenocytes of female C57BL6/J mice. Cells were cultured at 37°C, 5 % CO_2 in a media mix containing 50 % of RPMI-1640 (Gibco) and 50 % of DMEM F-12 (Gibco) and supplemented with 10 % fetal bovine serum (FBS), 100 units/ml penicillin (Gibco), 100 µg/ml streptomycin (Gibco) and 50 µM β-mercaptoethanol (Roth).

Lymphokine-activated killer cells (LAKs) were cultured at starting concentration of 10^6 cell/ml and supplemented with 6000 units/ml hIL-2. After every 2-3 days, 50 % of fresh

media was added and hIL-2 was replenished. Cells were harvested 8-9 days after seeding.

Cytokine-induced killer cells (CIKs) were seeded at 10^6 cells/ml in media containing 1000 units/ml IFNγ for 24 hours. Simultaneously, 10 cm culture dishes were coated with 10 μg/ml anti-CD3 (clone 145-2C11, Biolegend) in PBS rocking at 4°C. After pre-stimulation with IFNγ (Miltenyi Biotech), cells were transferred onto the aCD3-coated culture dishes and supplemented with 300 units/ml hIL-2. Following a 48-hour incubation period, cells were transferred on to normal tissue culture flasks, medium was replenished and fresh hIL-2 at 300 units/ml was added. Every 2-3 days, 50 % of fresh media was added and hIL-2 was replenished. Cells were harvested 8-9 days after initial seeding.

For differentiation of tumour-induced T-cells (CTLs), prior to seeding splenocytes, EA v1 cells were pre-treated with 50 μg/ml mitomycin C (Medac) for 24 hours in FBS-free media mix containing 50 % of RPMI and DMEM F-12. Before seeding splenocytes, tumour cells were washed four times with PBS. Subsequently, splenocytes were added in a 10:1 ratio (splenocytes to tumour cells) to pre-treated tumour cells at a density of 10^6 cells/ml in media containing 10 ng/ml IL-7, 2 μg/ml anti-CD28 (clone 37.51, Biolegend), 20 μg/ml anti-PD-1 (clone RMP1-14, BioXCell) and 10 units/ml hIL-2. Every 2-3 days, 50 % fresh media was added according to cell density in flasks and hIL-2 was appropriately replenished. Cells were harvested 8-9 days after initial seeding.

Prior to seeding γδT-cell culture, 10 cm culture dishes were coated with 10 μg/ml anti-γδTCR (clone UC7-13D5, Biolegend) for 24 hours rocking at 4°C. Subsequently, dishes were washed and splenocytes were seeded at a density of 10^6 cells/ml in media containing 100 units/ml hIL-2. Following a 48-hour incubation period, cells were transferred to normal, uncoated tissue culture flasks and supplemented with 100 units/ml hIL-2. Every 2-3 days, 50 % of fresh media was added and hIL-2 was replenished. Cells were harvested 8-9 days after initial seeding.

4.3 Results

4.3.1 Establishment of autochthonous EML4-ALK lung cancer model

To investigate EML4-ALK-driven lung cancer, I established an autochthonous EML4-ALK variant 1 model in our group using an EML4-ALK-adenoviral transduction method developed by Maddalo and colleagues [80]. Through this method, lung tumours are induced in wild-type mice by infection with an adenovirus carrying the EML4-ALK inversion (Ad-EA). Detection of target lesions was possible between 8-12 weeks after viral induction (Fig. 4.1A). To validate the sensitivity of our autochthonous mouse model to AKL inhibition therapy that is currently used in a clinical setting, I administered two different concentrations of the ALK TKI alectinib and monitored tumour growth using *in vivo* imaging techniques (Fig. S1A). Weekly CT or MRI scans were used to determine tumour lesion size and tumour growth was assessed using mouse-adapted RECIST criteria [81]. Upon treatment with 20 mg/kg bodyweight (BW) alectinib, I was able to achieve consistent reduction in tumour size with complete tumour remission in mice after seven weeks of treatment. Therapy using a reduced concentration of 6 mg/kg BW alectinib resulted in stable tumours for the first few weeks, compared to vehicle mice. However, eventual progression followed initial stable tumours in the 6mg/kg alectinib group (Fig. 4.1B). In best tumour response data, 20 mg/kg alectinib therapy clearly indicated highest rates of complete tumour remission, while 6 mg/kg alectinib conveyed partially responding or stable tumours (Fig. 4.1C). Final validation of tumour tissue with HE staining displayed successfully established EML4-ALK tumours in our cohorts that resembled tumour morphology from original developmental studies generating this specific type of EML4-ALK mouse model (Fig. 4.1D) [80]. As expected, I saw established tumour also in HE stains from 6 mg/kg alectinib group, while 20 mg/kg alectinib resulted in lung tissue cleared from tumour lesions (Fig. 4.1D). In summary, I established the working autochthonous EML4-ALK mouse model in our group to be able study EML4-ALK-driven NSCLC in a biologically realistic context. To ensure comparability of our experiments to other pre-clinical studies, I validated ALK TKI sensitivity in our model with concentrations of alectinib previously used by others [73,82]. Together, this autochthonous EML4-ALK model allows us to examine the lung tissue-specific microenvironment of tumours and elucidate changes in response to different therapy approaches, not only in the immune cell infiltrate, but also regarding acquisition of resistance mechanisms to ALK inhibition.

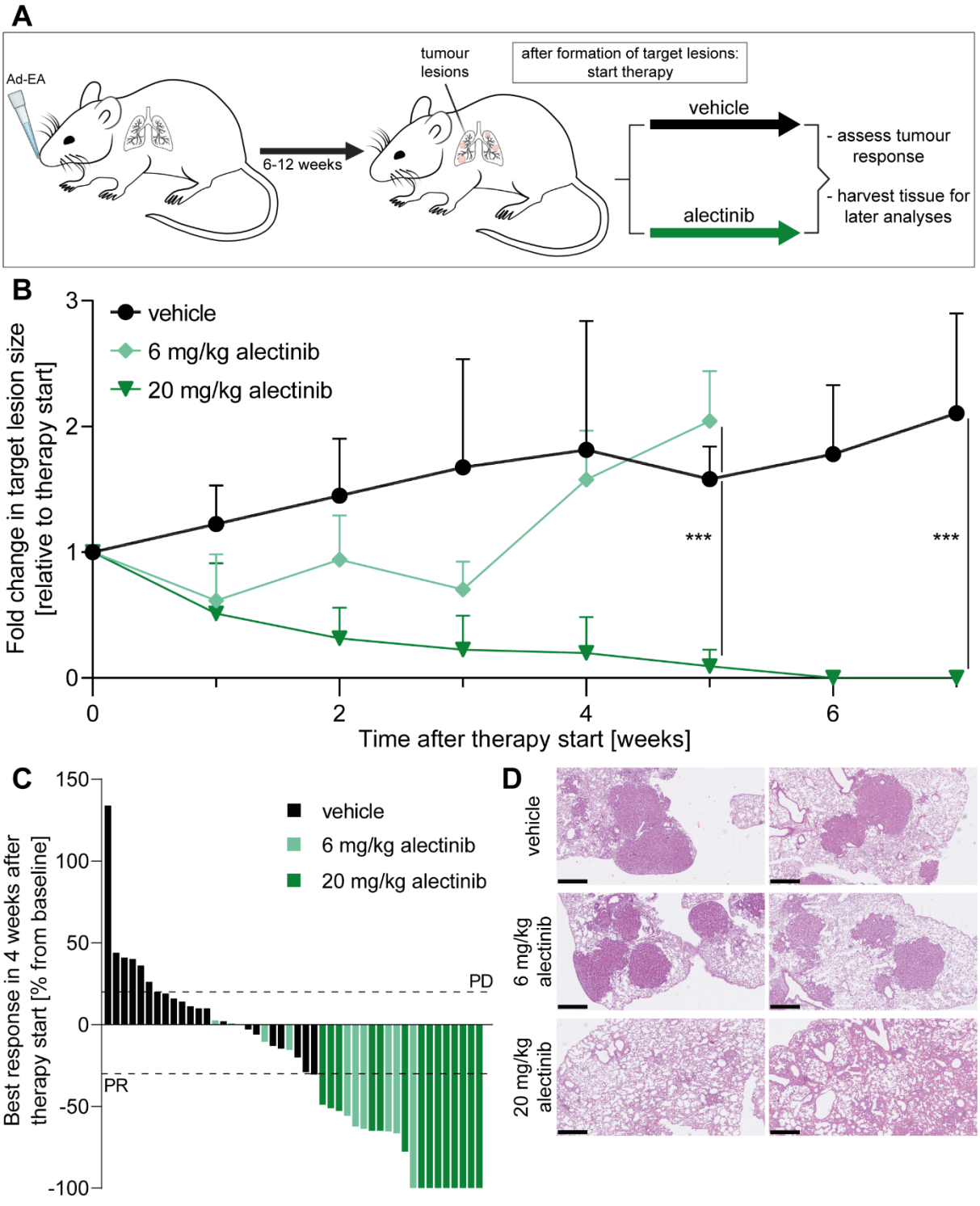

Figure 4.3 Establishment of autochthonous EML4-ALK NSCLC model. (**A**) Experimental set-up of tumour induction in EML4-ALK NSCLC mice with EML4-ALK-adenovirus (Ad-EA) and treatment strategies following the formation of target lesions. (**B**) Mean fold change of target lesion growth over time in indicated treatment groups: vehicle, 6 mg/kg body weight (BW) alectinib and 20 mg/kg BW alectinib. Data are shown as mean with SD; statistical analyses performed using Student's *t*-test; ***, p< 0.001. (**C**) Best response to therapy in first four weeks of treatment relative to therapy start (baseline). PD, progressive disease; PR, partial response. (**D**) Hematoxylin and eosin (HE) stain of formalin-fixed paraffin-embedded lung tissue samples of EML4-ALK mice. Two representative samples from each therapy group are shown. Scale bars depict 500 µm.

4.3.2 In vitro validation of sensitivity to ALK inhibition in murine EML4-ALK/p53 NSCLC cell lines

Another prominent genetic alteration is a *p53* mutation that can be found in approximately 50 % of all human cancers [83]. In ALK+ NSCLC, a subgroup of patients has been identified that carry mutated *p53*. This co-mutation has been associated with more aggressive cancers and poor clinical outcome compared to ALK+ NSCLC without *p53* mutation, demonstrating the need for further investigations of EML4-ALK/p53-driven subgroup to optimise therapies and improve outcome for patients [49,71,84]. In order to extend our studies on EML4-ALK NSCLC to include this particular subgroup tumours, we obtained murine NSCLC cell lines carrying *EML4-ALK* and *p53* mutations. These cell lines were kindly provided by the lab of Rocio Sotillo, and originated from primary tissue of either EML4-ALK variant 1/p53 (EAv1) or EML4-ALK variant 3/p53 (EAv3) tumours. To ensure consistency in our studies, I first validated sensitivity of primary cell lines to ALK inhibition through alectinib treatment. Viability studies were conducted using an established EML4-ALK variant 1/p53 NSCLC patient-derived cell line H3122 as control [85]. After viability testing, all four primary murine EML4-ALK/p53 cell lines, two containing EAv1 and two containing EAv3, displayed similar sensitivity pattern to alectinib compared to H3122 control cells (Fig 4.2A-D). Calculated IC50 values of cell lines for alectinib are EAv1.1: 85 nM, EAv1.2: 110 nM, EAv3.1: 105 nM and EAv3.2: 310 nM alectinib, all ranging around the H3122 control of 190 nM alectinib.

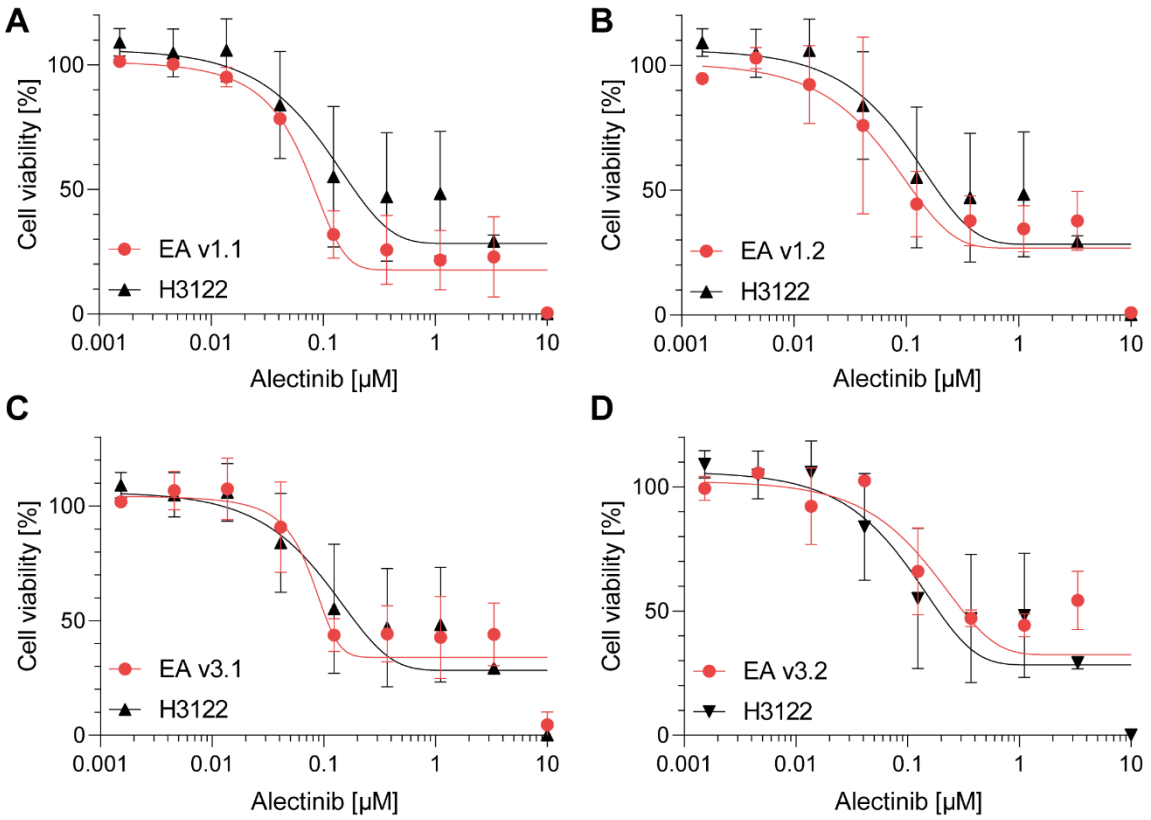

Figure 4.4 *in* vitro validation of sensitivity to ALK inhibition via alectinib in primary EML4-ALK/p53 NSCLC murine cell lines. (**A-D**) Cell viability assays with different EML4-ALK/p53 cell lines, either carrying EML4-ALK variant 1 (EA v1.1 and EA v1.2; **A,B**) or EML4-ALK variant 3 (EA v3.1 and EA v3.2; **C,D**). Primary murine cell lines were compared to established human H3122 control cell line containing *EML4-ALK/p53* mutations to confirm similar sensitivity to alectinib. Data are shown as mean with SD.

After confirmation of sensitivity to ALK inhibition through alectinib treatment, I started investigations in cellular processes and secretion of cytokines that are altered upon ALK inhibition in EML4-ALK/p53 NSCLC. At the same time, I sought to examine whether changes occur directly after start of treatment, or if some processes take longer to be altered. To this end, cells were treated with different concentrations of alectinib for either 4 or 24 hours before supernatants were collected to determine levels of secreted cytokines. In preliminary experiments, downregulation in G-CSF, GM-CSF and LIF cytokines could be observed in response to ALK inhibition. This trend was noted in both EAv1 (Fig. 4.3A) and EAv3 (Fig. 4.3B) cells. As cytokine levels did not decrease further after 24 hours of ALK inhibition, compared to 4 hours, these changes appear to be mediated directly after alectinib treatment. All three cytokines have been shown to be expressed by different cancer types and display tumour-promoting characteristics that instruct the immune response to tumours towards an

immunosuppressive phenotype [86,87]. This suggests, that ALK inhibition by alectinib also facilitates changes in the TME by directly modulating cytokine secretion of tumour cells. However, due to high variation between control samples, results will need to be verified in future experiments. While RNA samples from treated cells were also obtained for each time point, results remained inconclusive, suggesting that optimisation is required and it will be beneficial to include alternative approaches investigate not only the transcriptome of EA cells exposed to ALK inhibition, but also analyse proteomic alterations under different alectinib conditions.

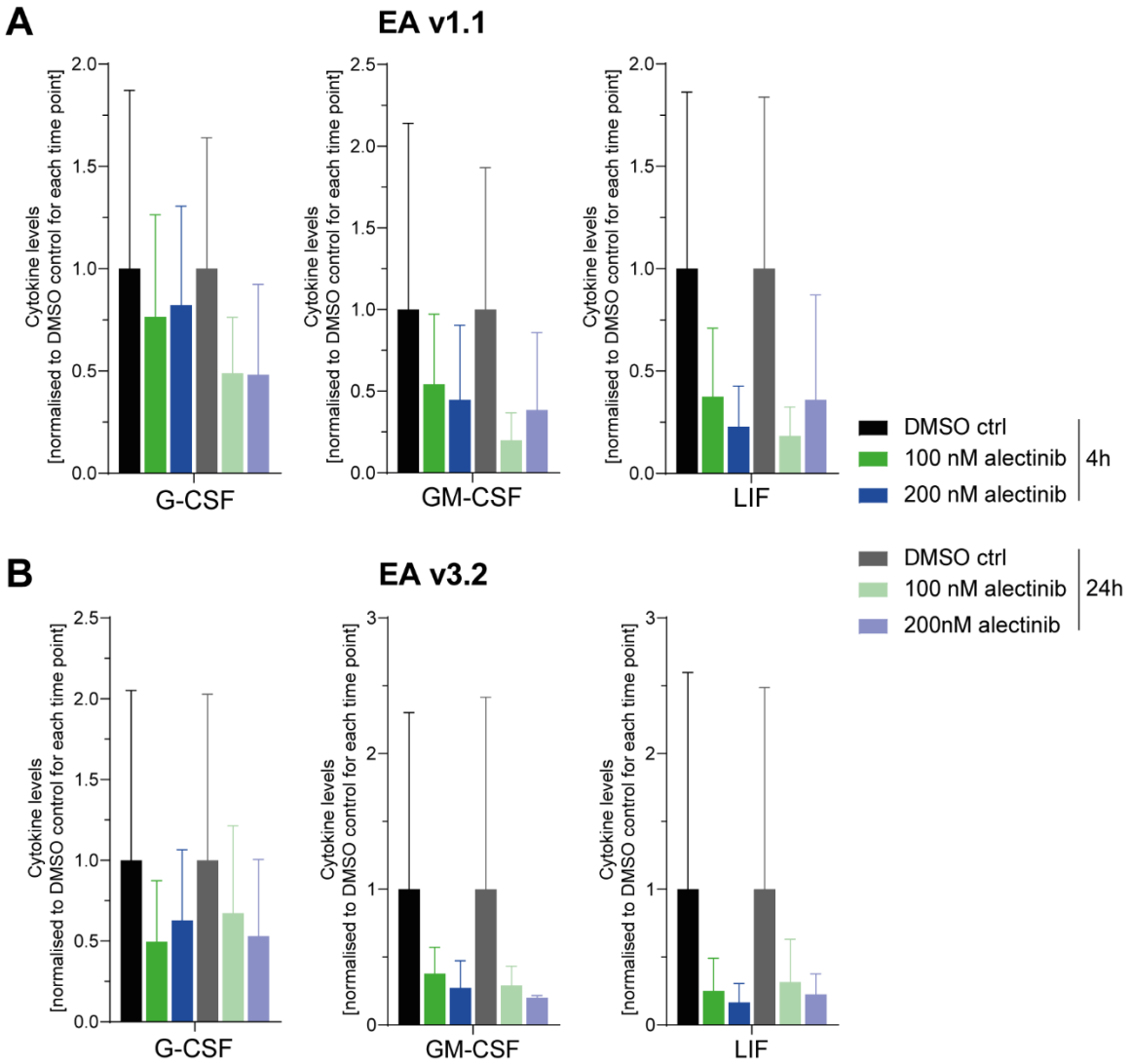

Figure 4.5 Cytokine analysis of EML4-ALK/p53 cells in response to ALK inhibition. (**A-B**) Levels of secreted cytokines G-CSF, GM-CSF and LIF in either EAv1.1 (**A**) or EAv3.2 (**B**) cells after alectinib treatment for 4 and 24 hours. Cytokine levels were normalised to DMSO control. Data are shown as mean with SD

In summary, we established the use of new primary murine EML4-ALK/p53 NSCLC cell lines in cellular assays that are sensitive to alectinib and can be used in further *in vitro* studies to shed light on exact changes in cellular processes that are altered by inhibition of oncogenic ALK signalling, as well as decipher the role of mutated *p53* in more aggressive cancers harbouring both mutations. This system can further be applied to elucidate the acquisition of resistance mechanisms in response to ALK TKI therapy in NSCLC patients. Lastly, generation of alectinib-resistant cells from primary cell lines will offer a platform that allows examination of different treatment strategies for TKI-insensitive NSCLC, and test novel therapy options on their potential benefits for TKI-resistant ALK+ patients.

4.3.3 Establishment of EML4-ALK/p53 subcutaneous mouse model

To follow up on the validation of primary murine EML4-ALK/p53 cell lines in cellular assays, I next sought to establish a syngeneic subcutaneous (s.c.) mouse model for EML4-ALK/p53-driven tumours. This was achieved by injection of either EAv1 or EAv3 cells in flanks of mice. Tumours rapidly developed within the first few weeks, resulting in established tumours, reaching a volume of 50 mm^3 after 1-2 weeks post injection (Fig. 4.4A). After that, therapy was initiated with either vehicle control or 20 mg/kg BW alectinib, the concentration that led to complete tumour reduction in the autochthonous EA model (Fig. 4.1B). I was able to confirm results in the s.c. EML4-ALK/p53 model, halting tumour growth and achieving a rapid reduction of tumour size in response to alectinib treatment. Not only in EAv1, but also in EAv3 tumours, ALK inhibition led to tumour volumes that were significantly decreased compared to vehicle controls (Fig. 4.4B, C). To initial insights into the TME and corresponding immune cell infiltrates of EML4-ALK/p53 cancers, flow cytometry analyses were established and carried out for tumour tissue samples, looking at levels of different cell types. While no changes were observed in T-cell levels in either EAv1 or EAv3 tumours after ALK inhibition compared to vehicle control, EAv1 tumour displayed slightly higher infiltration of NK cells in tumour following alectinib treatment. This trend was not depicted in EAv3 tumours (Fig. 4.4D, E). Additional T-cell subtype levels were also assessed by flow cytometry, but did not yield robust results (Fig. S2). Future analyses will be required to confirm and expand results on changes in the TME upon inhibition of oncogenic ALK signalling. A well-established understanding of the composition of the immune cell infiltrate in tumours will also offer essential foundational information that permits appropriate

assessment of anti-tumour immune response and other changes in the TME induced by novel therapy approaches.

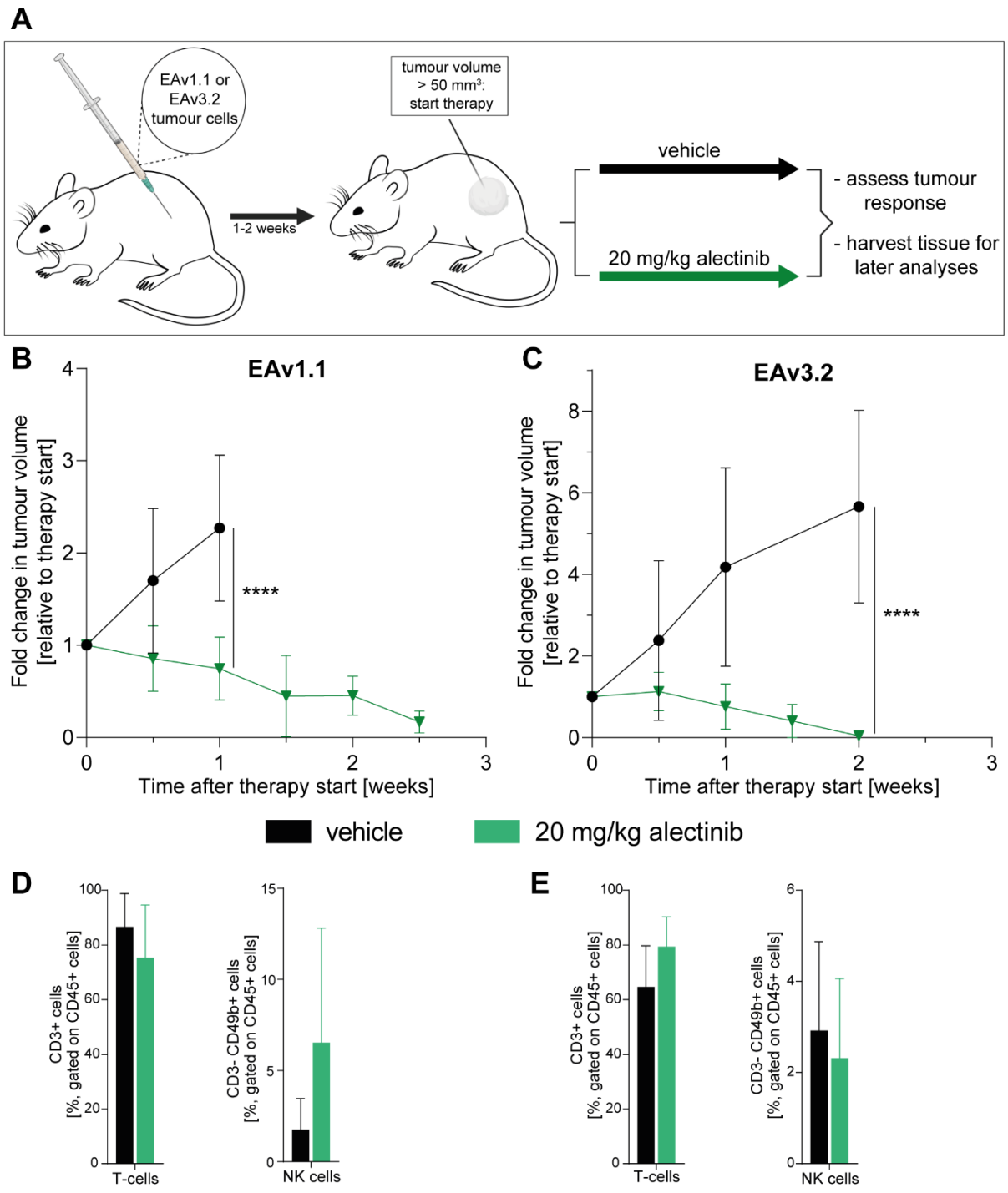

Figure 4.6 Establishment of subcutaneous EML4-ALK/p53 mouse model. (**A**) Experimental set-up of subcutaneous (s.c.) EML4-ALK/p53 NSCLC mouse model by injection of either EAv1.1 or EAv3.2 cells in flank of mice. After establishment of s.c. tumours, administration of treatment started in either vehicle- or 20 mg/kg BW alectinib-treated groups. (**B**) Mean fold change of s.c. EAv1.1 tumour growth over time in indicated treatment groups. (**C**) Mean fold change of s.c. EAv3.2 tumour growth over time in indicated treatment groups. (**D**) Flow cytometry data for intratumoral levels of T-cells (CD3+ CD49b- cells) and NK cells (CD3- CD49b+ cells) in EAv1.1 tumours, shown in percentage of CD45+ cells. (**E**) Flow cytometry data for intratumoral levels of T-cells (CD3+ CD49b- cells) and NK cells (CD3- CD49b+ cells) in EAv3.2 tumours, shown in percentage of CD45+ cells. (**B,C**) Statistical analyses performed using Student's *t*-test; ****, p< 0.0001. (**B-E**) Data are shown as mean with SD.

4.3.4 Investigation of different therapy approaches in autochthonous EML4-ALK model

As a proof of principle study to show that our mouse models can be used for studying alternative therapy modalities in EA NSCLC, I focussed on a novel immunotherapy approach that has been recently established in our group (Borchmann, Selenz *et al*., under revision). As mentioned, typical immunotherapy approaches via ICB have only offered limited benefits in oncogene-driven NSCLC, including those harbouring ALK+ tumours. A second immune-modulating treatment, that has gained a lot of attention over the last years is cellular transfer, in particular chimeric antigen receptor (CAR) T-cells, that uses autologous T-cells for expansion and stimulation *ex vivo* and followed by transfection to include receptors that specifically recognise tumour cells antigens [88]. Recently, the generation of ALK-specific CAR T-cell constructs has opened this approach for various ALK+ cancers [89]. Unfortunately, due the ALK domain residing intracellularly as part of the EML4-ALK fusion protein, the existing CAR T-cell constructs are not applicable for EML4-ALK tumours. An alternative adoptive cellular transfer (ACT) approach, which aims to re-instate an active immune cell infiltrate in tumours, was developed by our group (Borchmann, Selenz *et al*., under revision). For this approach, autologous immune cells are expanded *ex vivo* in stimulating conditions that results in differentiation or tumour cell-specific priming of immune cells, divided into lymphokine-activated killer cells (LAKs), cytokine-activated killer cells (CIKs), γδT-cells and cytotoxic tumour-specific lymphocytes (TILs). These are injected in lymphodepleted mice to substitute the immune cell infiltrate in tumours to stimulate an active and durable anti-tumour immune response (Fig. 4.5A). As this approach has shown promising results in melanoma models, NSCLC xenografts, and autochthonous KP-driven NSCLC tumours (Borchmann, Selenz *et al*., under revision), I wanted to test potential benefits of the ACT therapy on EML4-ALK-driven tumours. Additionally, I examined the effect of ACT on stable tumours, by combining ACT with 6 mg/kg alectinib therapy (Fig. 4.5B). While ACT treatment, as well as ACT and alectinib combi did show slower tumour progression compared to vehicle control, reduced tumour growth was also observed for the lymphodepletion monotherapy group that acted as control group for ACT (Fig. 4.5B). Moreover, no added benefits were noted in the ACT + alectinib group compared to alectinib monotherapy, suggesting that ACT and alectinib do not offer a synergistic effect when used in combination (Fig. 4.5B). After analysis of intratumoral T-cells by flow cytometry, no significant differences were detected between T-cell levels (Fig. 4.5C). Examining activation and proliferation

status of T-cells did also not indicate significant differences, although there may be a trend of increased activated T-cells in ACT + alectinib combi group, which could be interesting to examine more closely in future studies (Fig. 4.5C, E). Here, I have successfully administered new treatment modalities that focus on immune-modulating therapies and investigated its efficacy when combined with TKI-mediated ALK inhibition in our autochthonous EA NSCLC mouse model. Thus, this system can be used to explore novel therapy approaches and examine potential benefits involving other avenues of immunotherapy and combination regiments including targeted therapies in EA NSCLC.

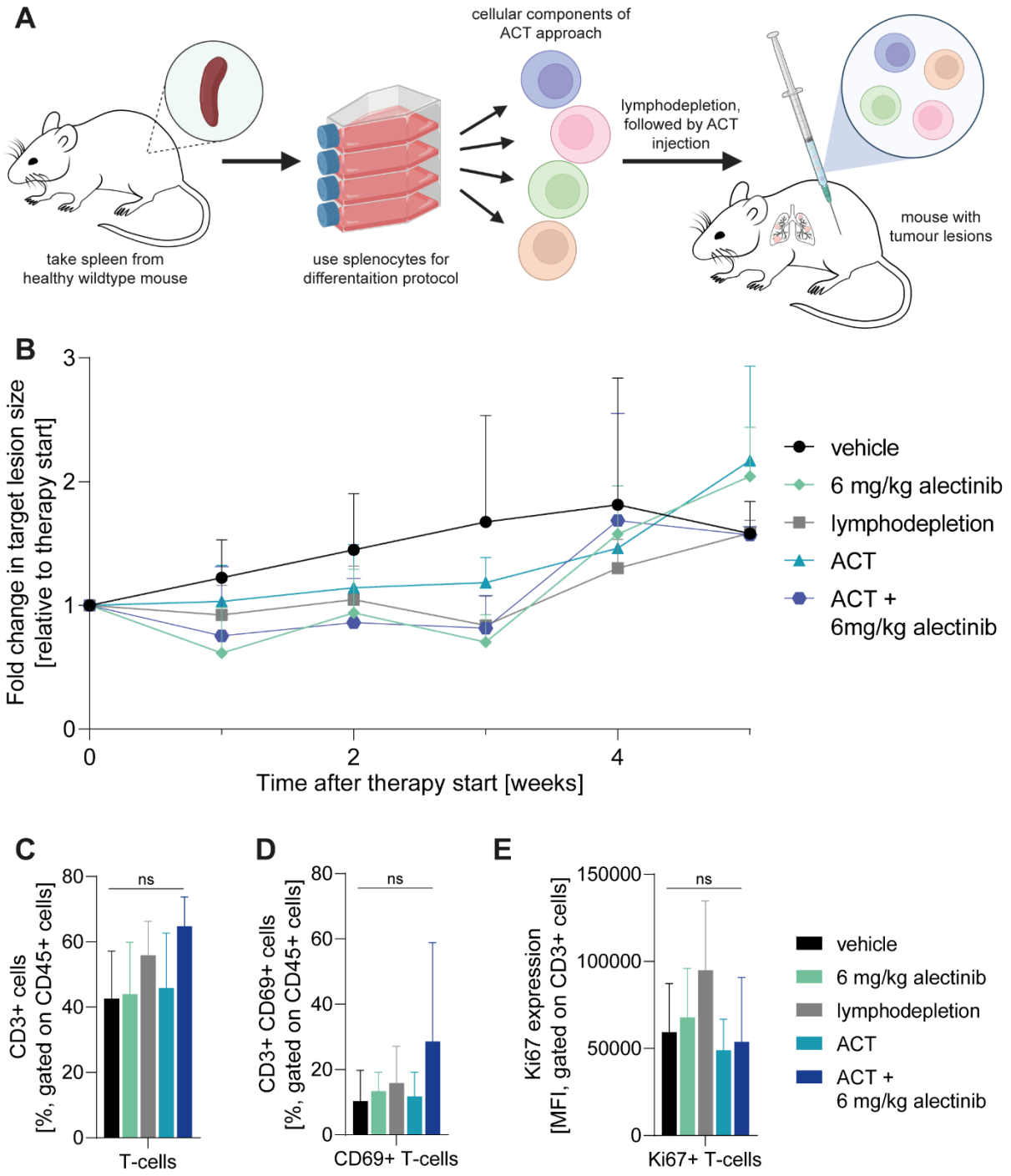

Figure 4.5 Investigation of different therapy approaches in autochthonous EML4-ALK model. (**A**) Schematic of adoptive cellular transfer (ACT) protocol and therapy strategy. (**B**) Mean fold change of tumour volume over time in indicated treatment groups: vehicle, 6 mg/kg BW alectinib, lymphodepletion, ACT and ACT + 6 mg/kg BW alectinib. Data are shown as mean with SD. (**C-E**) Anlysis of intratumoural T-cell infiltration by flow cytometry, looking at levels of T-cells (**C**), activation (**D**) and proliferation (**E**) of T-cells in different therapy groups. Statistical testing was conducted using either one-way ANOVA or Kruskal-Wallis test, ns= non-significant. Data are shown as mean with SD.

4.4 Discussion

In this study, my aim was to set up appropriate mouse model systems in order to study the resistance mechanisms and TME in EML4-ALK-driven NSCLC. This was approached by establishing an autochthonous mouse model using adenoviral induction, that enables us to investigate the intrinsic immune response and analyse the immune cell infiltrate in EML4-ALK-driven tumours (Fig. 4.1, 4.5C-E). To include the subgroup of NSCLC harbouring both *EML4-ALK* and *p53* mutations, that has been linked to particularly aggressive cancers and poorer clinical outcome compared to EML4-ALK-driven patients with wildtype *p53* [49,71,84], we obtained primary murine NSCLC cell lines carrying both mutations (Fig. 4.2). Using these cells, we can not only shed light on underlying mechanisms that are altered upon inhibition of oncogenic ALK signalling, but can also further our understanding on differences between distinct variants of EML4-ALK fusion proteins and their specific functions in various cellular processes (Fig. 4.3). Subsequently, we can readily validate initial results obtained from *in vitro* assays by translating them to our newly established pre-clinical syngeneic mouse model (Fig. 4.4). This does not only allow us to confirm our findings in an immunocompetent context, thus taking into account the effect of intratumoral immune cells and the whole TME, but also offers a unique possibility to compare results between autochthonous EA tumours and co-mutated EML4-ALK/p53 cancers.

4.5 Conclusion

In summary, I have established multiple systems of EML4-ALK-driven NSCLC to elucidate the effects of oncogenic ALK signalling and its inhibition, both in regards to intracellular processes as well as in a more complex biological environment of the TME. Moreover, previous studies have shown that development of resistance mechanisms are a crucially limiting factor for the benefits of targeted therapy via TKIs in EML4-ALK-driven cancers [75]. Therefore, it is essential to find other treatment strategies for TKI-insensitive EA tumours. The established mouse models in this study can be used to investigate alternative therapies, such as immunotherapy or combinatorial approaches, to improve anti-tumour response and establish a pro-inflammatory TME. This will also increase our understanding of underlying regulatory mechanisms and interactions in the TME that are necessary to induce an active and durable anti-tumour response in EML4-ALK-driven NSCLC.

Chapter 5 – Discussion

5.1 Inhibition of tumour VEGFR2 induces serine 897 EphA2-dependent tumour cell invasion and metastasis in NSCLC

Efforts to block angiogenesis, and thereby limit the supply of nutrients and oxygen delivered to cancer cells, have been applied in the clinic over the last decades. Although other pathways also contribute to angiogenesis, signalling through the receptor tyrosine kinase VEGFR2 has been the focus of most therapeutic approaches and anti-angiogenic treatments, with the first compounds mediating VEGFR2 inhibition approved for clinical use in the early 2000s [36]. Inhibition of VEGFR2 blocks an essential signal transduction pathway of the angiogenic process and thus inhibits a key contributor to tumour growth and progression. For this endeavour, multiple therapeutic approaches have been developed to date that target different levels of the VEGFR2 signalling cascade, such as neutralising antibodies against the ligand VEGF, or inhibitors that block tyrosine kinase activity of the VEGFR2 receptor. Unfortunately, despite good initial results from patients, monotherapy of VEGFR2 inhibition only shows limited long-term benefits, as resistance mechanisms are generally acquired [20]. Insensitivity to VEGFR2 monotherapy can occur through activation of alternative angiogenic pathways or increased levels of pro-angiogenic factors [21]. Of note, in addition to the emergence of resistance mechanisms, VEGFR2 inhibition has also shown to cause tumours to acquire a more aggressive phenotype, as also shown by our own studies on VEGFR2 inhibition in NSCLC. Furthermore, we identified the tyrosine kinase EphA2 as a key mediator for this invasive phenotype in response to VEGFR2 inhibition.

Interestingly, in recent years, EphA2 has gained more attention in association with tumour cell survival and growth. Eph receptors form the largest subfamily of receptor tyrosine kinases and conduct bi-directional activation of signalling by directly interacting with ligands bound to cell membranes. In previous studies, Eph receptors have revealed to possess both tumour-promoting and anti-tumour characteristics, depending on the biological context. Dysregulation and overexpression of EphA2 has been linked to multiple cancer entities and is associated with poor clinical outcome in patients [90]. In particular, upregulation of EphA2 was detected in not only lung carcinoma, but also in prostate and breast cancer, glioblastoma, and other types of malignancies [91]. In a cellular context, EphA2 is able to mediate signal transduction

both initiated by ligand-binding, as well as in a ligand-independent manner when multiple EphA2 proteins form homo-multimers in the absence of ligands. This can occur upon high concentration of receptors at the cell membrane. In contrast to ligand-dependent signalling, that negatively regulates multiple processes, including cell survival, proliferation, migration and epithelial to mesenchymal transition (EMT), non-canonical ligand-independent EphA2 signalling activates pathways such as PI3K/AKT and thereby stimulates cell migration, EMT and angiogenic potential [92–94]. In breast cancer, EphA2 has even demonstrated to be required for angiogenesis in the TME [95–97]. In NSCLC, genome-wide analyses revealed frequent EphA2 overexpression in tumours and linked it to poor clinical outcome in patients [98,99]. Moreover, EphA2 knockdown experiments with NSCLC cells lines exhibited limited tumour cells viability [100]. Furthermore, pre-clinical studies with NSCLC models investigating loss of EphA2 function in established tumours confirmed that presence of EphA2 is required to confer tumour growth, as knockdown of EphA2 was sufficient to limit tumour progression [100]. In an oncogenic KRAS-driven NSCLC model, EphA2 inhibition has shown to alter regulation of mitochondrial apoptosis by decreasing S6K1-mediated phosphorylation of BAD, thereby activating the pro-apoptotic factor, leading to BAD-mediated apoptosis. Interestingly, tumorigenic functions of EphA2 have been linked to ligand-independent binding of the receptor in NSCLC and other cancer entities, as stimulation with Ephrin-A1 ligand obstructed tumour cell proliferation [100,101]. In melanoma cells, EphA2 inhibition also slowed down tumour growth and induced apoptosis by reducing AKT and ERK phosphorylation [102]. In addition to promoting a pro-apoptotic phenotype of tumour cells, biomarker levels for cell proliferation and angiogenesis were reduced in a uterine cancer model in response to EphA2-targeted therapy [103]. Together, these findings confirm and underline our own conclusions that EphA2 is a key mediator for the invasive and more aggressive tumour cell phenotype detected upon VEGFR2 inhibition. More specifically, in lines with previous studies on thyroid cancer [104], phosphorylation of residue S897 is essential to enable this tumour-promoting function of EphA2 in NSCLC and presents a promising target for combination strategies with VEGFR2 inhibition.

5.2 EGFR inhibition strongly modulates the tumour immune microenvironment in EGFR-driven non-small-cell lung cancer

Oncogenic EGFR signalling has been extensively studied as a target for therapeutic intervention against cancer cells for many years [38,39]. The first small molecule inhibitors targeting specifically EGFR were introduced for clinical applications from 2004 onwards as first generation inhibitors, including gefitinib and erlotinib [38,39]. Since then, EGFR TKIs have become standard therapy for NSCLC patients harbouring *EGFR* mutations. First generation EGFR inhibitors abrogate EGFR signalling by reversibly binding to the tyrosine kinase domain of EGFR, thus blocking ATP from binding and preventing ATP-dependent phosphorylation by tyrosine kinase activity [40]. While patients respond well to TKI therapy, resistance mechanisms eventually emerge. Often, these occur in the form of novel secondary point mutations in EGFR that confer insensitivity towards TKIs by preventing physical interaction between the inhibitor and its previous binding site at the tyrosine kinase domain. Prompted by the acquired resistance mechanisms in EGFR-driven NSCLC, the search for advanced inhibitors combating this issue continued. This resulted in the development of second generation TKIs, that irreversibly bind to EGFR, and third generation TKIs including osimertinib, which also irreversibly bind and block the ATP-binding site of EGFR, as well as possess a higher specificity towards EGFR mutants carrying secondary mutations [43,105,106]. While treatment approaches with third generation TKIs or sequential administration of inhibitors have delayed tumour progression, the problem of acquired mutations leading to TKI insensitivity still remains, together with multiple other mechanisms of resistance that are autonomous from EGFR signalling. EGFR-independent resistance mechanisms include amplifications of MET, HER2 or FGRF receptors, which mediate bypass signalling in place of EGFR and activate the same downstream pathways, including PI3K-AKT and RAS-MAPK-ERK cascades [55,107–112]. Additionally, AXL and FAS/NFκB signalling can also function as bypass pathways upon EGFR inhibition [50,52,53,113]. Due to the limited benefits of EGFR-specific TKI monotherapy, approaches that combine EGFR TKIs with other treatment modalities have gained more attention over the last decade, with the goal of improving efficacy of EGFR-targeted therapy. To obstruct activation of bypass signalling, multiple clinical trials are ongoing that combine EGFR inhibition with other targeting compounds. For example, two studies specifically focus on targeting MET amplification in addition to oncogenic EGFR signalling [114,115]. In the TATTON study, EGFR-mutated and MET-

amplified NSCLC patients are selectively treated with a combination of osimertinib and savolitinib, a MET inhibitor [115]. Another trial (ORCHARD) focusses on patients, resistant to EGFR-TKI after first-line treatment with osimertinib that have acquired MET amplification and also administer a combination of osimertinib and savolitinib [114]. Apart from MET inhibition, more clinical trials investigate the potential benefits when blocking other key factors in EGFR downstream pathways of bypass signal transmission, such as abrogating JAK1 or AXL activity, in combination with inhibition of EGFR, to try and circumvent resistance mechanisms [116–118].

In contrast to the approaches mentioned above, that combine targeted therapy in an attempt to normalise aberrant oncogenic signalling in tumour cells, another focus lies on establishing treatment modalities that engage and stimulate other components of the TME to combat the tumour. Immunotherapy aims to modulate the immune cell infiltrate in the TME towards an inflamed, activated status that prompts a rapid and durable anti-tumour immune response. The most common type of immunotherapy currently applied in the clinic is inhibition of immune checkpoint signalling via ICB. In different cancer entities, ICB has shown very promising results [58]. Although it has also improved clinical outcome for some NSCLC patients, ICB has not offered a satisfactory alternative to targeted inhibition therapy in oncogene-driven NSCLC, due to poor response in patients harbouring oncogenic genetic alterations [62]. In line with this, subgroup analyses of larger clinical trials have revealed only limited benefits of ICB therapy for patients with EGFR-driven NSCLC [63–66]. Interestingly, PD-L1 expression has been reported to be linked to oncogenic EGFR signalling, thereby contributing to the escape of immune surveillance in tumours [62,119–122]. Furthermore, pre-clinical studies detected a downregulation of PD-L1 expression in response to EGFR inhibition via TKIs, which could be explained by the release of antigens upon TKI-induced tumour cell apoptosis, resulting in an enhanced immune response [121,122]. However, whether there is a robust correlation between PD-L1 expression and patient response to EGFR TKIs that can be used as a biomarker still needs to be firmly established, as previous studies hold conflicting views on the subject, either linking PD-L1 expression to a favourable prognosis upon EGFR TKI treatment [123], or proposing PD-L1 as a biomarker for TKI-resistance and thus associating poor response to EGFR inhibition in PD-L1 expressing EGFR-driven tumours [119,120].

In addition to ICB monotherapy, combinatorial approaches with EGFR inhibition and ICB treatment have also gained attention in recent years, striving to further improve and prolong tumour response over TKI treatment. This issue is still under investigation to date in multiple studies, both pre-clinical and in clinical trials, and has not yet reached a final conclusion. Different studies described toxicity issues upon combination of EGFR inhibition and ICB and no significant improvements in tumour response [124–127], while others observed durable response in EGFR-driven patients and tolerable reaction by combination therapy [128,129]. Of note is, that studies with good tolerability of combination therapy were conducted using erlotinib as TKI, instead of the third generation inhibitor osimertinib. In another retrospective study that examined sequential treatment of ICB followed by EGFR TKI, severe adverse effects were detected in the cohort of patients that received osimertinib, with no toxicity observed in patients receiving erlotinib following a ICB [130]. This suggests a potential cross-reactivity of osimertinib and ICB, leading to intolerable side effects that are absent with erlotinib. These findings indicate the importance of selecting the right EGFR TKI to conduct combinatorial studies on EGFR-driven NSCLC. Similar to clinical data, pre-clinical studies that examine a combination strategy using ICB and EGFR TKI have also not reached a final conclusion yet, due to some findings indicating potential benefits, while others do not see improvement over EGFR TKI monotherapy [131,132]. These conflicting results illustrate that investigations regarding combining EGFR TKIs with ICB still require further examination and clarification, not only in regards to overall tumour response, but also to elucidate and uncover the underlying mechanisms that are involved. Furthermore, it remains critical to clarify the direct and indirect role of oncogenic signalling of tumour cell in defining and modulating the TME, which significantly determines the success or failure of therapy approaches.

5.3 Establishment of two different EML4-ALK-driven NSCLC mouse models

NSCLC harbouring EML4-ALK chromosomal rearrangements constitute another prominent type of oncogene-driven NSCLC. This genetic alteration was first described in 2007 by Soda and colleagues and account for approximately 3-5% of NSCLC cases [70]. In this cancer subtype, oncogenic signalling is facilitated by the constitutively active tyrosine kinase domain of ALK, which is part of all EML4-ALK fusion variants. Similar to targeted therapy of EGFR-driven NSCLC, oncogenic ALK signalling is

treated with tyrosine kinase inhibitors that were first introduced in the clinic in 2011 with crizotinib [45]. Since then, ALK TKIs have advanced to newer generations of inhibitors, including alectinib, further improving tumour response in ALK+ patients and achieving a better transfer between the blood-brain-barrier [46,47]. Comparable with other therapy strategies that inhibit key oncogenic signalling pathways, ALK inhibitors initially offer good tumour responses in EML4-ALK patients, however tumours eventually progress due to the emergence of resistance mechanisms [133]. The complexity of designing an appropriate treatment strategy is further increased by differences between EML4-ALK variants regarding their metastatic potential and aggressive phenotype, leading to poorer clinical outcome in EML4-ALK variant 3 patients, compared to either variant 1 or variant 2 patients [134]. In line with these findings, EML4-ALK variant 3 patients have also displayed a higher tendency of developing resistant mechanisms in response to ALK inhibition, resulting in TKI insensitivity in tumours [135]. These factors illustrate the importance of differentiating between EML4-ALK variants and discourage the assumption that oncogenic mechanisms of one EML4-ALK variant can be universally applied to other variants. Mechanisms of resistance that have been identified in EML4-ALK tumours can be divided into processes dependent on ALK signalling, and ALK-independent mechanisms. Secondary and tertiary mutations in the *ALK* gene, leading to conformational changes of the fusion protein and thus preventing ALK inhibitors to bind to the tyrosine kinase domain, constitute the main resistance mechanisms reinstating oncogenic ALK signalling. ALK-independent mechanisms can involve activation of bypass signalling pathways, such as EGFR or MEK signalling, that contribute to tumour growth and progression in the absence of ALK signalling [50–53]. Epithelial-to-mesenchymal transition can also convey TKI insensitivity by enabling tumour cells to invade blood vessels and metastasise at secondary tumour sites [54]. In line with this, studies examining EML4-ALK NSCLC patients detected increased expression of the mesenchymal marker vimentin in ALK TKI-resistant cases, as well as a downregulation of the epithelial marker E-cadherin [136,137]. Furthermore, co-occurrence of other genetic alterations can also result in TKI resistance, such as mutations in the tumour suppressor gene *p53*, further promoting tumour cell survival and proliferation [85]. In line with this, overexpression of MYC, a transcriptional regulator for different tumour-promoting processes, was linked to both crizotinib- and alectinib-insensitive EML4-ALK NSCLC [138].

To overcome resistance mechanisms in EML4-ALK NSCLC, different approaches applying ALK inhibitory treatment in combination with other compounds targeting additional factors are currently under investigation. As MEK signalling is one main pathway that is not only induced by oncogenic ALK signalling, but also activated by bypass pathways following TKI resistance, multiple clinical trials are ongoing that investigate treatment strategies combining ALK TKIs with MEK inhibition (NCT03202940, NCT04005144). Other avenues of research are using other combinatorial approaches that also target the vascular system to normalise blood vessels in the TME, and combine ALK inhibitors with anti-angiogenic compound bevacizumab, targeting VEGF (NCT03779191, NCT04227028). Shifting focus to the clearance of tumour cells in TME facilitated by an active immune response, immunotherapy has also been an active field of study for EML4-ALK-driven NSCLC. Patient data of ALK+ NSCLC tumours indicated significantly higher expression of PD-L1 compared to ALK wildtype tumours [61]. This finding confirms pre-clinical data, detecting upregulation of PD-L1 expression in EML4-ALK-transfected cells, as well as increased levels of PD-L1 in patient-derived EML4-ALK variant 1 and variant 3 cells [139,140]. Studies have shown that upregulation of PD-L1 by EML4-ALK is mediated by activation of MEK/ERK and PI3K/AKT pathways in response to oncogenic ALK signalling. In line with these results, inhibition of ALK signalling either by TKI treatment or knockdown, blocked upregulation of PD-L1 in NSCLC cells, further confirming a regulatory role of ALK activity on PD-L1 levels in EML4-ALK-driven cancers [61,139]. Despite the regulatory link between inhibitory PD-L1 expression and oncogenic ALK signalling, initial results from case report studies or retrospective analyses of larger trials do not indicate satisfactory response in ALK+ patients treated with ICB [30]. First pre-clinical studies that have investigated potential benefits of combining ICB with ALK inhibition have yielded similar unsatisfactory results, with no higher efficacy observed in combination cohorts over TKI monotherapy [139,141]. While initial findings propose no improvement, due to low number of studies conducted on the subject of targeting both immune checkpoints and oncogenic ALK signalling, combinatorial approaches should not be disregarded yet. Further investigations can explore and optimise therapy administration strategies and timing, also in regards to TKI-resistant tumours. In general, it can be said that research efforts on immunotherapy approaches in the context of EML4-ALK-driven NSCLC are still in the early stages, such as initial strategies combining ALK inhibition with ICB or adoptive cellular transfer procedures.

Therefore, more studies are required to properly evaluate their potential benefits on tumour development and patient outcome, as well as their impact on the TME.

5.4 Concluding remarks

The development of targeted therapy for lung cancer, particularly for cases harbouring oncogenic driver mutations, has considerably enhanced tumour response and improved outcome and quality of life for patients compared to previous alternative treatment approaches. Simultaneously, more inhibitors are still being developed against new targets, further increasing treatment options for oncogene-driven NSCLC patients. Despite this success, targeted therapy still has inherent limitations due to the emergence of resistance in tumour cells. In addition, intratumoral molecular and cellular heterogeneity can make the choice of treatment even more complex. Apart from tumour cells, it is also imperative to elucidate the effects of targeted therapy on other cellular factors in close proximity to the cancer, as the TME represents a critical factor that facilitates or limits tumour response and an active immune response.

This work examined different targeted therapeutic approaches in oncogene-driven NSCLC and considered the impact of therapies on the different components of the TME. Studies on the consequences of anti-angiogenic treatment in the TME elucidate underlying mechanisms pertaining to an increasingly aggressive phenotype of tumours observed in response to anti-angiogenic treatment dependent on EphA2 (chapter 2). In addition, this work investigated inhibition of oncogenic signalling in EGFR-driven NSCLC and examined changes mediated by targeted therapy on the immune cell infiltrate of the TME (chapter 3). Lastly, essential steps were taken by establishing different oncogene-driven mouse models that allow investigation of acquired resistance mechanisms, as well as further exploration on the influence of oncogenic signalling on the TME (chapter 4).

General References

1. Sung, H.; Ferlay, J.; Siegel, R.L.; Laversanne, M.; Soerjomataram, I.; Jemal, A.; Bray, F. Global Cancer Statistics 2020: GLOBOCAN Estimates of Incidence and Mortality Worldwide for 36 Cancers in 185 Countries. *CA. Cancer J. Clin.* **2021**, *71*, 209–249, doi:10.3322/caac.21660.

2. Torre, L.A.; Bray, F.; Siegel, R.L.; Ferlay, J.; Lortet-Tieulent, J.; Jemal, A. Global Cancer Statistics, 2012. *CA. Cancer J. Clin.* **2015**, *65*, 87–108, doi:10.3322/caac.21262.

3. Miller, K.D.; Siegel, R.L.; Lin, C.C.; Mariotto, A.B.; Kramer, J.L.; Rowland, J.H.; Stein, K.D.; Alteri, R.; Jemal, A. Cancer Treatment and Survivorship Statistics, 2016. *CA. Cancer J. Clin.* **2016**, *66*, 271–289, doi:10.3322/caac.21349.

4. Denisenko, T. V.; Budkevich, I.N.; Zhivotovsky, B. Cell Death-Based Treatment of Lung Adenocarcinoma Article. *Cell Death Dis.* **2018**, *9*, doi:10.1038/s41419-017-0063-y.

5. Kris, M.G.; Johnson, B.E.; Berry, L.D.; Kwiatkowski, D.J.; Iafrate, A.J.; Wistuba, I.I.; Varella-Garcia, M.; Franklin, W.A.; Aronson, S.L.; Su, P.F.; et al. Using Multiplexed Assays of Oncogenic Drivers in Lung Cancers to Select Targeted Drugs. *JAMA - J. Am. Med. Assoc.* **2014**, *311*, 1998–2006, doi:10.1001/jama.2014.3741.

6. Wang, L.-H.; Wu, C.-F.; Rajasekaran, N.; Shin, Y.K. Loss of Tumor Suppressor Gene Function in Human Cancer: An Overview. *Cell. Physiol. Biochem.* **2018**, *51*, 2647–2693, doi:10.1159/000495956.

7. Shea, M.; Costa, D.B.; Rangachari, D. Management of Advanced Non-Small Cell Lung Cancers with Known Mutations or Rearrangements: Latest Evidence and Treatment Approaches. *Ther. Adv. Respir. Dis.* **2016**, *10*, 113–129, doi:10.1177/1753465815617871.

8. Pikor, L.A.; Ramnarine, V.R.; Lam, S.; Lam, W.L. Genetic Alterations Defining NSCLC Subtypes and Their Therapeutic Implications. *Lung Cancer* **2013**, *82*, 179–189, doi:10.1016/j.lungcan.2013.07.025.

9. Carpenter, G.; Lembach, K.J.; Morrison, M.M.; Cohen, S. Characterization of the Binding of 125I Labeled Epidermal Growth Factor to Human Fibroblasts. *J. Biol. Chem.* **1975**, *250*, 4297–4304, doi:10.1016/s0021-9258(19)41417-8.

10. Schlessinger, J. Receptor Tyrosine Kinases: Legacy of the First Two Decades. *Cold Spring Harb. Perspect. Biol.* **2014**, *6*, doi:10.1101/cshperspect.a008912.

11. Morgillo, F.; Della Corte, C.M.; Fasano, M.; Ciardiello, F. Mechanisms of Resistance to EGFR-Targeted Drugs: Lung Cancer. *ESMO Open* **2016**, *1*, 1–9, doi:10.1136/esmoopen-2016-000060.

12. De Luca, A.; Carotenuto, A.; Rachiglio, A.; Gallo, M.; Maiello, M.R.; Aldinucci, D.; Pinto, A.; Normanno, N. The Role of the EGFR Signaling in Tumor Microenvironment. *J. Cell. Physiol.* **2008**, *214*, 559–567, doi:10.1002/jcp.21260.

13. Jimeno, A.; Hidalgo, M. Pharmacogenomics of Epidermal Growth Factor Receptor (EGFR) Tyrosine Kinase Inhibitors. *Biochim. Biophys. Acta - Rev. Cancer* **2006**, *1766*, 217–229, doi:10.1016/j.bbcan.2006.08.008.

14. Da Cunha Santos, G.; Shepherd, F.A.; Tsao, M.S. EGFR Mutations and Lung Cancer. *Annu. Rev. Pathol. Mech. Dis.* **2011**, *6*, 49–69, doi:10.1146/annurev-pathol-011110-130206.

15. Mosesson, Y.; Yarden, Y. Oncogenic Growth Factor Receptors: Implications for Signal Transduction Therapy. *Semin. Cancer Biol.* **2004**, *14*, 262–270, doi:10.1016/j.semcancer.2004.04.005.

16. Woodburn, J.R. The Epidermal Growth Factor Receptor and Its Inhibition in Cancer Therapy. *Pharmacol. Ther.* **1999**, *82*, 241–250, doi:10.1016/S0163-7258(98)00045-X.

17. Papageorgiou, S.; Pashley, S.L.; Regan, L.O.; Khan, S.; Bayliss, R.; Fry, A.M. Alternative Treatment Options to ALK Inhibitor Monotherapy for EML4-ALK-Driven Lung Cancer. **2022**, 1–19.

18. Hanahan, D.; Weinberg, R.A. Hallmarks of Cancer: The next Generation. *Cell* **2011**, *144*, 646–674, doi:10.1016/j.cell.2011.02.013.

19. Altorki, N.K.; Markowitz, G.J.; Gao, D.; Port, J.L.; Saxena, A.; Stiles, B.; McGraw, T.; Mittal, V. The Lung Microenvironment: An Important Regulator of Tumour Growth and Metastasis. *Nat. Rev. Cancer* **2019**, *19*, 9–31, doi:10.1038/s41568-018-0081-9.

20. Taylor, A.P.; Rodriguez, M.; Adams, K.; Goldenberg, D.M.; Blumenthal, R.D. Altered Tumor Vessel Maturation and Proliferation in Placenta Growth Factor-Producing Tumors: Potential Relationship to Post-Therapy Tumor Angiogenesis and Recurrence. *Int. J. Cancer* **2003**, *105*, 158–164, doi:10.1002/ijc.11059.

21. Lopes-Coelho, F.; Martins, F.; Pereira, S.A.; Serpa, J. Anti-Angiogenic Therapy: Current Challenges and Future Perspectives. *Int. J. Mol. Sci.* **2021**, *22*, doi:10.3390/ijms22073765.

22. Santaniello, A.; Napolitano, F.; Servetto, A.; De Placido, P.; Silvestris, N.; Bianco, C.; Formisano, L.; Bianco, R. Tumour Microenvironment and Immune Evasion in EGFR Addicted NSCLC: Hurdles and Possibilities. *Cancers (Basel).* **2019**, *11*, 1419, doi:10.3390/cancers11101419.

23. Taube, J.M.; Galon, J.; Sholl, L.M.; Rodig, S.J.; Cottrell, T.R.; Giraldo, N.A.; Baras, A.S.; Patel, S.S.; Anders, R.A.; Rimm, D.L.; et al. Implications of the Tumor Immune Microenvironment for Staging and Therapeutics. *Mod. Pathol.* **2018**, *31*, 214–234, doi:10.1038/modpathol.2017.156.

24. Binnewies, M.; Roberts, E.W.; Kersten, K.; Chan, V.; Fearon, D.F.; Merad, M.; Coussens, L.M.; Gabrilovich, D.I.; Ostrand-Rosenberg, S.; Hedrick, C.C.; et al. Understanding the Tumor Immune Microenvironment (TIME) for Effective Therapy. *Nat. Med.* **2018**, *24*, 541–550, doi:10.1038/s41591-018-0014-x.

25. Tanaka, A.; Sakaguchi, S. Regulatory T Cells in Cancer Immunotherapy. *Cell Res.* **2017**, *27*, 109–118, doi:10.1038/cr.2016.151.

26. Tian, X.; Shen, H.; Li, Z.; Wang, T.; Wang, S. Microenvironment. **2019**, 1–18.

27. Giatromanolaki, A.; Banham, A.H.; Harris, A.L.; Koukourakis, M.I. FOXP3 Infiltrating Lymphocyte Density and PD-L1 Expression in Operable Non-Small Cell Lung Carcinoma. *Exp. Lung Res.* **2019**, *45*, 76–83,

doi:10.1080/01902148.2019.1617371.

28. Kargl, J.; Busch, S.E.; Yang, G.H.Y.; Kim, K.H.; Hanke, M.L.; Metz, H.E.; Hubbard, J.J.; Lee, S.M.; Madtes, D.K.; McIntosh, M.W.; et al. Neutrophils Dominate the Immune Cell Composition in Non-Small Cell Lung Cancer. *Nat. Commun.* **2017**, *8*, 1–11, doi:10.1038/ncomms14381.

29. Soo, R.A.; Lim, S.M.; Syn, N.L.; Teng, R.; Soong, R.; Mok, T.S.K.; Cho, B.C. Immune Checkpoint Inhibitors in Epidermal Growth Factor Receptor Mutant Non-Small Cell Lung Cancer: Current Controversies and Future Directions. *Lung Cancer* **2018**, *115*, 12–20, doi:10.1016/j.lungcan.2017.11.009.

30. Gainor, J.F.; Shaw, A.T.; Sequist, L. V.; Fu, X.; Azzoli, C.G.; Piotrowska, Z.; Huynh, T.G.; Zhao, L.; Fulton, L.; Schultz, K.R.; et al. EGFR Mutations and ALK Rearrangements Are Associated with Low Response Rates to PD-1 Pathway Blockade in Non-Small Cell Lung Cancer: A Retrospective Analysis. *Clin. Cancer Res.* **2016**, *22*, 4585–4593, doi:10.1158/1078-0432.CCR-15-3101.

31. Bindea, G.; Mlecnik, B.; Tosolini, M.; Kirilovsky, A.; Waldner, M.; Obenauf, A.C.; Angell, H.; Fredriksen, T.; Lafontaine, L.; Berger, A.; et al. Spatiotemporal Dynamics of Intratumoral Immune Cells Reveal the Immune Landscape in Human Cancer. *Immunity* **2013**, *39*, 782–795, doi:10.1016/j.immuni.2013.10.003.

32. Shroff, G.S.; de Groot, P.M.; Papadimitrakopoulou, V.A.; Truong, M.T.; Carter, B.W. Targeted Therapy and Immunotherapy in the Treatment of Non–Small Cell Lung Cancer. *Radiol. Clin. North Am.* **2018**, *56*, 485–495, doi:10.1016/j.rcl.2018.01.012.

33. Politi, K.; Herbst, R.S. Lung Cancer in the Era of Precision Medicine. *Clin. Cancer Res.* **2015**, *21*, 2213–2220, doi:10.1158/1078-0432.CCR-14-2748.

34. Yuan, M.; Huang, L.L.; Chen, J.H.; Wu, J.; Xu, Q. The Emerging Treatment Landscape of Targeted Therapy in Non-Small-Cell Lung Cancer. *Signal Transduct. Target. Ther.* **2019**, *4*, doi:10.1038/s41392-019-0099-9.

35. Aldea, M.; Andre, F.; Marabelle, A.; Dogan, S.; Barlesi, F.; Soria, J.C. Overcoming Resistance to Tumor-Targeted and Immune-Targeted Therapies. *Cancer Discov.* **2021**, *11*, 874–899, doi:10.1158/2159-8290.CD-20-1638.

36. Hurwitz, H.; Fehrenbacher, L.; Novotny, W.; Cartwright, T.; Hainsworth, J.; Heim, W.; Berlin, J.; Baron, A.; Griffing, S.; Holmgren, E.; et al. Bevacizumab plus Irinotecan, Fluorouracil, and Leucovorin for Metastatic Colorectal Cancer. *N. Engl. J. Med.* **2004**, *350*, 2335–2342, doi:10.1056/NEJMoa032691.

37. McCarty, M.F.; Wey, J.; Stoeltzing, O.; Liu, W.; Fan, F.; Bucana, C.; Mansfield, P.F.; Ryan, A.J.; Ellis, L.M. ZD6474, a Vascular Endothelial Growth Factor Receptor Tyrosine Kinase Inhibitor with Additional Activity against Epidermal Growth Factor Receptor Tyrosine Kinase, Inhibits Orthotopic Growth and Angiogenesis of Gastric Cancer. *Mol. Cancer Ther.* **2004**, *3*, 1041–1048, doi:10.1158/1535-7163.1041.3.9.

38. Cohen, M.H.; Williams, G.A.; Sridhara, R.; Chen, G.; Pazdur, R. FDA Drug Approval Summary: Gefitinib (ZD1839) (Iressa®) Tablets. *Oncologist* **2003**, *8*, 303–306, doi:10.1634/theoncologist.8-4-303.

39. Cohen, M.H.; Johnson, J.R.; Chen, Y.-F.; Sridhara, R.; Pazdur, R. FDA Drug Approval Summary: Erlotinib (Tarceva®) Tablets. *Oncologist* **2005**, *10*, 461–466, doi:10.1634/theoncologist.10-7-461.

40. Lynch, T.J.; Bell, D.W.; Sordella, R.; Gurubhagavatula, S.; Okimoto, R.A.; Brannigan, B.W.; Harris, P.L.; Haserlat, S.M.; Supko, J.G.; Haluska, F.G.; et al. Activating Mutations in the Epidermal Growth Factor Receptor Underlying Responsiveness of Non–Small-Cell Lung Cancer to Gefitinib. *N. Engl. J. Med.* **2004**, *350*, 2129–2139, doi:10.1056/NEJMoa040938.

41. Ohashi, K.; Maruvka, Y.E.; Michor, F.; Pao, W. Epidermal Growth Factor Receptor Tyrosine Kinase Inhibitor-Resistant Disease. *J. Clin. Oncol.* **2013**, *31*, 1070–1080, doi:10.1200/JCO.2012.43.3912.

42. Del Re, M.; Petrini, I.; Mazzoni, F.; Valleggi, S.; Gianfilippo, G.; Pozzessere, D.; Chella, A.; Crucitta, S.; Rofi, E.; Restante, G.; et al. Incidence of T790M in NSCLC Patients Progressed to Gefitinib, Erlotinib and Afatinib: A Study on Circulating Tumor DNA. *Clin. Lung Cancer* **2019**, 1–6, doi:10.1016/j.cllc.2019.10.003.

43. Cross, D.A.E.; Ashton, S.E.; Ghiorghiu, S.; Eberlein, C.; Nebhan, C.A.; Spitzler, P.J.; Orme, J.P.; Finlay, M.R. V.; Ward, R.A.; Mellor, M.J.; et al. AZD9291, an Irreversible EGFR TKI, Overcomes T790M-Mediated Resistance to EGFR Inhibitors in Lung Cancer. *Cancer Discov.* **2014**, *4*, 1046–1061, doi:10.1158/2159-8290.CD-14-0337.

44. Thress, K.S.; Paweletz, C.P.; Felip, E.; Cho, B.C.; Stetson, D.; Dougherty, B.; Lai, Z.; Markovets, A.; Vivancos, A.; Kuang, Y.; et al. Acquired EGFR C797S Mutation Mediates Resistance to AZD9291 in Non-Small Cell Lung Cancer Harboring EGFR T790M. *Nat. Med.* **2015**, *21*, 560–562, doi:10.1038/nm.3854.

45. Kazandjian, D.; Blumenthal, G.M.; Chen, H.-Y.; He, K.; Patel, M.; Justice, R.; Keegan, P.; Pazdur, R. FDA Approval Summary: Crizotinib for the Treatment of Metastatic Non-Small Cell Lung Cancer With Anaplastic Lymphoma Kinase Rearrangements. *Oncologist* **2014**, *19*, e5–e11, doi:10.1634/theoncologist.2014-0241.

46. Larkins, E.; Blumenthal, G.M.; Chen, H.; He, K.; Agarwal, R.; Gieser, G.; Stephens, O.; Zahalka, E.; Ringgold, K.; Helms, W.; et al. FDA Approval: Alectinib for the Treatment of Metastatic, ALK-Positive Non-Small Cell Lung Cancer Following Crizotinib. *Clin. Cancer Res.* **2016**, *22*, 5171–5176, doi:10.1158/1078-0432.CCR-16-1293.

47. Ly, A.C.; Olin, J.L.; Smith, M.B. Alectinib for Advanced ALK-Positive Non-Small-Cell Lung Cancer. *Am. J. Heal. Pharm.* **2018**, *75*, 515–522, doi:10.2146/ajhp170266.

48. Doebele, R.C.; Pilling, A.B.; Aisner, D.L.; Kutateladze, T.G.; Le, A.T.; Weickhardt, A.J.; Kondo, K.L.; Linderman, D.J.; Heasley, L.E.; Franklin, W.A.; et al. Mechanisms of Resistance to Crizotinib in Patients with ALK Gene Rearranged Non-Small Cell Lung Cancer. *Clin. Cancer Res.* **2012**, *18*, 1472–1482, doi:10.1158/1078-0432.CCR-11-2906.

49. Christopoulos, P.; Kirchner, M.; Bozorgmehr, F.; Endris, V.; Elsayed, M.; Budczies, J.; Ristau, J.; Penzel, R.; Herth, F.J.; Heussel, C.P.; et al. Identification

of a Highly Lethal V3 + TP53 + Subset in ALK + Lung Adenocarcinoma. *Int. J. Cancer* **2019**, *144*, 190–199, doi:10.1002/ijc.31893.

50. Liu, Q.; Yu, S.; Zhao, W.; Qin, S.; Chu, Q.; Wu, K. EGFR-TKIs Resistance via EGFR-Independent Signaling Pathways. *Mol. Cancer* **2018**, *17*, 1–9, doi:10.1186/s12943-018-0793-1.

51. Rosell, R.; Chaib, I.; Santarpia, M. Targeting MET Amplification in EGFR-Mutant Non-Small-Cell Lung Cancer. *Lancet Respir. Med.* **2020**, *8*, 1068–1070, doi:10.1016/S2213-2600(20)30171-5.

52. Okimoto, R.A.; Bivona, T.G. AXL Receptor Tyrosine Kinase as a Therapeutic Target in NSCLC. *Lung Cancer Targets Ther.* **2015**, *6*, 27–34, doi:10.2147/LCTT.S60438.

53. Raoof, S.; Mulford, I.J.; Frisco-Cabanos, H.; Nangia, V.; Timonina, D.; Labrot, E.; Hafeez, N.; Bilton, S.J.; Drier, Y.; Ji, F.; et al. Targeting FGFR Overcomes EMT-Mediated Resistance in EGFR Mutant Non-Small Cell Lung Cancer. *Oncogene* **2019**, *38*, 6399–6413, doi:10.1038/s41388-019-0887-2.

54. Mittal, V. Epithelial Mesenchymal Transition in Tumor Metastasis. *Annu. Rev. Pathol. Mech. Dis.* **2018**, *13*, 395–412, doi:10.1146/annurev-pathol-020117-043854.

55. Papadimitrakopoulou, V.A.; Wu, Y.-L.; Han, J.-Y.; Ahn, M.-J.; Ramalingam, S.S.; John, T.; Okamoto, I.; Yang, J.C.-H.; Bulusu, K.C.; Laus, G.; et al. Analysis of Resistance Mechanisms to Osimertinib in Patients with EGFR T790M Advanced NSCLC from the AURA3 Study. *Ann. Oncol.* **2018**, *29*, viii741, doi:10.1093/annonc/mdy424.064.

56. Weng, C.H.; Chen, L.Y.; Lin, Y.C.; Shih, J.Y.; Lin, Y.C.; Tseng, R.Y.; Chiu, A.C.; Yeh, Y.H.; Liu, C.; Lin, Y.T.; et al. Epithelial-Mesenchymal Transition (EMT) beyond EGFR Mutations per Se Is a Common Mechanism for Acquired Resistance to EGFR TKI. *Oncogene* **2019**, *38*, 455–468, doi:10.1038/s41388-018-0454-2.

57. Ramalingam, S.S.; Cheng, Y.; Zhou, C.; Ohe, Y.; Imamura, F.; Cho, B.C.; Lin, M.-C.; Majem, M.; Shah, R.; Rukazenkov, Y.; et al. Mechanisms of Acquired Resistance to First-Line Osimertinib: Preliminary Data from the Phase III FLAURA Study. *Ann. Oncol.* **2018**, *29*, viii740, doi:10.1093/annonc/mdy424.063.

58. Sadreddini, S.; Baradaran, B.; Aghebati-Maleki, A.; Sadreddini, S.; Shanehbandi, D.; Fotouhi, A.; Aghebati-Maleki, L. Immune Checkpoint Blockade Opens a New Way to Cancer Immunotherapy. *J. Cell. Physiol.* **2019**, *234*, 8541–8549, doi:10.1002/jcp.27816.

59. Anandappa, A.J.; Wu, C.J.; Ott, P.A. Directing Traffic: How to Effectively Drive T Cells into Tumors. *Cancer Discov.* **2020**, *10*, 185–197, doi:10.1158/2159-8290.CD-19-0790.

60. Wang, L.; Lui, V.W.Y. Emerging Roles of ALK in Immunity and Insights for Immunotherapy. *Cancers (Basel).* **2020**, *12*, doi:10.3390/cancers12020426.

61. Ota, K.; Azuma, K.; Kawahara, A.; Hattori, S.; Iwama, E.; Tanizaki, J.; Harada, T.; Matsumoto, K.; Takayama, K.; Takamori, S.; et al. Induction of PD-L1 Expression by the EML4–ALK Oncoprotein and Downstream Signaling

Pathways in Non–Small Cell Lung Cancer. *Clin. Cancer Res.* **2015**, *21*, 4014–4021, doi:10.1158/1078-0432.CCR-15-0016.

62. Soo, R.A.; Kim, H.R.; Asuncion, B.R.; Fazreen, Z.; Omar, M.F.M.; Herrera, M.C.; Yun Lim, J.S.; Sia, G.; Soong, R.; Cho, B.C. Significance of Immune Checkpoint Proteins in EGFR-Mutant Non-Small Cell Lung Cancer. *Lung Cancer* **2017**, *105*, 17–22, doi:10.1016/j.lungcan.2017.01.008.

63. Gettinger, S.; Rizvi, N.A.; Chow, L.Q.; Borghaei, H.; Brahmer, J.; Ready, N.; Gerber, D.E.; Shepherd, F.A.; Antonia, S.; Goldman, J.W.; et al. Nivolumab Monotherapy for First-Line Treatment of Advanced Non-Small-Cell Lung Cancer. *J. Clin. Oncol.* **2016**, *34*, 2980–2987, doi:10.1200/JCO.2016.66.9929.

64. Garon, E.B.; Hellmann, M.D.; Rizvi, N.A.; Carcereny, E.; Leighl, N.B.; Ahn, M.J.; Eder, J.P.; Balmanoukian, A.S.; Aggarwal, C.; Horn, L.; et al. Five-Year Overall Survival for Patients with Advanced Non-Small-Cell Lung Cancer Treated with Pembrolizumab: Results from the Phase i KEYNOTE-001 Study. *J. Clin. Oncol.* **2019**, *37*, 2518–2527, doi:10.1200/JCO.19.00934.

65. Lisberg, A.; Cummings, A.; Goldman, J.W.; Bornazyan, K.; Reese, N.; Wang, T.; Coluzzi, P.; Ledezma, B.; Mendenhall, M.; Hunt, J.; et al. A Phase II Study of Pembrolizumab in EGFR-Mutant, PD-L1+, Tyrosine Kinase Inhibitor Naïve Patients With Advanced NSCLC. *J. Thorac. Oncol.* **2018**, *13*, 1138–1145, doi:10.1016/j.jtho.2018.03.035.

66. Peters, S.; Gettinger, S.; Johnson, M.L.; Jänne, P.A.; Garassino, M.C.; Christoph, D.; Toh, C.K.; Rizvi, N.A.; Chaft, J.E.; Costa, E.C.; et al. Phase II Trial of Atezolizumab as First-Line or Subsequent Therapy for Patients with Programmed Death-Ligand 1-Selected Advanced Non-Small-Cell Lung Cancer (BIRCH). *J. Clin. Oncol.* **2017**, *35*, 2781–2789, doi:10.1200/JCO.2016.71.9476.

67. Xia, B.; Nagasaka, M.; Zhu, V.W.; Ou, S.H.I.; Soo, R.A. How to Select the Best Upfront Therapy for Metastatic Disease? Focus on ALK-Rearranged Non-Small Cell Lung Cancer (NSCLC). *Transl. Lung Cancer Res.* **2020**, *9*, 2521–2534, doi:10.21037/tlcr-20-331.

68. Wu, L.; Ke, L.; Zhang, Z.; Yu, J.; Meng, X. Development of EGFR TKIs and Options to Manage Resistance of Third-Generation EGFR TKI Osimertinib: Conventional Ways and Immune Checkpoint Inhibitors. *Front. Oncol.* **2020**, *10*, doi:10.3389/fonc.2020.602762.

69. Klebanoff, C.A.; Rosenberg, S.A.; Restifo, N.P. Prospects for Gene-Engineered T Cell Immunotherapy for Solid Cancers. *Nat. Med.* **2016**, *22*, 26–36, doi:10.1038/nm.4015.

70. Soda, M.; Choi, Y.L.; Enomoto, M.; Takada, S.; Yamashita, Y.; Ishikawa, S.; Fujiwara, S.I.; Watanabe, H.; Kurashina, K.; Hatanaka, H.; et al. Identification of the Transforming EML4-ALK Fusion Gene in Non-Small-Cell Lung Cancer. *Nature* **2007**, *448*, 561–566, doi:10.1038/nature05945.

71. Zhang, S.S.; Nagasaka, M.; Zhu, V.W.; Ou, S.H.I. Going beneath the Tip of the Iceberg. Identifying and Understanding EML4-ALK Variants and TP53 Mutations to Optimize Treatment of ALK Fusion Positive (ALK+) NSCLC. *Lung Cancer* **2021**, *158*, 126–136, doi:10.1016/j.lungcan.2021.06.012.

72. Bayliss, R.; Choi, J.; Fennell, D.A.; Fry, A.M.; Richards, M.W. Molecular

Mechanisms That Underpin EML4-ALK Driven Cancers and Their Response to Targeted Drugs. *Cell. Mol. Life Sci.* **2016**, *73*, 1209–1224, doi:10.1007/s00018-015-2117-6.

73. Sakamoto, H.; Tsukaguchi, T.; Hiroshima, S.; Kodama, T.; Kobayashi, T.; Fukami, T.A.; Oikawa, N.; Tsukuda, T.; Ishii, N.; Aoki, Y. CH5424802, a Selective ALK Inhibitor Capable of Blocking the Resistant Gatekeeper Mutant. *Cancer Cell* **2011**, *19*, 679–690, doi:10.1016/j.ccr.2011.04.004.

74. Caccese, M.; Ferrara, R.; Pilotto, S.; Carbognin, L.; Grizzi, G.; Caliò, A.; Brunelli, M.; Cuppone, F.; Petraglia, S.; Scarpa, A.; et al. Current and Developing Therapies for the Treatment of Non-Small Cell Lung Cancer with ALK Abnormalities: Update and Perspectives for Clinical Practice. *Expert Opin. Pharmacother.* **2016**, *17*, 2253–2266, doi:10.1080/14656566.2016.1242578.

75. Pan, Y.; Deng, C.; Qiu, Z.; Cao, C.; Wu, F. The Resistance Mechanisms and Treatment Strategies for ALK-Rearranged Non-Small Cell Lung Cancer. *Front. Oncol.* **2021**, *11*, 1–13, doi:10.3389/fonc.2021.713530.

76. Taube, J.M.; Galon, J.; Sholl, L.M.; Rodig, S.J.; Cottrell, T.R.; Giraldo, N.A.; Baras, A.S.; Patel, S.S.; Anders, R.A.; Rimm, D.L.; et al. Implications of the Tumor Immune Microenvironment for Staging and Therapeutics. *Mod. Pathol.* **2018**, *31*, 214–234, doi:10.1038/modpathol.2017.156.

77. Fukui, T.; Tachihara, M.; Nagano, T.; Kobayashi, K. Review of Therapeutic Strategies for Anaplastic Lymphoma Kinase-Rearranged Non-Small Cell Lung Cancer. *Cancers (Basel).* **2022**, *14*, doi:10.3390/cancers14051184.

78. Spigel, D.R.; Reynolds, C.; Waterhouse, D.; Garon, E.B.; Chandler, J.; Babu, S.; Thurmes, P.; Spira, A.; Jotte, R.; Zhu, J.; et al. Phase 1/2 Study of the Safety and Tolerability of Nivolumab Plus Crizotinib for the First-Line Treatment of Anaplastic Lymphoma Kinase Translocation — Positive Advanced Non–Small Cell Lung Cancer (CheckMate 370). *J. Thorac. Oncol.* **2018**, *13*, 682–688, doi:10.1016/j.jtho.2018.02.022.

79. Patel, S.P.; Pakkala, S.; Pennell, N.A.; Reckamp, K.L.; Lanzalone, S.; Polli, A.; Tarazi, J.; Robert-Vizcarrondo, F. Phase Ib Study of Crizotinib plus Pembrolizumab in Patients with Previously Untreated Advanced Non-Small Cell Lung Cancer with ALK Translocation . *Oncologist* **2020**, *25*, 562-e1012, doi:10.1634/theoncologist.2020-0034.

80. Maddalo, D.; Manchado, E.; Concepcion, C.P.; Bonetti, C.; Vidigal, J.A.; Han, Y.C.; Ogrodowski, P.; Crippa, A.; Rekhtman, N.; Stanchina, E. De; et al. In Vivo Engineering of Oncogenic Chromosomal Rearrangements with the CRISPR/Cas9 System. *Nature* **2014**, *516*, 423–428, doi:10.1038/nature13902.

81. Meder, L.; Schuldt, P.; Thelen, M.; Schmitt, A.; Dietlein, F.; Klein, S.; Borchmann, S.; Wennhold, K.; Vlasic, I.; Oberbeck, S.; et al. Combined VEGF and PD-L1 Blockade Displays Synergistic Treatment Effects in an Autochthonous Mouse Model of Small Cell Lung Cancer. *Cancer Res.* **2018**, *78*, 4270–4281, doi:10.1158/0008-5472.CAN-17-2176.

82. Kodama, T.; Tsukaguchi, T.; Yoshida, M.; Kondoh, O.; Sakamoto, H. Selective ALK Inhibitor Alectinib with Potent Antitumor Activity in Models of Crizotinib Resistance. *Cancer Lett.* **2014**, *351*, 215–221, doi:10.1016/j.canlet.2014.05.020.

83. Vogelstein, B.; Lane, D.; J. Levine, A. Surfing P53 Network. *Nature* **2000**, *408*, 307–310.

84. Aisner, D.L.; Sholl, L.M.; Berry, L.D.; Rossi, M.R.; Chen, H.; Fujimoto, J.; Moreira, A.L.; Ramalingam, S.S.; Villaruz, L.C.; Otterson, G.A.; et al. The Impact of Smoking and Tp53 Mutations in Lung Adenocarcinoma Patients with Targetable Mutations—the Lung Cancer Mutation Consortium (LCMC2). *Clin. Cancer Res.* **2018**, *24*, 1038–1047, doi:10.1158/1078-0432.CCR-17-2289.

85. Alidousty, C.; Baar, T.; Martelotto, L.G.; Heydt, C.; Wagener, S.; Fassunke, J.; Duerbaum, N.; Scheel, A.H.; Frank, S.; Holz, B.; et al. Genetic Instability and Recurrent MYC Amplification in ALK-Translocated NSCLC: A Central Role of TP53 Mutations. *J. Pathol.* **2018**, *246*, 67–76, doi:10.1002/path.5110.

86. Viswanadhapalli, S.; Dileep, K. V.; Zhang, K.Y.J.; Nair, H.B.; Vadlamudi, R.K. Targeting LIF/LIFR Signaling in Cancer. *Genes Dis.* **2022**, *9*, 973–980, doi:10.1016/j.gendis.2021.04.003.

87. Aliper, A.M.; Frieden-Korovkina, V.P.; Buzdin, A.; Roumiantsev, S.A.; Zhavoronkov, A. A Role for G-CSF and GM-CSF in Nonmyeloid Cancers. *Cancer Med.* **2014**, *3*, 737–746, doi:10.1002/cam4.239.

88. Hucks, G.; Rheingold, S.R. The Journey to CAR T Cell Therapy: The Pediatric and Young Adult Experience with Relapsed or Refractory B-ALL. *Blood Cancer J.* **2019**, *9*, doi:10.1038/s41408-018-0164-6.

89. Walker, A.J.; Majzner, R.G.; Zhang, L.; Wanhainen, K.; Long, A.H.; Nguyen, S.M.; Lopomo, P.; Vigny, M.; Fry, T.J.; Orentas, R.J.; et al. Tumor Antigen and Receptor Densities Regulate Efficacy of a Chimeric Antigen Receptor Targeting Anaplastic Lymphoma Kinase. *Mol. Ther.* **2017**, *25*, 2189–2201, doi:10.1016/j.ymthe.2017.06.008.

90. Surawska, H.; Ma, P.C.; Salgia, R. The Role of Ephrins and Eph Receptors in Cancer. *Cytokine Growth Factor Rev.* **2004**, *15*, 419–433, doi:10.1016/j.cytogfr.2004.09.002.

91. Ireton, R.; Chen, J. EphA2 Receptor Tyrosine Kinase as a Promising Target for Cancer Therapeutics. *Curr. Cancer Drug Targets* **2005**, *5*, 149–157, doi:10.2174/1568009053765780.

92. Miao, H.; Burnett, E.; Kinch, M.; Simon, E.; Wang, B. Activation of EphA2 Kinase Suppresses Integrin Function and Causes Focal-Adhesion-Kinase Dephosphorylation. *Nat. Cell Biol.* **2000**, *2*, 62–69, doi:10.1038/35000008.

93. Zantek, N.D.; Azimi, M.; Fedor-Chaiken, M.; Wang, B.; Brackenbury, R.; Kinch, M.S. E-Cadherin Regulates the Function of the EphA2 Receptor Tyrosine Kinase. *Cell Growth Differ.* **1999**, *10*, 629–638.

94. Brantley-Sieders, D.M.; Caughron, J.; Hicks, D.; Pozzi, A.; Ruiz, J.C.; Chen, J. EphA2 Receptor Tyrosine Kinase Regulates Endothelial Cell Migration and Vascular Assembly through Phosphoinositide 3-Kinase-Mediated Rac1 GTPase Activation. *J. Cell Sci.* **2004**, *117*, 2037–2049, doi:10.1242/jcs.01061.

95. Brantley-Sieders, D.M.; Zhuang, G.; Hicks, D.; Wei, B.F.; Hwang, Y.; Cates, J.M.M.; Coffman, K.; Jackson, D.; Bruckheimer, E.; Muraoka-Cook, R.S.; et al. The Receptor Tyrosine Kinase EphA2 Promotes Mammary Adenocarcinoma

Tumorigenesis and Metastatic Progression in Mice by Amplifying ErbB2 Signaling. *J. Clin. Invest.* **2008**, *118*, 64–78, doi:10.1172/JCI33154.

96. Fang, W. Bin; Brantley-Sieders, D.M.; Parker, M.A.; Reith, A.D.; Chen, J. A Kinase-Dependent Role for EphA2 Receptor in Promoting Tumor Growth and Metastasis. *Oncogene* **2005**, *24*, 7859–7868, doi:10.1038/sj.onc.1208937.

97. Brantley-Sieders, D.M.; Fang, W. Bin; Hicks, D.J.; Zhuang, G.; Shyr, Y.; Chen, J. Impaired Tumor Microenvironment in EphA2-deficient Mice Inhibits Tumor Angiogenesis and Metastatic Progression. *FASEB J.* **2005**, *19*, 1884–1886, doi:10.1096/fj.05-4038fje.

98. Brannan, J.M.; Dong, W.; Prudkin, L.; Behrens, C.; Lotan, R.; Bekele, B.N.; Wistuba, I.; Johnson, F. Expression of the Receptor Tyrosine Kinase EphA2 Is Increased in Smokers and Predicts Poor Survival in Non -Small Cell Lung Cancer. *Clin. Cancer Res.* **2009**, *15*, 4423–4430, doi:10.1158/1078-0432.CCR-09-0473.

99. Kinch, M.S.; Moore, M.B.; Harpole, D.H. Predictive Value of the EphA2 Receptor Tyrosine Kinase in Lung Cancer Recurrence and Survival. *Clin. Cancer Res.* **2003**, *9*, 613–618.

100. Amato, K.R.; Gray, N.S.; Chen, J.; Amato, K.R.; Wang, S.; Hastings, A.K.; Youngblood, V.M.; Santapuram, P.R.; Chen, H.; Cates, J.M.; et al. Genetic and Pharmacologic Inhibition of EPHA2 Promotes Apoptosis in NSCLC. **2014**, *124*, 2037–2049, doi:10.1172/JCI72522.increases.

101. Brannan, J.M.; Sen, B.; Saigal, B.; Prudkin, L.; Behrens, C.; Solis, L.; Dong, W.; Bekele, B.N.; Wistuba, I.; Johnson, F.M. EphA2 in the Early Pathogenesis and Progression of Non-Small Cell Lung Cancer. *Cancer Prev. Res.* **2009**, *2*, 1039–1049, doi:10.1158/1940-6207.CAPR-09-0212.

102. Miao, B.; Ji, Z.; Tan, L.; Taylor, M.; Zhang, J.; Choi, H.G.; Frederick, D.T.; Kumar, R.; Wargo, J.A.; Flaherty, K.T.; et al. EPHA2 Is a Mediator of Vemurafenib Resistance and a Novel Therapeutic Target in Melanoma. *Cancer Discov.* **2015**, *5*, 274–287, doi:10.1158/2159-8290.CD-14-0295.

103. Merritt, W.M.; Kamat, A.A.; Hwang, J.Y.; Bottsford-Miller, J.; Lu, C.; Lin, Y.G.; Coffey, D.; Spannuth, W.; Nugent, E.; Han, L.Y.; et al. Clinical and Biological Impact of EphA2 Overexpression and Angiogenesis in Endometrial Cancer. *Cancer Biol. Ther.* **2010**, *10*, 1306–1314, doi:10.4161/cbt.10.12.13582.

104. Allocca, C.; Cirafici, A.M.; Laukkanen, M.O.; Castellone, M.D. Serine 897 Phosphorylation of EPHA2 Is Involved in Signaling of Oncogenic ERK1/2 Drivers in Thyroid Cancer Cells. *Thyroid* **2021**, *31*, 76–87, doi:10.1089/thy.2019.0728.

105. Dungo, R.T.; Keating, G.M. Afatinib: First Global Approval. *Drugs* **2013**, *73*, 1503–1515, doi:10.1007/s40265-013-0111-6.

106. Greig, S.L. Osimertinib: First Global Approval. *Drugs* **2016**, *76*, 263–273, doi:10.1007/s40265-015-0533-4.

107. Remon, J.; Steuer, C.E.; Ramalingam, S.S.; Felip, E. Osimertinib and Other Third-Generation EGFR TKI in EGFR-Mutant NSCLC Patients. *Ann. Oncol.* **2018**, *29*, i20–i27, doi:10.1093/annonc/mdx704.

108. Kim, T.M.; Song, A.; Kim, D.W.; Kim, S.; Ahn, Y.O.; Keam, B.; Jeon, Y.K.; Lee, S.H.; Chung, D.H.; Heo, D.S. Mechanisms of Acquired Resistance to AZD9291: A Mutation-Selective, Irreversible EGFR Inhibitor. *J. Thorac. Oncol.* **2015**, *10*, 1736–1744, doi:10.1097/JTO.0000000000000688.

109. Tang, Z.H.; Lu, J.J. Osimertinib Resistance in Non-Small Cell Lung Cancer: Mechanisms and Therapeutic Strategies. *Cancer Lett.* **2018**, *420*, 242–246, doi:10.1016/j.canlet.2018.02.004.

110. Le, X.; Puri, S.; Negrao, M. V.; Nilsson, M.B.; Robichaux, J.; Boyle, T.; Kevin Hicks, J.; Lovinger, K.L.; Roarty, E.; Rinsurongkawong, W.; et al. Landscape of EGFR-Dependent and -Independent Resistance Mechanisms to Osimertinib and Continuation Therapy beyond Progression in EGFR-Mutant NSCLC. *Clin. Cancer Res.* **2018**, *24*, 6195–6203, doi:10.1158/1078-0432.CCR-18-1542.

111. Ortiz-Cuaran, S.; Scheffler, M.; Plenker, D.; Dahmen, L.; Scheel, A.H.; Fernandez-Cuesta, L.; Meder, L.; Lovly, C.M.; Persigehl, T.; Merkelbach-Bruse, S.; et al. Heterogeneous Mechanisms of Primary and Acquired Resistance to Third-Generation EGFR Inhibitors. *Clin. Cancer Res.* **2016**, *22*, 4837–4847, doi:10.1158/1078-0432.CCR-15-1915.

112. Piotrowska, Z.; Niederst, M.J.; Karlovich, C.A.; Wakelee, H.A.; Neal, J.W.; Mino-Kenudson, M.; Fulton, L.; Hata, A.N.; Lockerman, E.L.; Kalsy, A.; et al. Heterogeneity Underlies the Emergence of EGFRT790wild-Type Clones Following Treatment of T790M-Positive Cancers with a Third-Generation EGFR Inhibitor. *Cancer Discov.* **2015**, *5*, 713–723, doi:10.1158/2159-8290.CD-15-0399.

113. Bivona, T.G.; Hieronymus, H.; Parker, J.; Chang, K.; Taron, M.; Rosell, R.; Moonsamy, P.; Dahlman, K.; Miller, V.A.; Costa, C.; et al. FAS and NF-KB Signalling Modulate Dependence of Lung Cancers on Mutant EGFR. *Nature* **2011**, *471*, 523–526, doi:10.1038/nature09870.

114. Cho, B.C.; Piotrowska, Z.; Le, X.; Goldberg, S.B.; Goldman, J.; De Langen, A.; Okamoto, I.; Smith, P.; Mensi, I.; Maidment, J.; et al. P76.27 ORCHARD: A Biomarker-Directed Phase 2 Platform Study in Pts with Advanced EGFRm NSCLC Progressing on First-Line Osimertinib. *J. Thorac. Oncol.* **2021**, *16*, S598, doi:10.1016/j.jtho.2021.01.1084.

115. Oxnard, G.R.; Yang, J.C.H.; Yu, H.; Kim, S.W.; Saka, H.; Horn, L.; Goto, K.; Ohe, Y.; Mann, H.; Thress, K.S.; et al. TATTON: A Multi-Arm, Phase Ib Trial of Osimertinib Combined with Selumetinib, Savolitinib, or Durvalumab in EGFR-Mutant Lung Cancer. *Ann. Oncol.* **2020**, *31*, 507–516, doi:10.1016/j.annonc.2020.01.013.

116. La Monica, S.; Cretella, D.; Bonelli, M.; Fumarola, C.; Cavazzoni, A.; Digiacomo, G.; Flammini, L.; Barocelli, E.; Minari, R.; Naldi, N.; et al. Trastuzumab Emtansine Delays and Overcomes Resistance to the Third-Generation EGFR-TKI Osimertinib in NSCLC EGFR Mutated Cell Lines. *J. Exp. Clin. Cancer Res.* **2017**, *36*, 1–12, doi:10.1186/s13046-017-0653-7.

117. Wright, N.M.A.; Goss, G.D. Third-Generation Epidermal Growth Factor Receptor Tyrosine Kinase Inhibitors for the Treatment of Non-Small Cell Lung Cancer. **2019**, *8*, doi:10.21037/tlcr.2019.06.01.

118. Lim, S.M.; Syn, N.L.; Cho, B.C.; Soo, R.A. Acquired Resistance to EGFR Targeted Therapy in Non-Small Cell Lung Cancer: Mechanisms and Therapeutic Strategies. *Cancer Treat. Rev.* **2018**, *65*, 1–10, doi:10.1016/j.ctrv.2018.02.006.

119. Haratani, K.; Hayashi, H.; Tanaka, T.; Kaneda, H.; Togashi, Y.; Sakai, K.; Hayashi, K.; Tomida, S.; Chiba, Y.; Yonesaka, K.; et al. Tumor Immune Microenvironment and Nivolumab Efficacy in EGFR Mutation-Positive Non-Small-Cell Lung Cancer Based on T790M Status after Disease Progression during EGFR-TKI Treatment. *Ann. Oncol.* **2017**, *28*, 1532–1539, doi:10.1093/annonc/mdx183.

120. Su, S.; Dong, Z.-Y.; Xie, Z.; Yan, L.-X.; Li, Y.-F.; Su, J.; Liu, S.-Y.; Yin, K.; Chen, R.-L.; Huang, S.-M.; et al. Strong Programmed Death Ligand 1 Expression Predicts Poor Response and De Novo Resistance to EGFR Tyrosine Kinase Inhibitors Among NSCLC Patients With EGFR Mutation. *J. Thorac. Oncol.* **2018**, *13*, 1668–1675, doi:10.1016/j.jtho.2018.07.016.

121. Moschella, F.; Proietti, E.; Capone, I.; Belardelli, F. Combination Strategies for Enhancing the Efficacy of Immunotherapy in Cancer Patients. *Ann. N. Y. Acad. Sci.* **2010**, *1194*, 169–178, doi:10.1111/j.1749-6632.2010.05464.x.

122. Akbay, E.A.; Koyama, S.; Carretero, J.; Altabef, A.; Tchaicha, J.H.; Christensen, C.L.; Mikse, O.R.; Cherniack, A.D.; Beauchamp, E.M.; Pugh, T.J.; et al. Activation of the PD-1 Pathway Contributes to Immune Escape in EGFR-Driven Lung Tumors. *Cancer Discov.* **2013**, *3*, 1355–1363, doi:10.1158/2159-8290.CD-13-0310.

123. Lin, K.; Cheng, J.; Yang, T.; Li, Y.; Zhu, B. EGFR-TKI down-Regulates PD-L1 in EGFR Mutant NSCLC through Inhibiting NF-KB. *Biochem. Biophys. Res. Commun.* **2015**, *463*, 95–101, doi:10.1016/j.bbrc.2015.05.030.

124. Oshima, Y.; Tanimoto, T.; Yuji, K.; Tojo, A. EGFR-TKI-Associated Interstitial Pneumonitis in Nivolumab-Treated Patients with Non-Small Cell Lung Cancer. *JAMA Oncol.* **2018**, *4*, 1112–1115, doi:10.1001/jamaoncol.2017.4526.

125. Ahn, M.J.; Yang, J.; Yu, H.; Saka, H.; Ramalingam, S.; Goto, K.; Kim, S.W.; Yang, L.; Walding, A.; Oxnard, G.R. 136O: Osimertinib Combined with Durvalumab in EGFR-Mutant Non-Small Cell Lung Cancer: Results from the TATTON Phase Ib Trial. *J. Thorac. Oncol.* **2016**, *11*, S115, doi:10.1016/S1556-0864(16)30246-5.

126. Gibbons, D.L.; Chow, L.Q.; Kim, D.W.; Kim, S.W.; Yeh, T.; Song, X.; Jiang, H.; Taylor, R.; Karakunnel, J.; Creelan, B. 57O Efficacy, Safety and Tolerability of MEDI4736 (Durvalumab [D]), a Human IgG1 Anti-Programmed Cell Death-Ligand-1 (PD-L1) Antibody, Combined with Gefitinib (G): A Phase I Expansion in TKI-Naïve Patients (Pts) with EGFR Mutant NSCLC. *J. Thorac. Oncol.* **2016**, *11*, S79, doi:10.1016/S1556-0864(16)30171-X.

127. Ma, B.B.Y.; Rudin, C.M.; Cervantes, A.; Dowlati, A.; Costa, D.; Schmid, P.; Heist, R.; Villaflor, V.M.; Sarkar, I.; Huseni, M.A.; et al. 441O Preliminary Safety and Clinical Activity of Erlotinib plus Atezolizumab from a Phase Ib Study in Advanced NSCLC. *Ann. Oncol.* **2016**, *27*, ix141, doi:10.1016/S0923-7534(21)00599-8.

128. Antonia, S.J.; Brahmer, J.R.; Gettinger, S.; Chow, L.Q.; Juergens, R.; Shepherd,

F.A.; Laurie, S.A.; Gerber, D.E.; Goldman, J.; Shen, Y.; et al. Nivolumab (Anti-PD-1; BMS-936558, ONO-4538) in Combination With Platinum-Based Doublet Chemotherapy (PT-DC) in Advanced Non-Small Cell Lung Cancer (NSCLC). *Int. J. Radiat. Oncol.* **2014**, *90*, S2, doi:10.1016/j.ijrobp.2014.08.024.

129. Gettinger, S.; Hellmann, M.D.; Chow, L.Q.M.; Borghaei, H.; Antonia, S.; Brahmer, J.R.; Goldman, J.W.; Gerber, D.E.; Juergens, R.A.; Shepherd, F.A.; et al. Nivolumab Plus Erlotinib in Patients With EGFR-Mutant Advanced NSCLC. *J. Thorac. Oncol.* **2018**, *13*, 1363–1372, doi:10.1016/j.jtho.2018.05.015.

130. Schoenfeld, A.J.; Arbour, K.C.; Rizvi, H.; Iqbal, A.N.; Gadgeel, S.M.; Girshman, J.; Kris, M.G.; Riely, G.J.; Yu, H.A.; Hellmann, M.D. Severe Immune-Related Adverse Events Are Common with Sequential PD-(L)1 Blockade and Osimertinib. *Ann. Oncol.* **2019**, 1–11, doi:10.1093/annonc/mdz077.

131. Ayeni, D.; Miller, B.; Kuhlmann, A.; Ho, P.C.; Robles-Oteiza, C.; Gaefele, M.; Levy, S.; De Miguel, F.J.; Perry, C.; Guan, T.; et al. Tumor Regression Mediated by Oncogene Withdrawal or Erlotinib Stimulates Infiltration of Inflammatory Immune Cells in EGFR Mutant Lung Tumors. *J. Immunother. Cancer* **2019**, *7*, 1–15, doi:10.1186/s40425-019-0643-8.

132. Sugiyama, E.; Togashi, Y.; Takeuchi, Y.; Shinya, S.; Tada, Y.; Kataoka, K.; Tane, K.; Sato, E.; Ishii, G.; Goto, K.; et al. Blockade of EGFR Improves Responsiveness to PD-1 Blockade in EGFR-Mutated Non-Small Cell Lung Cancer. *Sci. Immunol.* **2020**, *5*, doi:10.1126/sciimmunol.aav3937.

133. Okada, K.; Araki, M.; Sakashita, T.; Ma, B.; Kanada, R.; Yanagitani, N.; Horiike, A.; Koike, S.; Oh-hara, T.; Watanabe, K.; et al. Prediction of ALK Mutations Mediating ALK-TKIs Resistance and Drug Re-Purposing to Overcome the Resistance. *EBioMedicine* **2019**, *41*, 105–119, doi:10.1016/j.ebiom.2019.01.019.

134. Christopoulos, P.; Endris, V.; Bozorgmehr, F.; Elsayed, M.; Kirchner, M.; Ristau, J.; Buchhalter, I.; Penzel, R.; Herth, F.J.; Heussel, C.P.; et al. EML4-ALK Fusion Variant V3 Is a High-Risk Feature Conferring Accelerated Metastatic Spread, Early Treatment Failure and Worse Overall Survival in ALK+ Non-Small Cell Lung Cancer. *Int. J. Cancer* **2018**, *142*, 2589–2598, doi:10.1002/ijc.31275.

135. Lin, J.J.; Zhu, V.W.; Yoda, S.; Yeap, B.Y.; Schrock, A.B.; Dagogo-Jack, I.; Jessop, N.A.; Jiang, G.Y.; Le, L.P.; Gowen, K.; et al. Impact of EML4-ALK Variant on Resistance Mechanisms and Clinical Outcomes in ALK-Positive Lung Cancer. *J. Clin. Oncol.* **2018**, *36*, 1199–1206, doi:10.1200/JCO.2017.76.2294.

136. Guo, F.; Liu, X.; Qing, Q.; Sang, Y.; Feng, C.; Li, X.; Jiang, L.; Su, P.; Wang, Y. EML4-ALK Induces Epithelial-Mesenchymal Transition Consistent with Cancer Stem Cell Properties in H1299 Non-Small Cell Lung Cancer Cells. *Biochem. Biophys. Res. Commun.* **2015**, *459*, 398–404, doi:10.1016/j.bbrc.2015.02.114.

137. Voena, C.; Varesio, L.M.; Zhang, L.; Menotti, M.; Poggio, T.; Panizza, E.; Wang, Q.; Minero, V.G.; Fagoonee, S.; Compagno, M.; et al. Oncogenic ALK Regulates EMT in Non-Small Cell Lung Carcinoma through Repression of the Epithelial Splicing Regulatory Protein 1. *Oncotarget* **2016**, *7*, 33316–33330, doi:10.18632/oncotarget.8955.

138. Rihawi, K.; Alfieri, R.; Fiorentino, M.; Fontana, F.; Capizzi, E.; Cavazzoni, A.;

Terracciano, M.; La Monica, S.; Ferrarini, A.; Buson, G.; et al. MYC Amplification as a Potential Mechanism of Primary Resistance to Crizotinib in ALK-Rearranged Non-Small Cell Lung Cancer: A Brief Report. *Transl. Oncol.* **2019**, *12*, 116–121, doi:10.1016/j.tranon.2018.09.013.

139. Hong, S.; Chen, N.; Fang, W.; Zhan, J.; Liu, Q.; Kang, S.; He, X.; Liu, L.; Zhou, T.; Huang, J.; et al. Upregulation of PD-L1 by EML4-ALK Fusion Protein Mediates the Immune Escape in ALK Positive NSCLC: Implication for Optional Anti-PD-1/PD-L1 Immune Therapy for ALK-TKIs Sensitive and Resistant NSCLC Patients. *Oncoimmunology* **2016**, *5*, 1–12, doi:10.1080/2162402X.2015.1094598.

140. Koh, J.; Jang, J.Y.; Keam, B.; Kim, S.; Kim, M.Y.; Go, H.; Kim, T.M.; Kim, D.W.; Kim, C.W.; Jeon, Y.K.; et al. EML4-ALK Enhances Programmed Cell Death-Ligand 1 Expression in Pulmonary Adenocarcinoma via Hypoxia-Inducible Factor (HIF)-1α and STAT3. *Oncoimmunology* **2016**, *5*, 1–13, doi:10.1080/2162402X.2015.1108514.

141. Pyo, K.H.; Lim, S.M.; Park, C.W.; Jo, H.N.; Kim, J.H.; Yun, M.R.; Kim, D.; Xin, C.F.; Lee, W.; Gheorghiu, B.; et al. Comprehensive Analyses of Immunodynamics and Immunoreactivity in Response to Treatment in ALK-Positive Non-Small-Cell Lung Cancer. *J. Immunother. cancer* **2020**, *8*, doi:10.1136/jitc-2020-000970.

Erklärung zur Dissertation
gemäß der Promotionsordnung vom 12. März 2020

Hiermit versichere ich an Eides statt, dass ich die vorliegende Dissertation selbstständig und ohne die Benutzung anderer als der angegebenen Hilfsmittel und Literatur angefertigt habe. Alle Stellen, die wörtlich oder sinngemäß aus veröffentlichten und nicht veröffentlichten Werken dem Wortlaut oder dem Sinn nach entnommen wurden, sind als solche kenntlich gemacht. Ich versichere an Eides statt, dass diese Dissertation noch keiner anderen Fakultät oder Universität zur Prüfung vorgelegen hat; dass sie - abgesehen von unten angegebenen Teilpublikationen und eingebundenen Artikeln und Manuskripten - noch nicht veröffentlicht worden ist sowie, dass ich eine Veröffentlichung der Dissertation vor Abschluss der Promotion nicht ohne Genehmigung des Promotionsausschusses vornehmen werde. Die Bestimmungen dieser Ordnung sind mir bekannt. Darüber hinaus erkläre ich hiermit, dass ich die Ordnung zur Sicherung guter wissenschaftlicher Praxis und zum Umgang mit wissenschaftlichem Fehlverhalten der Universität zu Köln gelesen und sie bei der Durchführung der Dissertation zugrundeliegenden Arbeiten und der schriftlich verfassten Dissertation beachtet habe und verpflichte mich hiermit, die dort genannten Vorgaben bei allen wissenschaftlichen Tätigkeiten zu beachten und umzusetzen. Ich versichere, dass die eingereichte elektronische Fassung der eingereichten Druckfassung vollständig entspricht.

Teilpublikationen:

Volz, C.*, Breid, S.*, **Selenz, C.***, *et al.*, 2020 “Inhibition of Tumor VEGFR2 Induces Serine 897 EphA2- Dependent Tumor Cell Invasion and Metastasis in NSCLC”, *Cell Reports* 31(4).

* shared-first author

Selenz, C., *et al.*, 2022 “EGFR Inhibition Strongly Modulates the Tumour Immune Microenvironment in EGFR-Driven Non-Small-Cell Lung Cancer”, *Cancers* 14(16).

Borchmann, S., **Selenz, C.**, *et al.* “Tripartite antigen-agnostic combination immunotherapy cures established poorly immunogenic tumors“, *Journal for Immunotherapy of Cancer*, under 2nd review.

08.09.2022, Carolin Selenz 

Datum, Name und Unterschrift

Weitere Publikation, welche nicht in dieser Dissertation eingebunden ist:

Meder, L., Orschel, C., Otto, C., Koker, M., Brägelmann, J., Ercanoglu, M.S., Dähling, S., Compes, A., **Selenz, C.**, *et al.* “Integrin beta-1 signaling mediates tumor cell invasion and metastasis in small cell lung cancer“, *Science Translational Medicine* under submission.

Appendix

Chapter 2 – Supplementary materials

Cell Reports, Volume *31*

Supplemental Information

Inhibition of Tumor VEGFR2 Induces Serine 897 EphA2-Dependent Tumor Cell Invasion and Metastasis in NSCLC

Caroline Volz, Sara Breid, Carolin Selenz, Alina Zaplatina, Kristina Golfmann, Lydia Meder, Felix Dietlein, Sven Borchmann, Sampurna Chatterjee, Maike Siobal, Jakob Schöttle, Alexandra Florin, Mirjam Koker, Marieke Nill, Luka Ozretić, Niklas Uhlenbrock, Steven Smith, Reinhard Büttner, Hui Miao, Bingcheng Wang, H. Christian Reinhardt, Daniel Rauh, Michael Hallek, Amparo Acker-Palmer, Lukas C. Heukamp, and Roland T. Ullrich

Supplemental Figures

Figure S1

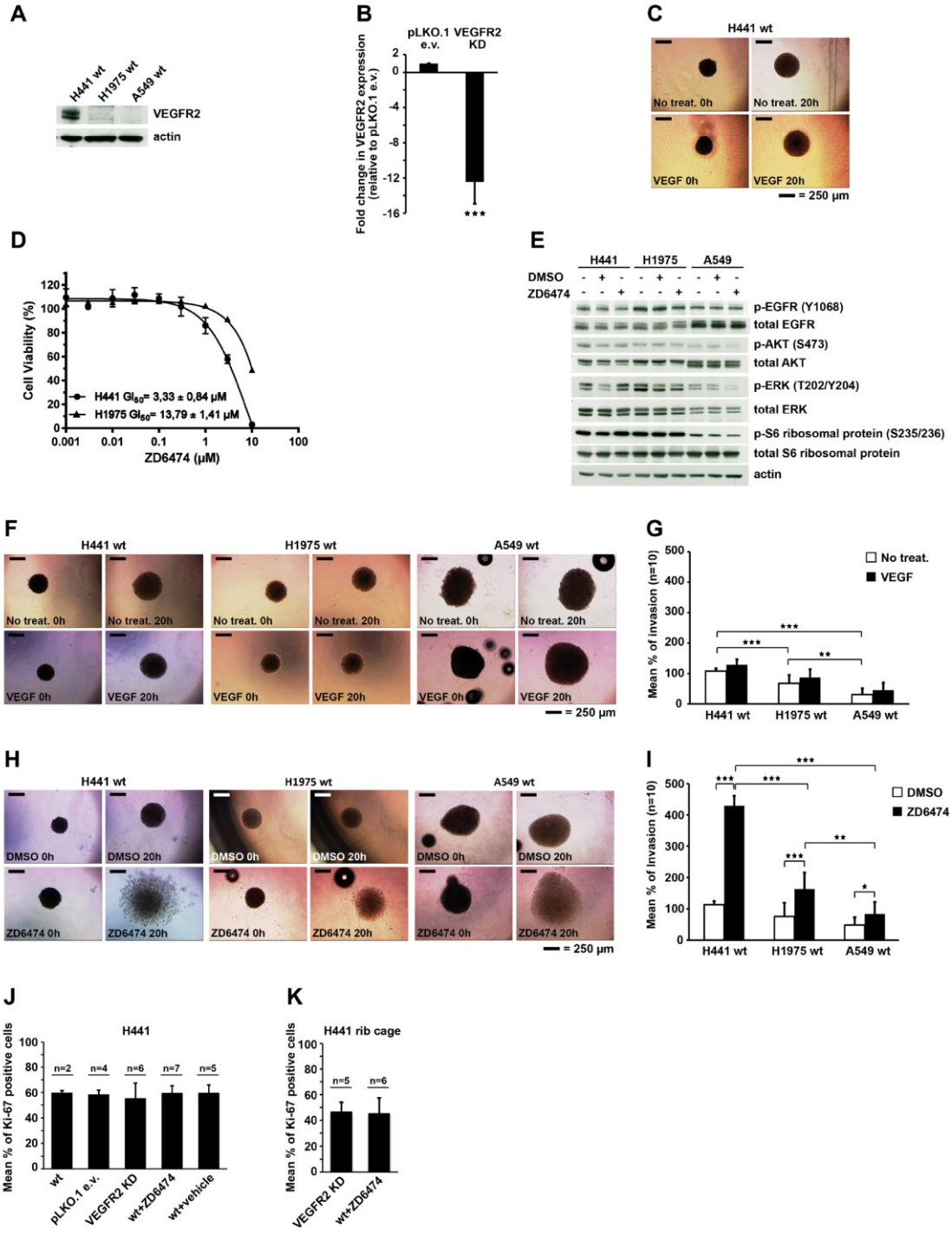

Figure S1. Specific knockdown of tumor VEGFR2 or drug-induced inhibition of VEGFR2 signaling in NSCLC cells induces an invasive phenotype *in vitro* and *in vivo*. Related to Figure 1. A, Western blot analysis of VEGFR2 expression in NSCLC cells. Actin served as loading control. H441 NSCLC cells have the highest VEGFR2 expression compared to H1975 and A549 NSCLC. **B**, qRT-PCR of VEGFR2 expression in H441 pLKO.1 e.v. and VEGFR2 KD cells. VEGFR2 KD cells showed up to 14 times reduced VEGFR2 expression compared to pLKO.1 e.v. cells. (***$p<0.001$) **C**, Representative invasion assay images for H441 wt spheroids with or without VEGF stimulation. **D**, Cell viability curve from CTG®-Assay with GI50 values for H441 and H1975 with ZD6474 treatment. **E**, Western blot analysis of resistance to EGFR inhibition by ZD6474 in three cell lines as indicated. Downstream signaling also showed no alteration upon ZD6474 treatment compared to DMSO control. **F-I**, Representative invasion assay images and the corresponding quantification as mean % of invasion (n=10) in three different NSCLC cell lines. H441, H1975 and A549 spheroids were not stimulated, VEGF- stimulated or treated with DMSO or ZD6474. VEGF stimulation had no effect on invasion whereas ZD6474 increased invasion all cell lines compared to DMSO control. (*$p<0.005$, **$p<0.01$,***$p<0.001$) **J and K**, Quantification of Ki-67- positive cells for orthotopically injected H441 tumors and rib cages as indicated. Line with number represents the number of mice for each group.

Figure S2

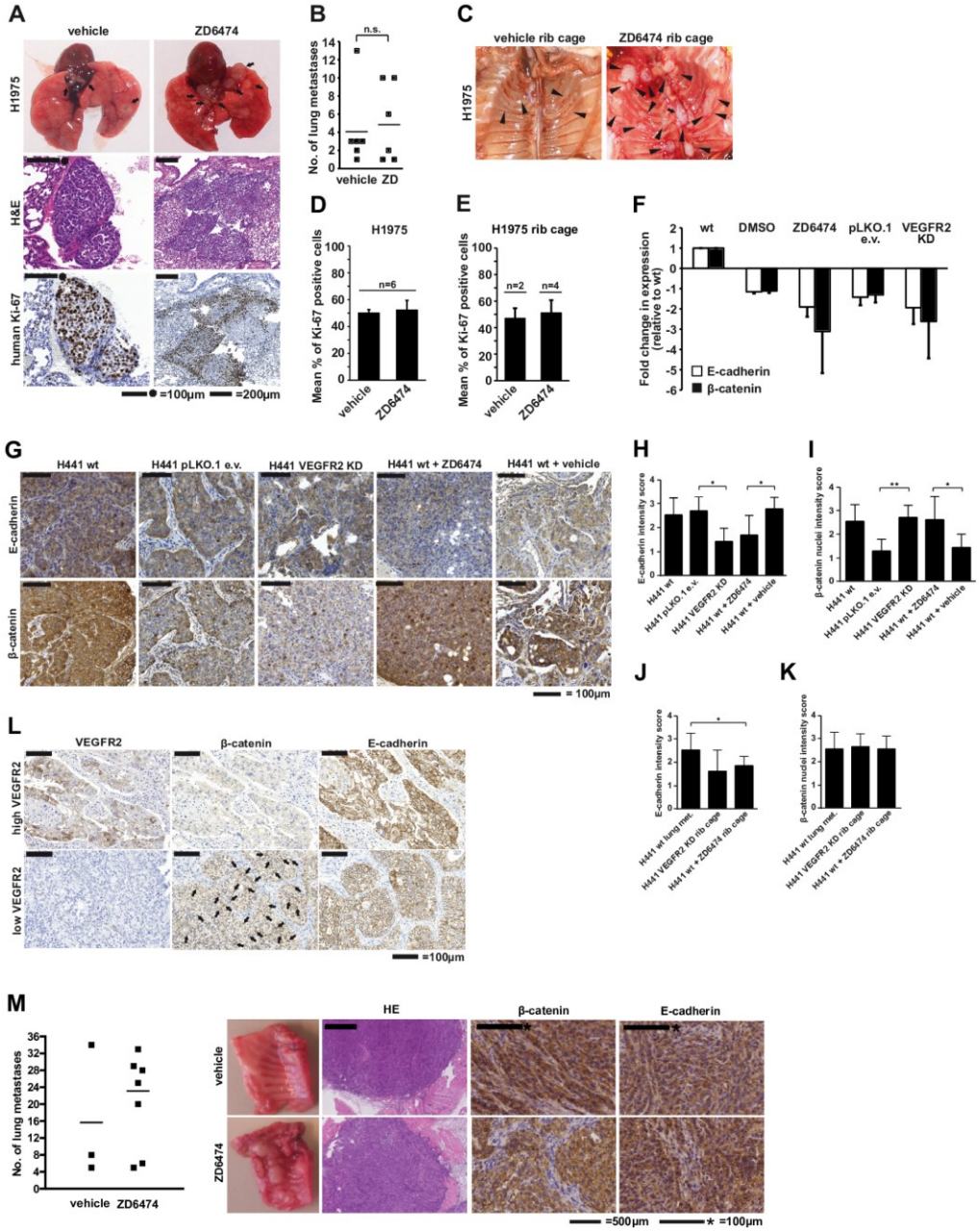
A
vehicle
ZD6474
H1975
H&E
human Ki-67
=100µm
=200µm
B
n.s.
No. of lung metastases
vehicle ZD
C
vehicle rib cage
ZD6474 rib cage
H1975
D
H1975
Mean % of Ki-67 positive cells
n=6
vehicle
ZD6474
E
H1975 rib cage
Mean % of Ki-67 positive cells
n=2
n=4
vehicle
ZD6474
F
wt
DMSO
ZD6474
pLKO.1 e.v.
VEGFR2 KD
Fold change in expression (relative to wt)
E-cadherin
β-catenin
G
H441 wt
H441 pLKO.1 e.v.
H441 VEGFR2 KD
H441 wt + ZD6474
H441 wt + vehicle
E-cadherin
β-catenin
= 100µm
H
E-cadherin intensity score
I
β-catenin nuclei intensity score
J
E-cadherin intensity score
K
β-catenin nuclei intensity score
L
VEGFR2
β-catenin
E-cadherin
high VEGFR2
low VEGFR2
=100µm
M
No. of lung metastases
vehicle ZD6474
HE
β-catenin
E-cadherin
vehicle
ZD6474
=500µm
=100µm

Figure S2. Drug-induced inhibition of VEGFR2 signaling in NSCLC cells induces a strong invasive phenotype *in vivo* in H1975 NSCLC and syngenic KP938.3 NSCLC. Related to Figure 1. A-C, Summary of orthotopically injected H1975 cells into lungs of nude mice. **A,** Representative photos and IHCs of resected lungs of the H1975 setting. Mice received vehicle (n=6) or ZD6474 (50mg/kg every second day) (n=6). ZD6474 treatment results in invasive tumor growth for H1975 cells. Black arrows indicate lung metastases. IHC staining of resected lungs for hematoxylin and eosin (H&E) and human Ki-67, indicating injected human tumor cells. Scale bars: 200µm or 100µm as indicated. **B,** Total amount of lung metastases for all mice in the H1975 setting. Each square represents one mouse (n.s.= not significant) and the line indicates the mean. **C,** Images of rib cages after lung resection. Vehicle treatment resulted in rib cages with very few infiltrating metastases. ZD6474 treatment shows strong infiltration of the rib cages with tumor mass. Black arrows highlight tumors. **D and E,** Quantification of Ki-67-positive cells for orthotopically injected H1975 tumors and rib cages as indicated. Line with number represents the number of mice for each group. **VEGFR2 inhibition induces an EMT-like phenotype**. **F,** qRT-PCR of E-cadherin and β-catenin expression in H441 wt, H441 pLKO.1 e.v. and VEGFR2 KD cells. The data are plotted relative to H441 wt cells. VEGFR2 inhibition reduced the expression of the two EMT-markers. **G,** Representative IHC stainings for E-cadherin and β-catenin of resected lungs from different H441 cells as indicated. Scale bars: 100µm. E-cadherin expression is slightly reduced under VEGFR2 inhibition compared to H441 wt. β-catenin shows increased translocation to the nucleus for VEGFR2 inhibition (KD or ZD6474) whereas wt cells showed membrane staining. **G-K,** Quantification of E-cadherin and β-catenin staining for resected lungs and rib cages as indicated. (*$p<0.005$, **$p<0.01$) n=9 for each group **L,** Two IHC examples for VEGFR2-high and -low expression in human NSCLC patient samples. The VEGFR2-high-expressing sample displayed β-catenin and E-cadherin expression at the membrane whereas the low-VEGFR2 sample showed higher incidence of β-catenin at the nucleus and lower expression of E-cadherin compared to the VEGFR2-high sample. Black arrows indicate nuclear staining for β-catenin. Scale bars: 100µm. **M,** Number of lung metastases found in the rib cage of the syngenic mouse model injected with KP938.3 tumor cells, either treated with vehicle or ZD6474. Each square represents one mouse and the line indicates the mean. Next to the number of lung metastases, representative images of the rib cage from vehicle-

and ZD6474-treated mice, and IHC stainings for H&E and EMT markers E-cadherin and β-catenin are shown. Scale bars: 100μm and 500μm.

Figure S3

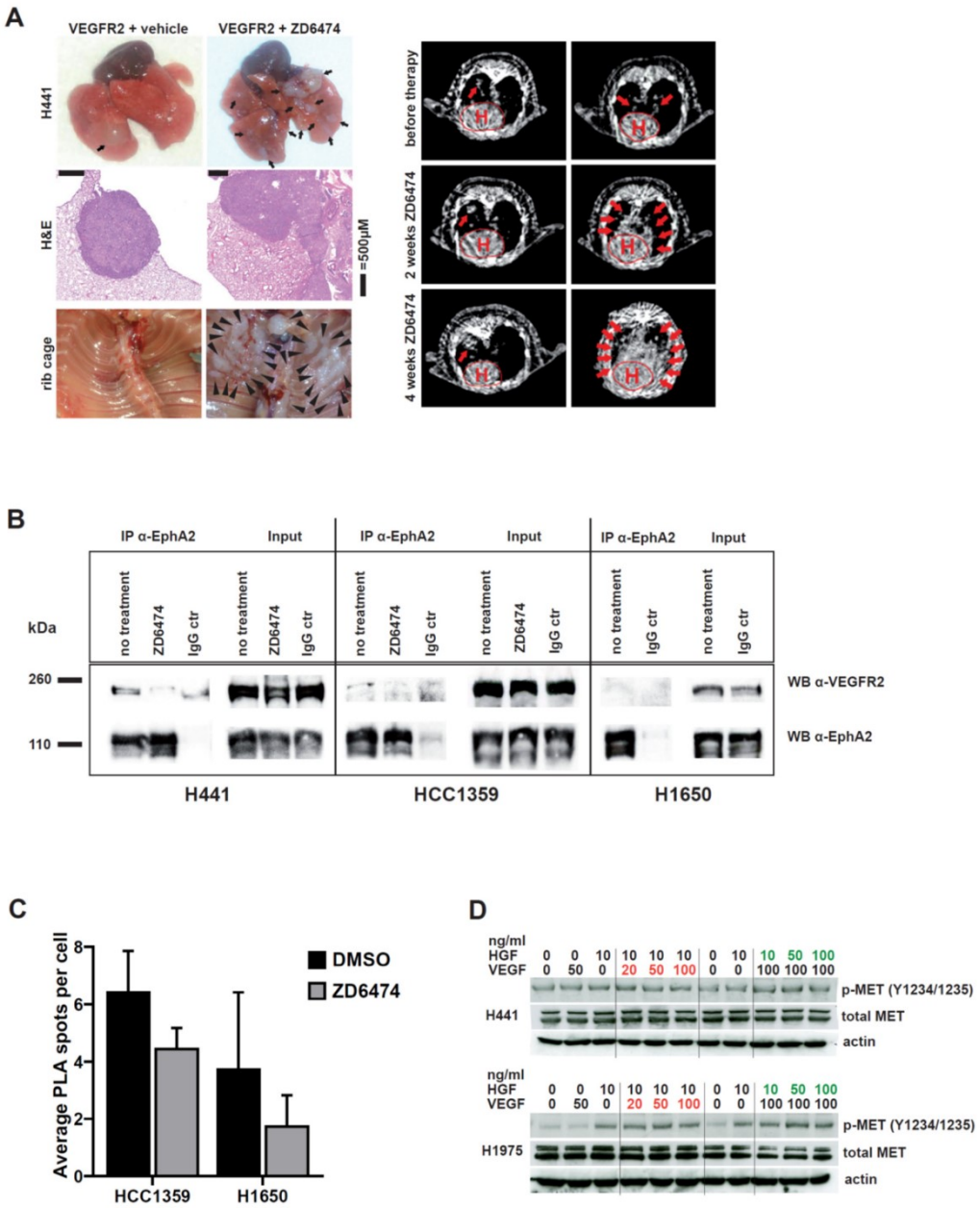

Figure S3. Inhibition of tumor cell VEGFR2 signaling and not antivascular effects within the tumor microenvironment induces an invasive phenotype in NSCLC. Related to Figure 2. A, Images, IHCs of resected lungs, µCT and rib cage images of orthotopically injected H441 VEGFR2 NSCLC cells into nude mice. Mice carrying H441 VEGFR2 cells received vehicle (n=6) or ZD6474 (n=6). Lung metastases are indicated by black arrows. IHC stainings of resected lungs for H&E. Images of infiltrated rib cages for VEGFR2 injected cells under vehicle and ZD6474 treatment. Representative µCT images before therapy, two and four weeks of ZD6474 or vehicle therapy. The heart is marked in red with a circle and the capital letter H. The tumors are indicated by red arrows. **Formation of VEGFR2-EphA2 heterocomplex is reduced upon VEGFR2 inhibition in HCC1359 and H1650 NSCLC cells. B**, Western blot analysis of VEGFR2 and EphA2 immunoprecipitation (IP) in H441, HCC1359 and H1650 NSCLC cells. Next to the normal cell lines without any treatment (no treatment), H441 and HCC1359 cells were also treated with ZD6474 and an unspecific IgG antibody was included as control. For input control, whole cell lysate was loaded using 10% of protein concentration used for the IP. **C**, HCC1359 and H1650 cells were used for PLA with ZD6474 treatment and DMSO as control. Quantfication of average PLA spots per cell in both cell lines as indicated. A decrease of interaction between VEGFR2 and EphA2 upon ZD6474 treatment can be observed. **MET signaling has no effect on VEGFR2 signaling in NSCLC. D**, Western blot analysis for pMET in H441 and H1975 cells. Cells were stimulated with different concentrations of VEGF and HGF or in combination as indicated. Western blots were stained for pMET, total MET and actin as loading control. VEGF or HGF stimulation had no effect on pMET in either cell lines.

Figure S4

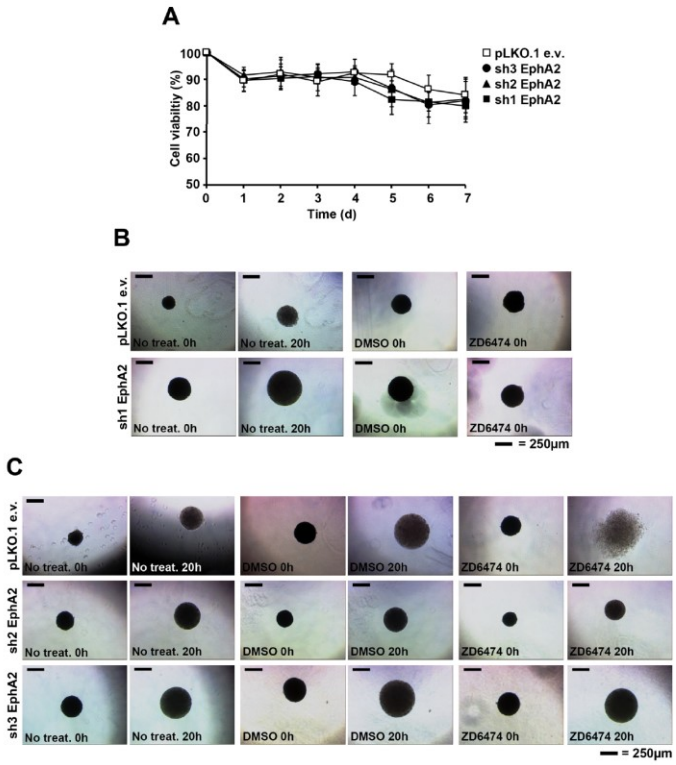

Figure S4. **EphA2 KD prevents VEGFR2 inhibition-induced tumor cell invasion *in vitro*. Related to Figure 3. A**, Viability curves of H441 pLKO.1 e.v. and sh-EphA2 harboring cells. EphA2 KD does not affect cell viability (n=9 for each group). **B**, Representative images of invasion assay for H441 pLKO.1 e.v. and sh1-EphA2 cells for no stimulation and the corresponding 0h images for DMSO and ZD6474 treatment. The 20h images are in Figure 3C. **C**, Representative images of invasion assay with H441 pLKO.1 e.v., sh2-EphA2 and sh3-EphA2 cells without stimulation, with DMSO and ZD6474 treatment. ZD6474 induced invasion in pLKO.1 e.v. cells, whereas the sh-constructs inhibited invasion.

Figure S5

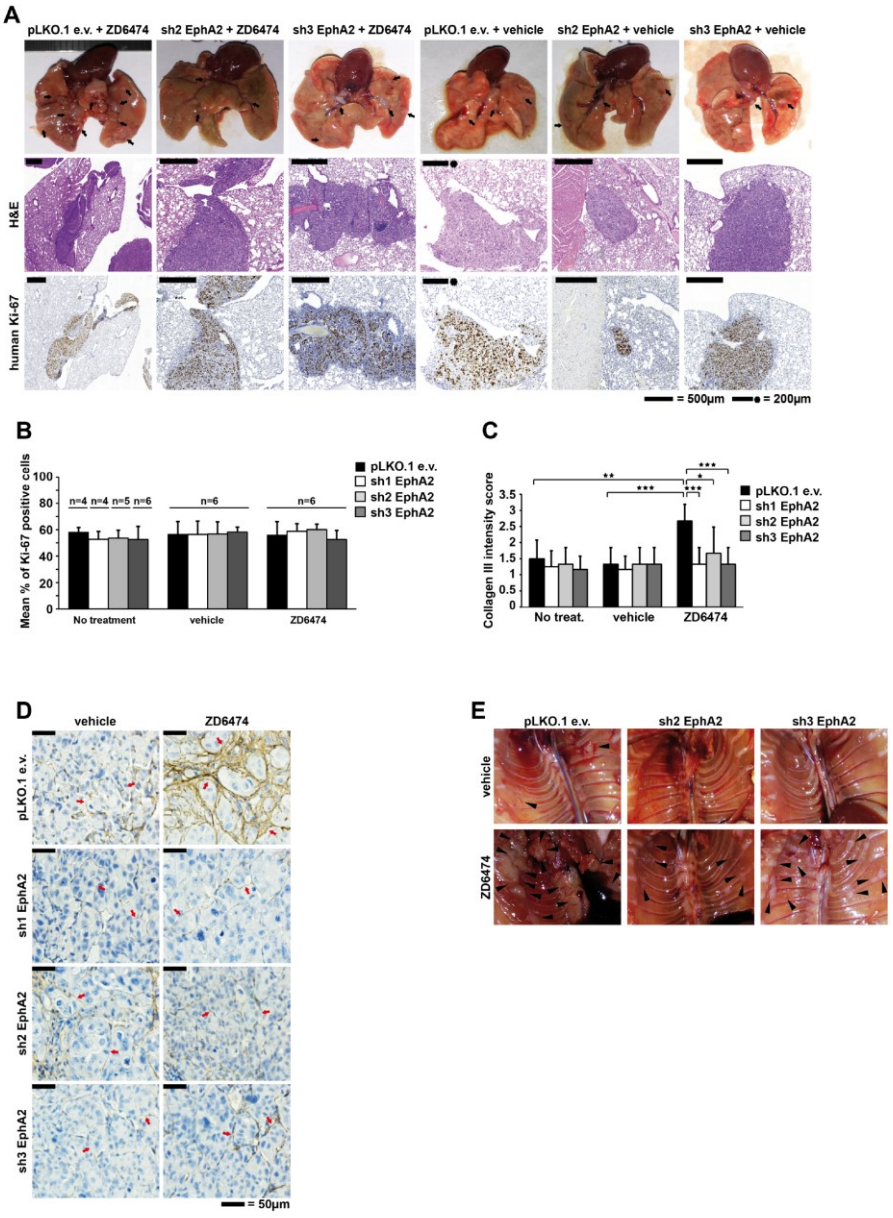
A
pLKO.1 e.v. + ZD6474
sh2 EphA2 + ZD6474
sh3 EphA2 + ZD6474
pLKO.1 e.v. + vehicle
sh2 EphA2 + vehicle
sh3 EphA2 + vehicle
H&E
human Ki-67
= 500µm
= 200µm
B
Mean % of Ki-67 positive cells
n=4 n=4 n=5 n=6
n=6
n=6
No treatment
vehicle
ZD6474
pLKO.1 e.v.
sh1 EphA2
sh2 EphA2
sh3 EphA2
C
Collagen III intensity score
No treat.
vehicle
ZD6474
D
vehicle
ZD6474
pLKO.1 e.v.
sh1 EphA2
sh2 EphA2
sh3 EphA2
= 50µm
E
pLKO.1 e.v.
sh2 EphA2
sh3 EphA2
vehicle
ZD6474

Figure S5. EphA2 KD prevents VEGFR2 inhibition-induced tumor cell invasion *in vivo*. Related to Figure 3. A, Summary of pLKO.1 e.v., sh2-EphA2 and sh3-EphA2 orthotopically injected H441 cells. Representative photos of resected lungs and IHCs are shown. Mice were treated every second day with either vehicle or ZD6474 (50mg/kg). Each setting included 6 mice. Black arrows indicate lung metastases. IHC staining of resected lungs for Hematoxylin and Eosin (H&E) and human Ki-67, indicating injected human tumor cells. Scale bars: 500µm or 200µm as indicated. **B**, Quantification of Ki-67-positive cells for orthotopically injected H441 tumors as indicated. Line with number represents the number of mice for each group. **C**, Quantification of collagen III staining for H441 pLKO.1 e.v. and sh-EphA2 tumors under different treatment conditions as indicated ((n=6 per group), *p<0.05, **p<0.01, ***p<0.001) **D**, Representative images for collagen III staining for H441 pLKO.1 e.v. and sh-EphA2 tumors under vehicle and ZD6474 treatment. The sh-EphA2 tumors showed reduced collagen III staining with well-ordered collagen fibers. **E**, Images of rib cages after lung resection for pLKO.1 e.v., sh2 and sh3 EphA2 injected cells. Vehicle treatment resulted in clean healthy rib cages. ZD6474 treatment showed increased infiltration of the rib cages with tumor mass for pLKO.1 e.v. injected mice. The sh-EphA2 injected mice showed a slight infiltration. Black arrows highlight tumors.

Figure S6

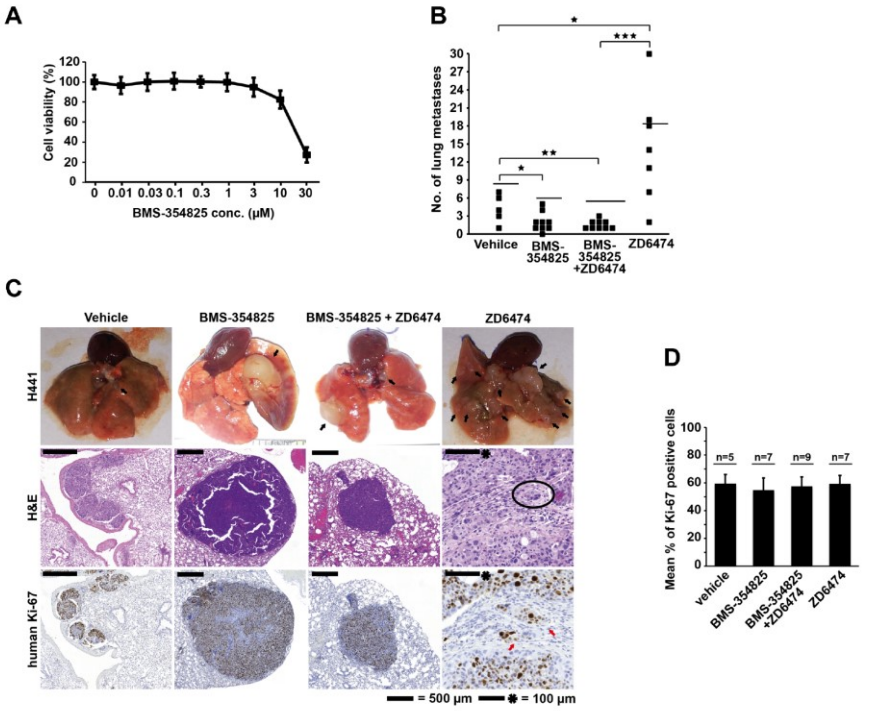

Figure S6. Drug-induced inhibition of EphA2 abrogates tumor cell invasion during VEGFR2-targeted treatment. Related to Figure 3. A, Viability curve for H441 cells with BMS-354825 incubation for 96h in increasing concentrations as indicated. **B**, Total numbers of lung metastases for all mice under different treatment conditions with ZD6474 and BMS-354825 as indicated. Each square represents one mouse. (*p<0.05, **p<0.01, ***p<0.001) **C**, Representative photos and IHCs of resected lungs of orthotopically injected H441 wt cells. Mice received vehicle (n=5), BMS-354825 (n=8), BMS-354825 + ZD6474 (n=9) or ZD6474 (n=7). IHC staining of resected lungs for H&E and human Ki-67. BMS-354825 reduced the incidences of lung metastases and animals with rib cage infiltrations. **D**, Quantification of Ki-67-positive cells for orthotopically injected H441 tumors with different treatment conditions as indicated. Line with number represent the amount of mice for each group.

Figure S7

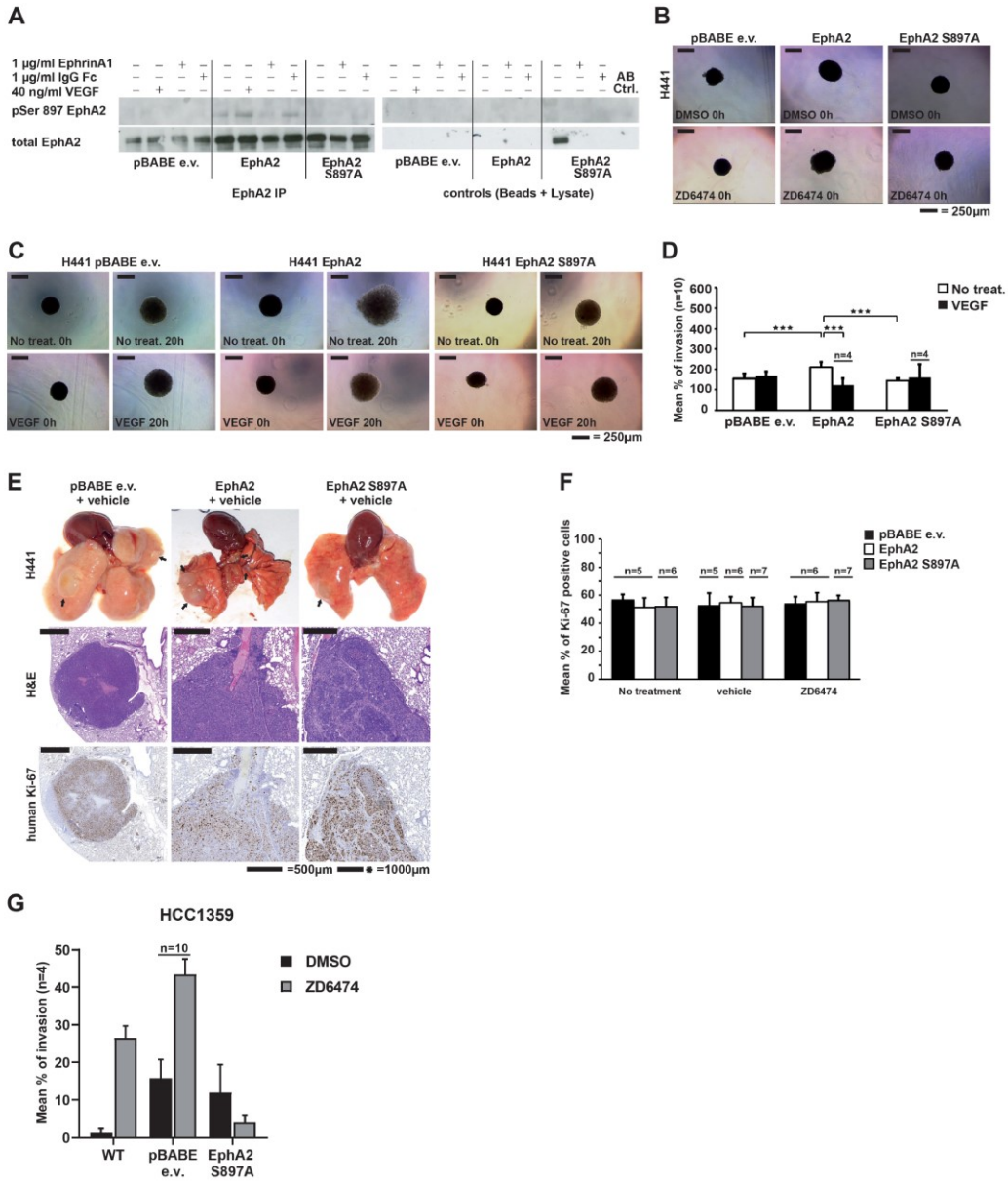
A
1 µg/ml EphrinA1
1 µg/ml IgG Fc
40 ng/ml VEGF
AB Ctrl.
pSer 897 EphA2
total EphA2
pBABE e.v.
EphA2
EphA2 S897A
EphA2 IP
controls (Beads + Lysate)
B
pBABE e.v.
EphA2
EphA2 S897A
H441
DMSO 0h
ZD6474 0h
= 250µm
C
H441 pBABE e.v.
H441 EphA2
H441 EphA2 S897A
No treat. 0h
No treat. 20h
VEGF 0h
VEGF 20h
= 250µm
D
No treat.
VEGF
Mean % of invasion (n=10)
***
n=4
pBABE e.v.
EphA2
EphA2 S897A
E
pBABE e.v. + vehicle
EphA2 + vehicle
EphA2 S897A + vehicle
H441
H&E
human Ki-67
=500µm
=1000µm
F
pBABE e.v.
EphA2
EphA2 S897A
Mean % of Ki-67 positive cells
n=5
n=6
n=7
No treatment
vehicle
ZD6474
G
HCC1359
DMSO
ZD6474
Mean % of invasion (n=4)
n=10
WT
pBABE e.v.
EphA2 S897A

Figure S7. EphA2 S897 phosphorylation is required for tumor cell invasion upon VEGFR2 inhibition in H441 and HCC1359 cells. Related to Figure 4. A, Western blot analysis of IP for EphA2. H441 wt, EphA2 and EphA2 S897A cells were treated with EphrinA1, IgG control or VEGF. IPs were stained for pS897 antibody (AB) to confirm S897A mutation. EphrinA1 reduced pS897 activation whereas VEGF treatment did not affect pS897 phosphorylation. EphA2 total staining shows that EphA2 was targeted by the AB, and that EphA2 and EphA2 S897A cells overexpress the constructs. Control lysates represent lysate incubated with beads without AB. **B**, Corresponding spheroid images of invasion assay for pBABE e.v., EphA2 and EphA2 S897A cells at 0h. The 20h end-results are shown in Figure 4A. **C and D**, Representative images and quantification as mean percentage of invasion assay for H441 pBABE e.v., EphA2 and EphA2 S897A with and without VEGF stimulation. EphA2 overexpression increased invasion compared to e.v. and S897A cells without stimulation. VEGF reduced invasion in EphA2 overexpressing cells but had no effect on invasion in e.v. and S897A expressing cells. (***$p<0.001$); Scale bars: 250µm. **E**, Representative photos of resected lungs and IHCs of pBABE e.v. (n=5), EphA2 (n=6) and EphA2 S897A (n=6) injected mice with vehicle treatment. Black arrows indicate lung metastases. IHC staining of resected lungs for H&E and human Ki-67, indicating injected human tumor cells. Scale bars: 500µm or 1000µm as indicated. The ZD6474-treated settings are shown in Figure 4D. **F**, Quantification of Ki-67-positive cells for orthotopically injected H441 tumors with different constructs and different treatment conditions as indicated. Line with number represent the amount of mice for each group. **G**, Invasion assay using HCC1359 wt, pBABE e.v. and EphA2 S897A mutant cells. Quantification was performed using mean percentage of invasion after 20h. Spheroids were treated with ZD6474 or DMSO as control. An increased invasive phenotype upon VEGFR2 inhibition can be observed in cells expressing only wild-type EphA2.

Figure S8

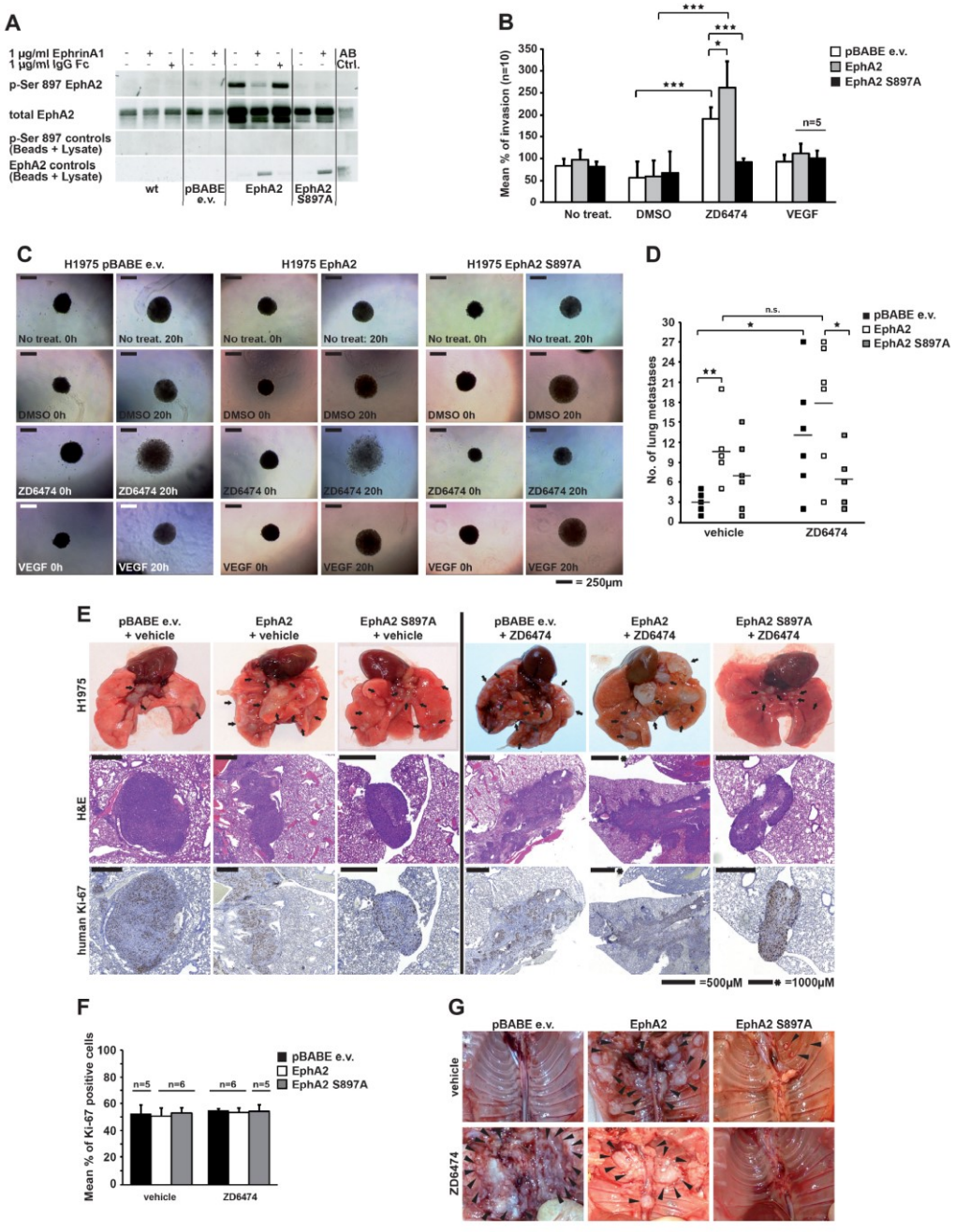
A
1 µg/ml EphrinA1
1 µg/ml IgG Fc
AB Ctrl.
p-Ser 897 EphA2
total EphA2
p-Ser 897 controls (Beads + Lysate)
EphA2 controls (Beads + Lysate)
wt
pBABE e.v.
EphA2
EphA2 S897A
B
Mean % of invasion (n=10)
pBABE e.v.
EphA2
EphA2 S897A
n=5
No treat.
DMSO
ZD6474
VEGF
C
H1975 pBABE e.v.
H1975 EphA2
H1975 EphA2 S897A
No treat. 0h
No treat. 20h
DMSO 0h
DMSO 20h
ZD6474 0h
ZD6474 20h
VEGF 0h
VEGF 20h
= 250µm
D
No. of lung metastases
n.s.
pBABE e.v.
EphA2
EphA2 S897A
vehicle
ZD6474
E
pBABE e.v. + vehicle
EphA2 + vehicle
EphA2 S897A + vehicle
pBABE e.v. + ZD6474
EphA2 + ZD6474
EphA2 S897A + ZD6474
H1975
H&E
human Ki-67
=500µM
=1000µM
F
Mean % of Ki-67 positive cells
pBABE e.v.
EphA2
EphA2 S897A
n=5
n=6
n=6
n=5
vehicle
ZD6474
G
pBABE e.v.
EphA2
EphA2 S897A
vehicle
ZD6474

Figure S8. EphA2 S897 phosphorylation is required for tumor cell invasion upon VEGFR2 inhibition in H1975 cells. Related to Figure 4. A, Western blot analysis of IP for EphA2. H1975 wt, pBABE e.v., EphA2, and EphA2 S897A cells were treated with EphrinA1 or IgG control. IPs were stained for pS897 antibody (AB) to confirm S897A mutation. EphrinA1 reduced pS897 activation in EphA2 overexpressing cells. EphA2 total staining shows that EphA2 was targeted by the AB and that EphA2 and EphA2 S897A cells overexpress the constructs. Control cell lysates represent lysate incubated with beads without AB. **B and C**, Quantification and representative images of invasion assay of H1975 pBABE e.v., EphA2 and EphA2 S897A spheroids. ZD6474 treatment induced an invasive phenotype compared to untreated, DMSO or VEGF-stimulated settings. VEGF had no effect on invasion. (*$p<0.05$, **$p<0.001$); Scale bars: 250µm **D**, Number of lung metastases for all mice in the H1975 pBABE e.v., EphA2 and EphA2 S897A setting. Each square represents one mouse. The mean is indicated by a line. (*$p<0.05$, **$p<0.001$, n.s.=not significant). ZD6474 treatment (50mg/kg every second day) increased the number of lung metastases in pBABE e.v. and EphA2 mice. EphA2 S897A injected mice reduced lung metastases. **E**, Representative photos and IHCs of resected lungs of H1975 pBABE e.v. (vehicle n=5, ZD6474 n=6), EphA2 (vehicle n=6, ZD6474 n=6) and EphA2 S897A (vehicle n=6, ZD6474 n=5) orthotopically injected mice. ZD6474 treatment results in invasive tumor growth of H1975 pBABE e.v. and EphA2 cells. H1975 EphA2 S897A tumors showed compact encapsulated shape. Black arrows indicate lung metastases. IHC staining of resected lungs for Hematoxylin and Eosin (H&E) and human Ki-67, indicating injected human tumor cells. Scale bars: 500µm or 1000µm as indicated. **F**, Quantification of Ki-67-positive cells for orthotopically injected H1975 tumors using different constructs and different treatment conditions as indicated. Line with number represents the amount of mice for each group. **G**, Images of rib cages after lung resection. Vehicle treatment resulted in nearly empty rib cages, however EphA2 overexpression showed strong infiltration. ZD6474 treatment shows increased infiltration of the rib cages with tumor mass for pBABE e.v. and EphA2 mice. EphA2 S897A mice had clean empty rib cages. Black arrows highlight tumors.

Figure S9

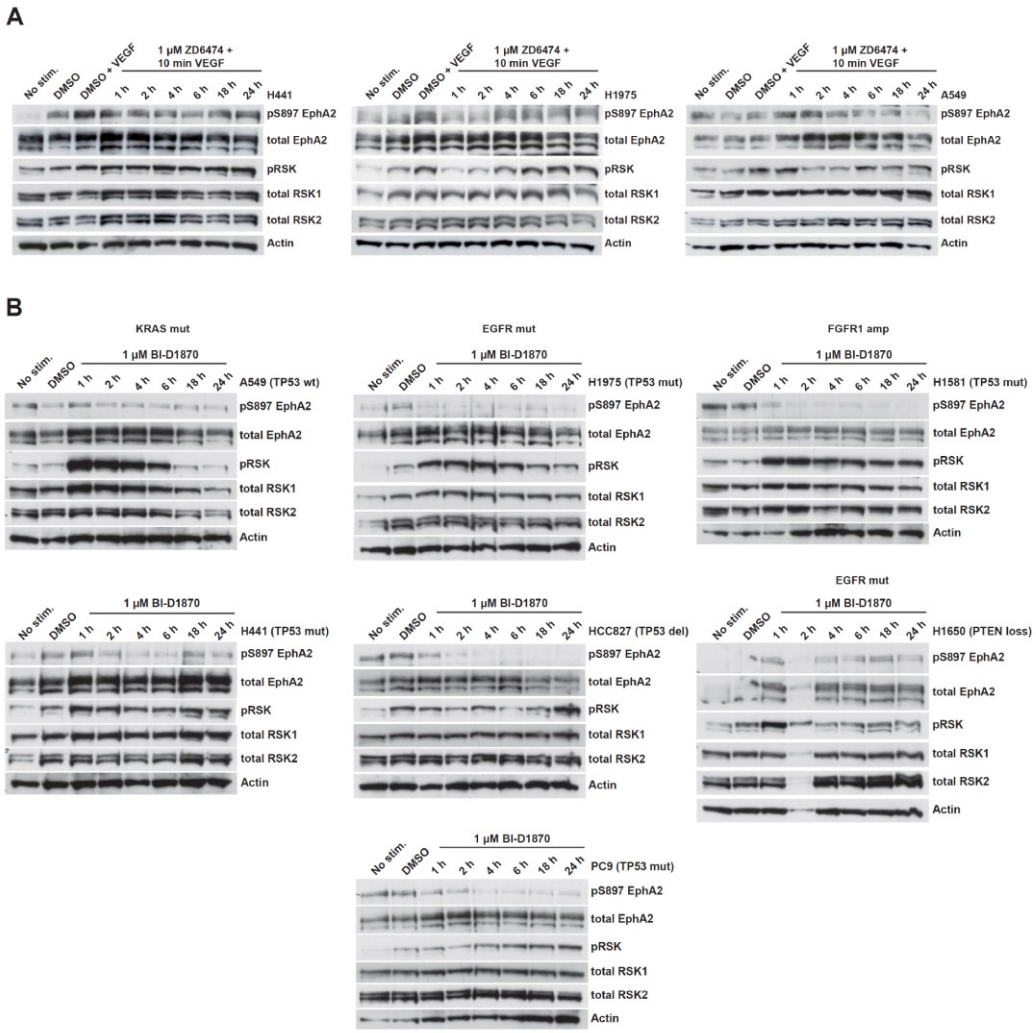
A
No stim.
DMSO
DMSO + VEGF
1 µM ZD6474 + 10 min VEGF
1 h
2 h
4 h
6 h
18 h
24 h
H441
H1975
A549
pS897 EphA2
total EphA2
pRSK
total RSK1
total RSK2
Actin
B
KRAS mut
EGFR mut
FGFR1 amp
1 µM BI-D1870
A549 (TP53 wt)
H1975 (TP53 mut)
H1581 (TP53 mut)
H441 (TP53 mut)
HCC827 (TP53 del)
H1650 (PTEN loss)
PC9 (TP53 mut)
C
HCC827
PC9
H1650
H1581
DMSO
10 µM BI-D1870

Figure S9. VEGFR2 inhibition does not induce S897 EphA2 in vitro. Related to Figure 4 and 5. A, Western blot analysis of H441, H1975 and A549 cells for pS897 EphA2, pRSK signaling under VEGFR2 inhibition with ZD6474 and DMSO control. Lysates were generated at different time-points as indicated. **RSK controls S897 EphA2 phosphorylation. B**, Western blot analysis of NSCLC cell lines for pS897 EphA2 and pRSK signaling under RSK inhibition with 1μM BI- D1870 and DMSO control. Actin served as loading control. Lysates were generated at different time points as indicated. Cell lines are sorted in columns depending on the mutation status. RSK inhibition reduced pS897 EphA2 in all cell lines except for H1650. **C**, Western blot analysis of NSCLC cells under 4h 10μM BI-D1870 and DMSO treatment for pS897 EphA2 and pRSK. Actin served as loading control. BI- D1870 inhibited pS897 EphA2 in most cell lines.

Figure S10

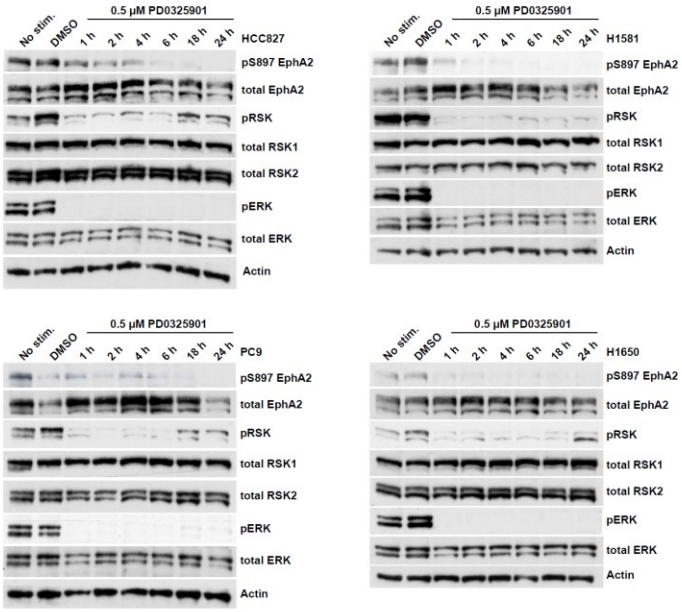

Figure S10. MEK inhibition reduces S897 EphA2 phosphorylation. Related to Figure 5. Western blot analysis of NSCLC cells for pS897 EphA2, pRSK and pERK signaling under MEK inhibition with 0.5µM PD0325901 and DMSO control as indicated. Lysates were generated at different time-points as indicated. PD0325901 reduced pS897 EphA2 in all cell lines as well as phosphorylation of downstream pRSK.

Figure S11

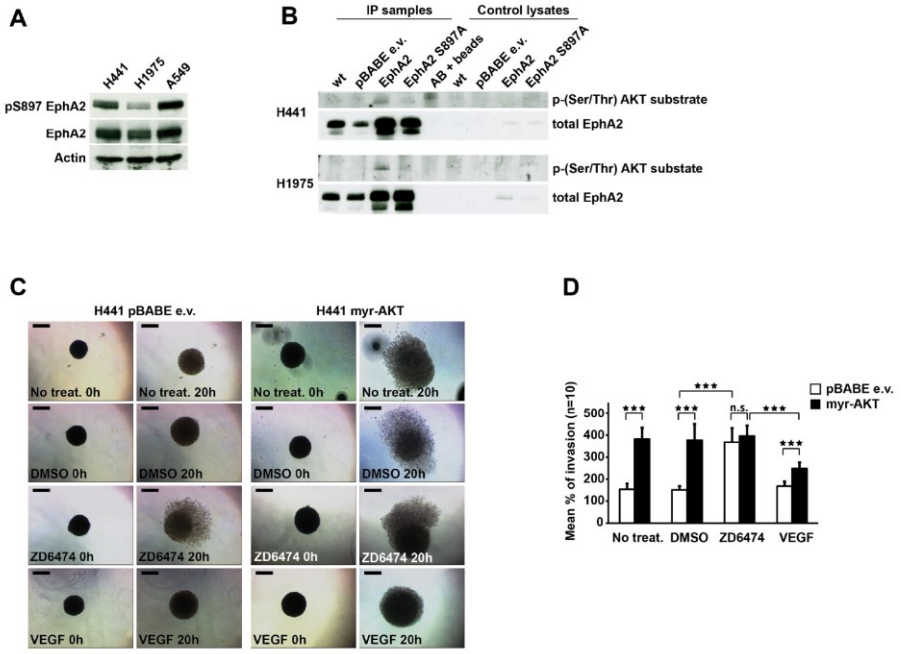

Figure S11. EphA2 S897 is a substrate of AKT. Related to Figure 5 and Graphical abstract. A, Western blot analysis of pS897 expression in NSCLC cell lines. Actin served as loading control. H441 and A549 present similar amount of pS897 whereas H1975 show the lowest. **B**, Western blot analysis of IP for EphA2 in pBABE e.v., EphA2 and EphA2 S897A-expressing H441 and H1975 NSCLC cells. Staining with an AKT substrate antibody confirmed that S897 is a substrate of AKT since the mutant showed no signal. **Activated AKT induces invasion**. **C and D**, Representative images of spheroids from the invasion assay and corresponding quantification of mean-% of invasion with H441 pBABE e.v. (control) and myr-AKT transduced cells. Myr-AKT cells induced invasion which could be reduced upon VEGF treatment (n=10 per group, **$p<0.01$, ***$p<0.001$).

Figure S12

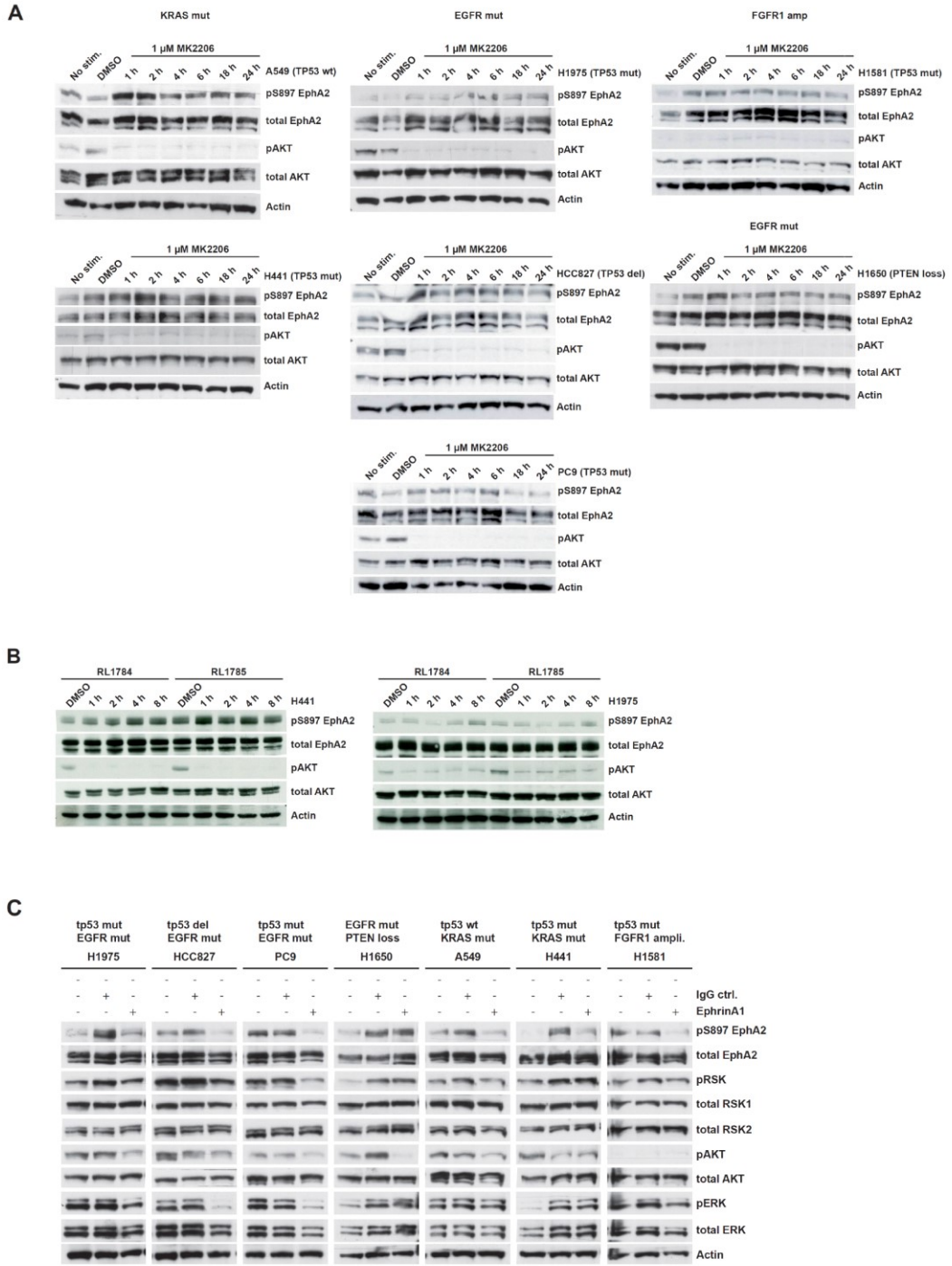
A
KRAS mut
EGFR mut
FGFR1 amp
EGFR mut
1 µM MK2206
No stim.
DMSO
1 h
2 h
4 h
6 h
18 h
24 h
A549 (TP53 wt)
H1975 (TP53 mut)
H1581 (TP53 mut)
H441 (TP53 mut)
HCC827 (TP53 del)
H1650 (PTEN loss)
PC9 (TP53 mut)
pS897 EphA2
total EphA2
pAKT
total AKT
Actin
B
RL1784
RL1785
DMSO
1 h
2 h
4 h
8 h
H441
H1975
pS897 EphA2
total EphA2
pAKT
total AKT
Actin
C
tp53 mut EGFR mut H1975
tp53 del EGFR mut HCC827
tp53 mut EGFR mut PC9
EGFR mut PTEN loss H1650
tp53 wt KRAS mut A549
tp53 mut KRAS mut H441
tp53 mut FGFR1 ampli. H1581
IgG ctrl.
EphrinA1
pS897 EphA2
total EphA2
pRSK
total RSK1
total RSK2
pAKT
total AKT
pERK
total ERK
Actin

Figure S12. AKT inhibition does not reduce pS897 EphA2. Related to Figure 5 and Graphical abstract. A, Western blot analysis of NSCLC cell lines for pS897 EphA2 and pAKT signaling under AKT inhibition with MK2206 and DMSO control. Actin served as loading control. Lysates were generated at different time points as indicated. Cell lines are sorted in columns depending on the mutation status. AKT inhibition did not result in pS897 EphA2 reduction. **B**, Western blot analysis of H441 and H1975 with a covalent- allosteric AKT inhibitor RL1784 and the reversible counterpart RL1785 (not commercially available) for pS897 EphA2 and pAKT signaling. Actin served as loading control. The inhibitors did not alter S897 phosphorylation upon target inhibition. **EphrinA1 is a negative regulator of S897 EphA2 phosphorylation. C**, Western blot analysis of NSCLC cells with 30 min EphrinA1, corresponding IgG control or no treatment for pS897 EphA2, pRSK, pAKT and pERK status. Actin served as loading control. In all cell lines with the exception of H1650, the presence of EphrinA1 reduced S897 EphA2 phosphorylation.

cancers

MDPI

Supplementary materials

EGFR Inhibition Strongly Modulates the Tumour Immune Microenvironment in EGFR-Driven Non-Small-Cell Lung Cancer

Carolin Selenz [1,2], Anik Compes [1,2,3], Marieke Nill [1,2], Sven Borchmann [1], Margarete Odenthal [4], Alexandra Florin [4], Johannes Brägelmann [2,3,5], Reinhard Büttner [4], Lydia Meder [1,2,3]*, and Roland T. Ullrich [1,2,*]

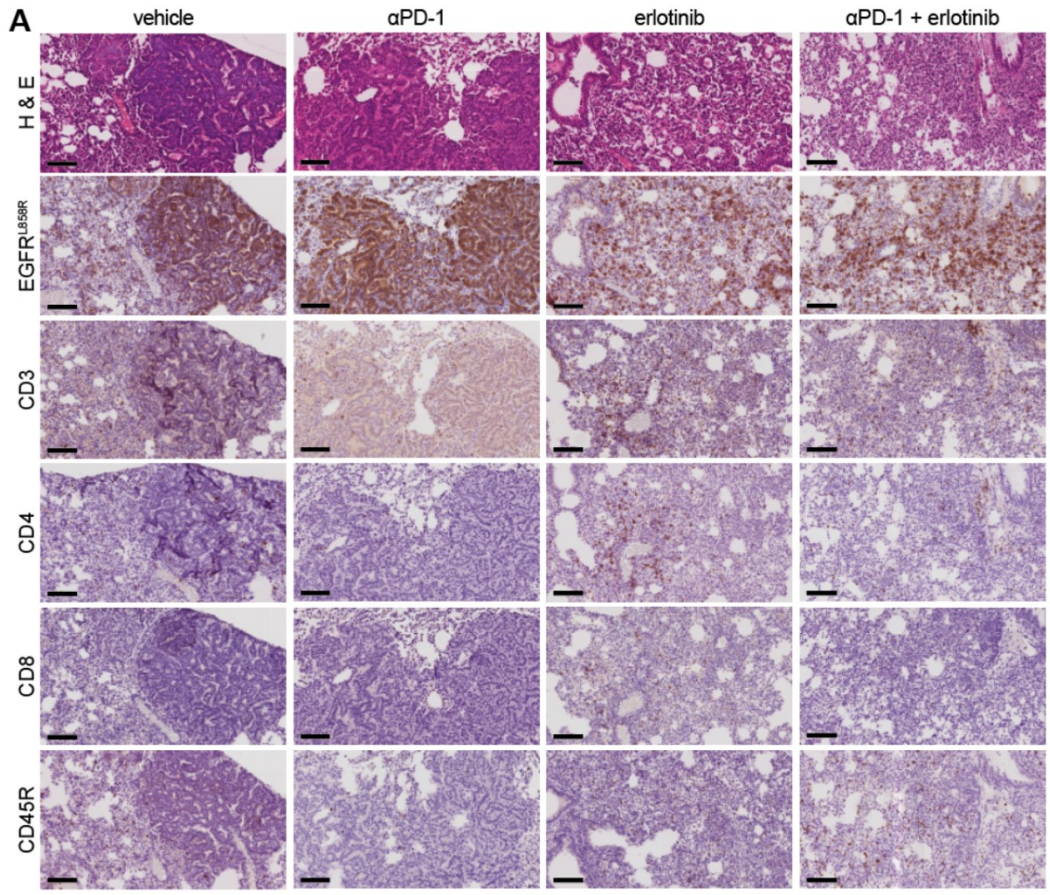

Figure S1. Infiltration of immune cells in EGFR^{L585R}-driven tumours is elevated upon EGFR inhibition. (**A**) Images from stained FFPE tumour material either after H&E or immunohistochemistry staining with the indicated antibodies, identifying EGFR^{L858R+} tumour cells, general T−cells, CD4^{+} T−cells, CD8^{+} T−cells and CD45^{+} B−cells. One representative lesion from each therapy group is shown. Scale bars indicate 100 µm.

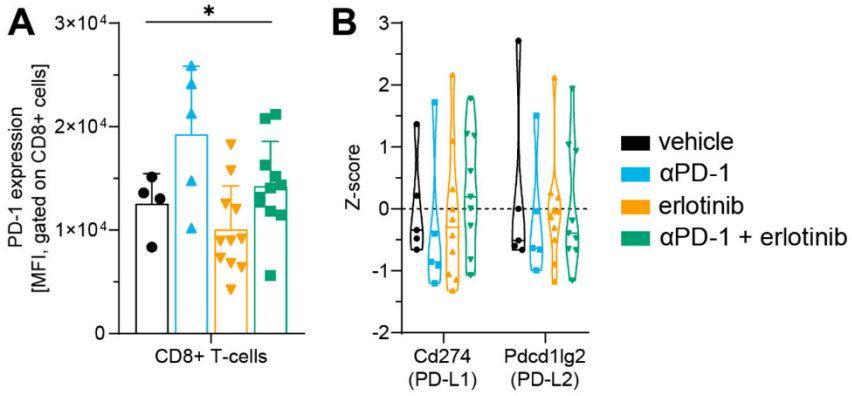

Figure S2. EGFR inhibition does not increase PD−1 levels. (**A**) Mean fluorescent intensity data of PD−1 expression of cytotoxic $CD8^+$ T−cells. Data are shown as the mean with SD, statistical test used was the Kruskal−Wallis test to compare all therapy groups (statistically significant changes are indicated across all groups as follows: *, $p < 0.05$). (**B**) Mean gene expression *z*-score of Cd274 (PD−L1) and Pdcd1lg2 (PD−L2). Data are shown as violin plots.

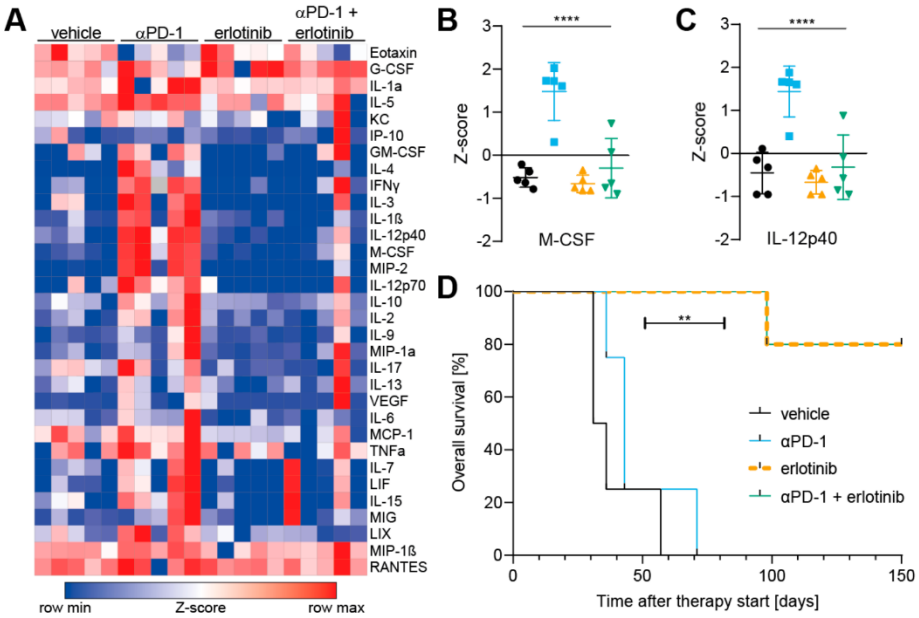

Figure S3. EGFR inhibition does not increase circulating cytokines. (**A**) Heatmap of *z*-scores of circulating cytokines quantified by multiplex Luminex analysis in sera of mice treated with vehicle, aPD−1, erlotinib or aPD−1 + erlotinib, as indicated. Colour gradient ranges from minimum (blue) to maximum (red) *z*-score value for each cytokine. (**B-C**) Circulating levels of cytokines (**B**) M−CSF and (**C**) IL12−p40 in sera of mice (**D**) Kaplan-Meier survival curve of mice bearing $EGFR^{L858R}$-driven lung tumours from indicated therapy groups (statistically significant changes are indicated as follows: **, $p < 0.01$; ****, $p < 0.0001$).

Table S1. Immune cell-specific transcripts.

Cell type	Genes							
mDC	CCL13	CCL17	CCL22	HSD11B1				
iDC	CD1A	CD1B	CD1E	F13A1	SYT17			
aDC	CCL1	EBI3	IDO1	LAMP3	OAS3			
pDC	IL3A							
Macrophages	APOE	CCL7	CD68	CHIT1	CXCL5	MARCO	MSR1	
Mast cells	CMA1	CTSG	KIT	MS4A2	PRG2	TPSAB1		
Neutrophils	CSF3R	FPR2	MME					
Eosinophils	CCR3	IL5RA	PTGDR2	SMPD3	THBS1			
B-cells	BLK	CD19	CR2	HLA-DOB	MS4A1	TNFRSF17		
T-cells	CD2	CD3E	CD3G	CD6				
Th1	CD38	CSF2	IFNG	IL12RB2	LTA	CTLA4	TXB21	STAT4
Th2	CXCR6	GATA3	IL26	LAIR2	PMCH	SMAD2	STAT6	
Th17	IL17A	IL17RA	RORC					
Tfh	CXCL13	MAF	PDCD1	BCL6				
Treg	FOXP3							
Cytotoxic CD8	CD8A	CD8B	FLT3LG	GZMM	PRF1			
gdTcells	CD160	FEZ1	TARP					
NK cells	BCL2	FUT5	NCR1	ZNF205				
CD56bright	FOXJ1	MPPED1	PLA2G6	RRAD				
CD56dim	GTF3C1	GZMB	IL21R					

Supplementary figures

Establishment of multiple EML4-ALK-driven NSCLC mouse models

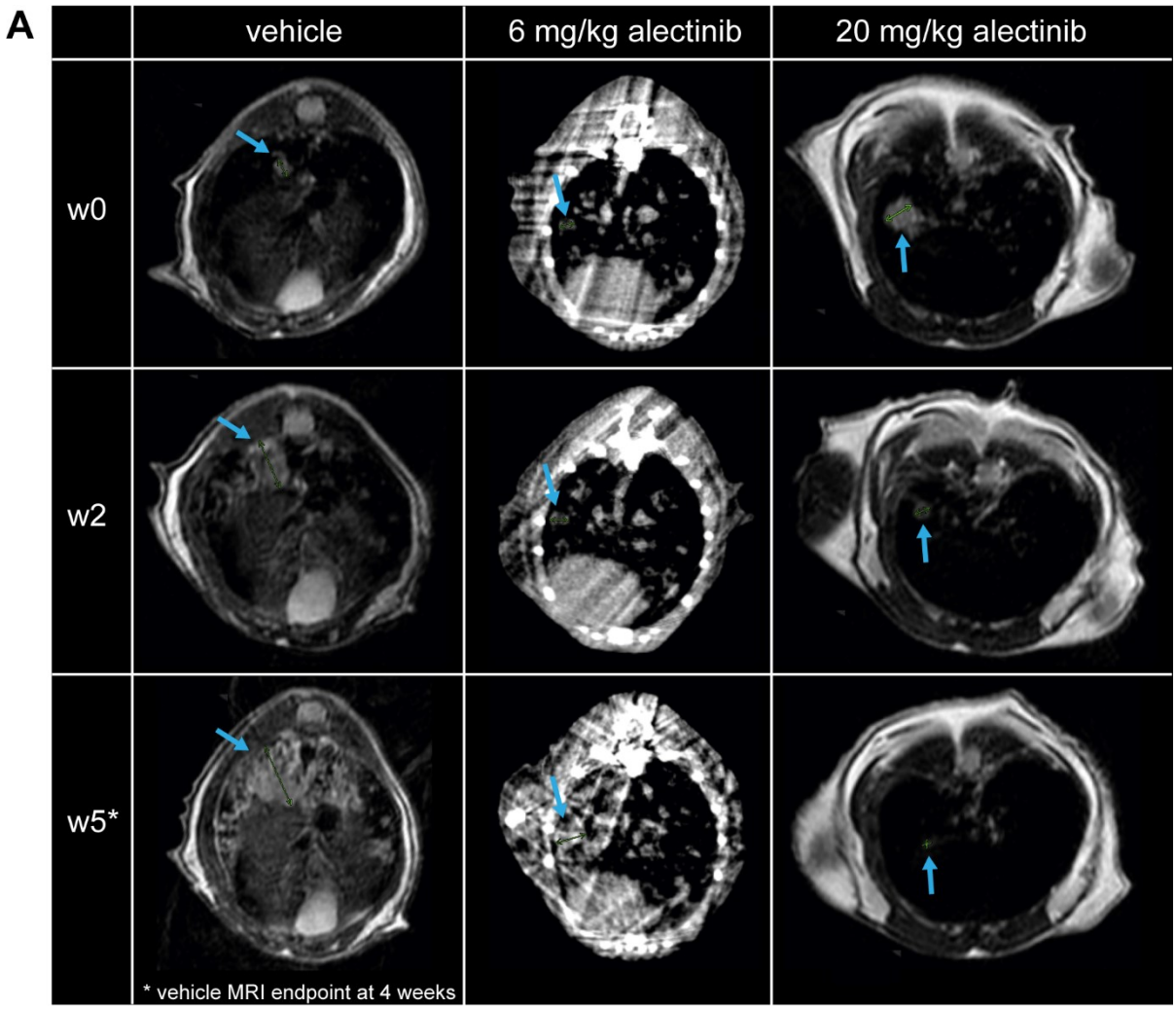

Figure S7. Scans of autochthonous EML4-ALK NSCLC mouse model. (A) Lung scans are shown of representative mice from each therapy group at different time points (w0= directly before therapy start, w2, w5= 2 and 5 weeks after therapy start, respectively), blue arrows indicate target lesions.

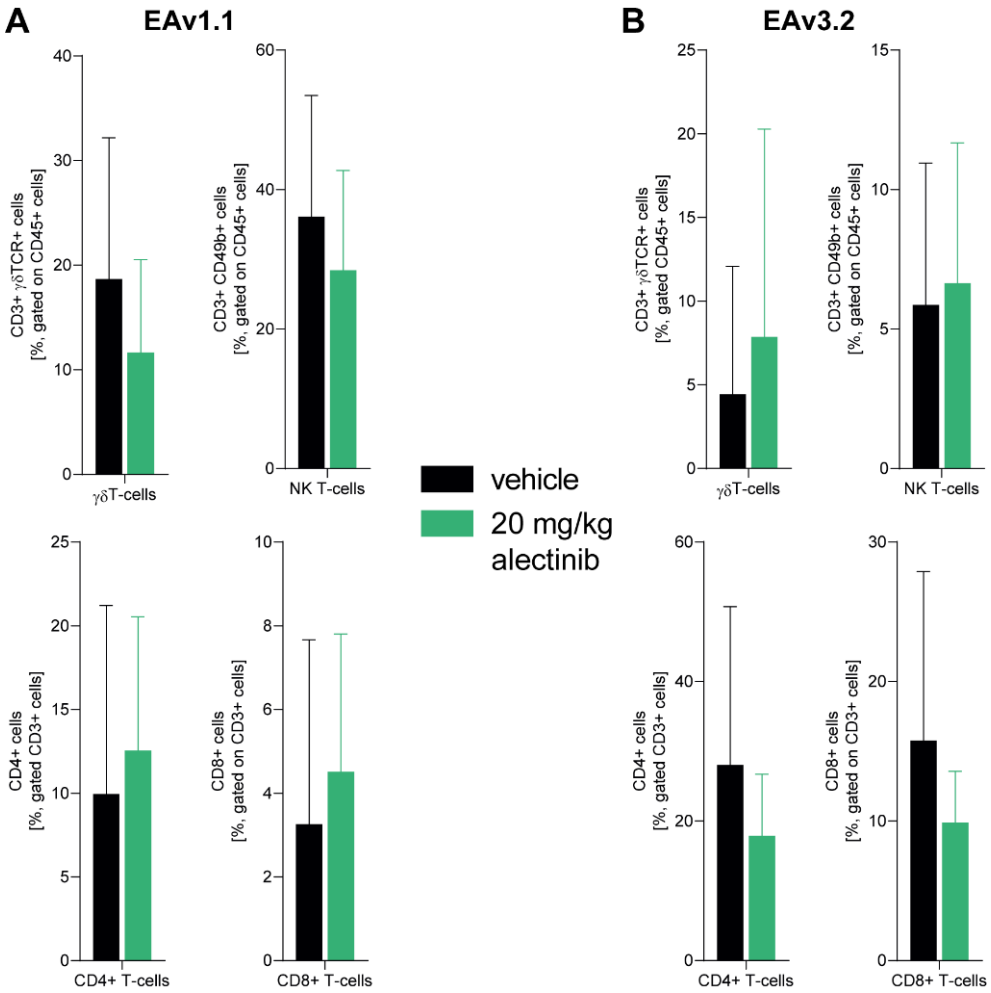

Figure S8. T-cell subtypes in murine EML4-ALK/p53 tumours in response to ALK inhibition. (A-B) Flow cytometry analysis of s.c. EML4-ALK/p53 variant 1 (EAv1.1; A) and variant 3 (EAv3.2; B) tumours, looking at intratumoral infiltration of γδT-cells, NK T-cells, CD4+ and CD8+ T-cells in vehicle and alectinib treated tumours. Data are shown as mean with SD.

Danksagung

Zum Abschluss möchte ich mich ganz herzlich bei den zahlreichen Kolleg/innen und Freund/innen bedanken, die mir in den letzten Jahren zur Seite gestanden haben.

Mein besonderer Dank gilt Roland Ullrich, der mir die Arbeit an meinen Projekten ermöglichte und mich über die gesamte Zeit hinweg betreute. Sehr geschätzt habe ich u.a. seine unkomplizierte Art, die es möglich machte, sich auch spontan über Projekte auszutauschen oder für eine Besprechung im Büro vorbeizuschauen.

Darüber hinaus bedanke ich mich bei Björn Schumacher und Matthias Fischer, die mich als Betreuer und Gutachter meiner Dissertation unterstützt haben.

Ein großer Dank gilt auch Lydia Meder, die mir nicht nur im Labor-Alltag eine große Hilfe und Ratgeberin war, sondern sich auch als unentbehrlich erwies, um die Vorgänge und Prozesse an der Uniklinik zu durchschauen.

Auch Marieke Nill darf an dieser Stelle nicht unerwähnt bleiben, die mir nicht nur stets im Labor zur Seite stand, sondern auch mit ausgiebigen Gesprächen über diverse kulinarische Themen für eine sehr willkommene Abwechslung zu den experimentellen Tätigkeiten sorgte.

Mein Dank gilt zudem auch allen weiteren Mitgliedern der AG Ullrich, mit denen ich in den letzten Jahren Seite an Seite zusammenarbeiten durfte und die das Labor zu einem zweiten Zuhause gemacht haben. Dafür bedanke ich mich ganz herzlich bei: Anik Compes, Philip Lützen, Jonathan Bochtler, Mirjam Koker, Luis Tetenborg, Charlotte Orschel, Claudia Orschel, David Stahl, Philipp Gödel, Tabea Gewalt, Hilal Bhat, Hanna Ludwig, Sven Borchmann und Julia Mattlener.

Ebenso haben die Mitglieder der AG Klein für mich dazu beigetragen, eine einzigartige Arbeitsumgebung zu schaffen, in der es nie langweilig wurde. Im geteilten Büro, Labor und in der Küche habe ich den Austausch in den letzten Jahren sehr geschätzt und dafür bedanke mich bei: Hanna Janicki, Meryam Seda Ercanoglu, Michael Korenkov, Nareshkumar Poopalasingam, Elvin Ahmadov, Artem Ashurov, Sabrina Dähling, Susanne Detmer, Timm Weber, Svea Rose, Leon Ullrich, Matthias Zehner, Christoph Kreer und Lutz Gieselmann.

Zu guter Letzt möchte ich auch meiner Familie und meinen Freund/innen Danke sagen, da ich ohne ihre bedingungslose Unterstützung und ihren Rückhalt diesen Punkt nicht erreicht hätte.